UNIVERSITY OF INSUBRIA

Ph.D. COURSE IN LIFE SCIENCES AND BIOTECHNOLOGY

XXXVI CYCLE

Characterization of PRODH regulation and function in lung adenocarcinomas: a role for tyrosine kinase receptors?

Caratterizzazione della regolazione e della funzione di PRODH in adenocarcinoma del polmone: un ruolo per i recettori tirosin chinasici?

Supervisor: Prof. **Paola Campomenosi**

Ph.D. thesis of:
Priscilla Chiofalo
Matr. 747154

Dep. of Biotechnology and Life Sciences - University of Insubria

Academic year 2020-2021

SUMMARY

ABSTRACT

Lung cancer is a global health concern. Targeted therapies improve survival and, among them, Epidermal Growth Factor Receptor (EGFR) inhibitors (TKIs) are used for lung adenocarcinoma (ADC) treatment. However, variable response and resistance mechanisms invariably occur.

We hypothesized that proline dehydrogenase (PRODH), an enzyme key in proline catabolism, played a role in EGFR-mutant lung ADCs, since we previously found a correlation with PRODH expression.

Overexpressing wild-type or mutant EGFR constructs led to decreased PRODH levels in various cell lines, with the EGFR p.E746-A750del mutant showing the strongest effect. EGFR inhibition in cell lines harboring the p.E746-A750del EGFR mutation increased PRODH mRNA, confirming that EGFR negatively regulates PRODH expression.

Bioinformatic analysis identified putative response elements for STAT3, a signaling molecule downstream of EGFR, in *PRODH* intron 1. We show that STAT3 indeed mediates EGFR modulation of PRODH. PRODH repression may represent a mechanism by which EGFR, via STAT3, contributes to tumor progression.

This project also aimed to advance the knowledge of PRODH's role in lung cancer progression. We observed increased PRODH expression in two EGFR-mutant lung ADC cell lines with *in-vitro* acquired resistance to TKIs compared to their TKI-sensitive counterparts. PRODH inhibition affected 2D/3D-growth of TKI-resistant but not TKI-sensitive cells.

Our results suggest different PRODH functions at different lung cancer stages.

INTRODUCTION

LUNG CANCER

Lung cancer is a highly heterogeneous disease: histologically, it comprises Small Cell Lung Cancer (SCLC, 15% of the cases) and Non-Small Cell Lung Cancer (NSCLC, 85%), which includes adenocarcinomas and squamocellular carcinomas (55% and 45% of NSCLCs, respectively). Lung cancer is heterogeneous also considering the genetic alterations and gene expression profiles, even within each histotype (Chen et al., 2014).

The common denominator of this type of cancer is its notoriously poor prognosis. Despite the advances in diagnostic techniques and the advent of new therapies, lung cancer remains a leading cause of cancer-related mortality, representing a health problem worldwide.

Lung cancer epidemiology: incidence, mortality, and survival

In recent years, the incidence of lung cancer has decreased, mainly among males, due to increasing quitting of smoking habit. Since 2006, a constant but slower decrease was also observed in women, who also took up smoking habit later than males (Siegel et al., 2023).

Despite this, lung cancer remains the second tumor worldwide for incidence: in 2020 about 1,4 million and more than 700000 new cases were diagnosed in men and females, respectively (Schabath and Cote, 2019; Sung et al., 2021). In both sexes, the incidence rate depends on the geographic localization. In Europe, it accounts for 20% of worldwide cases. The same trend was also observed in Italy, where about 28000 and 14000 new cases were estimated in males and females respectively by the Italian Association of Medical Oncology (AIOM, 2022). Thus, it represents the second type of

tumor for frequency in males and the third in females, with variable frequency based on the age of patients (AIOM, 2021).

The advances in lung cancer treatment, the implementation of prevention mechanisms, as well as earlier diagnosis led to a decrease in lung cancer mortality. Nevertheless, lung neoplasms are still the leading cause of cancer death worldwide. In 2020, the estimated deaths were more than 1,1 million in men and 600000 in women with variation between countries (Figure 1). The highest rate of mortality was observed in the Asian continent. In Italy, it represents the first cause of death for cancer in men and the second cause of death in females (Schabath and Cote, 2019; AIOM, 2021).

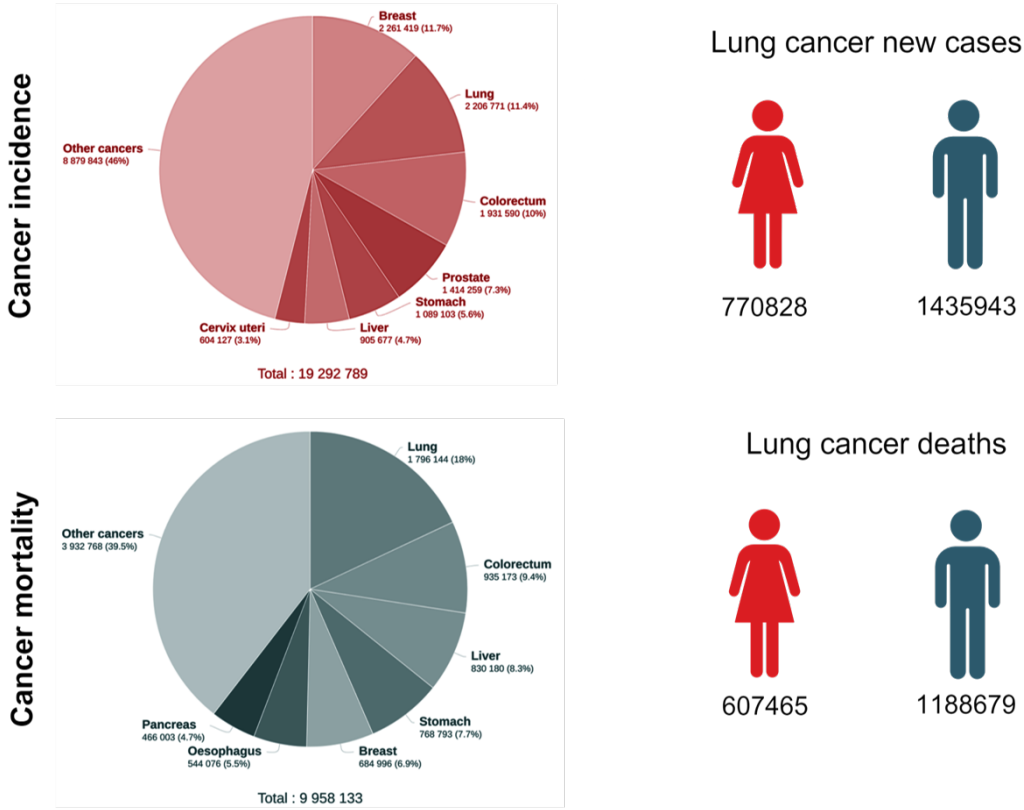

Figure 1. The graphic displays the incidence and deaths of the most common types of cancer in 2020 through a pie chart on the left. On the right, it shows the new estimated cases and mortality of lung cancer between the two sexes. Data was obtained from the Global Cancer Statistics 2020 report by Sung et al. 2021. Created with Biorender.com.

Late diagnosis is the main responsible for the large number of deaths. The 5-year survival rate depends on the stage of tumors at diagnosis. Overall, it is equal to 19%, with differences among the tumor subtypes. In Italy, it reaches 11% in men and 14% in women (Schabath and Cote, 2019; AIOM, 2021).

Lung cancer risk factors

The implementation of anti-smoking campaigns in the 2000s resulted in a decrease in lung cancer cases and highlighted the importance of identifying predisposing factors for malignancies. Over the past years, numerous risk factors have been described, including smoking, radon, occupational exposures, and infections (Bade and Dela Cruz, 2020).

As I said before, one of the main risk factors for lung cancer development is tobacco smoking, indeed in the United States, about 80-90% of lung cancers arise in persons with a history of tobacco exposure. Cigarettes contain 4000 chemicals, 69 of which are recognized as carcinogens by the International Agency for Research on Cancer (IARC). Among these, polycyclic aromatic hydrocarbons, aromatic amines, N-nitrosamines, benzene, arsenic, radon, and chromium are the most dangerous. These metabolites determine the formation of DNA adducts and the production of free radicals. Due to this, the risk of lung cancer in smokers is 10 to 30-fold higher compared to non-smokers. Moreover, the number of cigarettes consumed (pack years: packets of cigarettes/day x years of smoking), the grade of inhalation, the tar, and the nicotine amount affect the risk (Schabath and Cote, 2019; Bade and Dela Cruz, 2020).

The combustion of cigarettes between puffs is responsible for second-hand smoke, also known as environmental tobacco smoke. Carcinogens, such as benzene, benzo-a-pyrene, and cotinine are found in the serum of non-smokers. Moreover, DNA adducts generated from carcinogens are found in urine samples of never smokers. An increase of more than 20% in lung cancer risk has been described in second-hand smokers compared to non-smokers (Hori et al., 2016; Kim et al., 2018; Schabath and Cote, 2019). Other types of tobacco, such as pipers, have been correlated to an increased risk of lung cancer, whereas the correlation between the use of recreational drugs (like

cocaine or marijuana) and lung cancer has been still unclear, due to the usual concomitant use with cigarettes smoking (Schabath and Cote, 2019). Unknown is still the role of electronic cigarettes. The compounds contained in the vapor produced by these cigarettes hold carcinogens (such as formaldehyde, acetaldehyde, and acetone) that affect lung functionality, generating oxidative stress. This leads to cell permeability alterations, causing inflammation, and cytotoxicity. However, the effects of long exposure have still to be elucidated.

In the USA, only a minimum number of smokers develop lung cancer (about 15-20%), therefore other risk factors are responsible for the high incidence of lung cancer cases. Among carcinogens, biomass burning, such as wood burning, is also included. In addition, it has been demonstrated that air pollution, in particular fine particulate, and sulfur oxide, increases the risk of lung cancer (Bade and Dela Cruz, 2020).

The second risk factor for lung cancer is radon-exposure. Radon is an invisible, odorless gas, produced by the radioactive decay of radium. It is present in soil and rocks; its concentration varies with geographic localization and over time. About 4-13% of lung cancer is associated with radon exposure. The association between radon and lung cancer has emerged in working miners. Nowadays, radon exposure is mostly associated with occupational exposure being limited to underground workers and uranium miners. The level of exposure is also determined by the amount of radon in soil. The decay products of radon enter with particulate matter in the respiratory tract, causing persistent inflammation and DNA damage to respiratory epithelial cells.

Occupational carcinogens increase the risk of lung cancer, with 10% of tumors attributed to this cause. Occupational carcinogens include arsenic, beryllium, cadmium, chromium, nickel, diesel fumes, and asbestos (Schabath and Cote, 2019; Bade and Dela Cruz, 2020).

Asbestos is a strong natural silicate fiber, consisting of serpentine and amphibole. The mechanism by which it contributes to carcinogenesis is still unclear. It determines chronic inflammation, oxidative stress, genetic and epigenetic alterations, cellular toxicity, and fibrosis. The risk increases with dose exposure, the types of fibers, and

concomitant cigarette smoking (Schabath and Cote, 2019; Bade and Dela Cruz, 2020).

Chronic lung diseases, such as chronic obstructive pulmonary disease (COPD), as well as asthma, which causes chronic inflammation, have also been associated with lung cancer.

Lung infections have also a role in the development of neoplasia. Indeed, sequences from human papillomavirus have been found in 21% of lung cancer samples. Moreover, the virus has been detected in bronchial squamous cell lesions. Microorganisms such as *Streptococcus pneumoniae* and *Chlamydia pneumoniae* have been associated with lung cancer inflammation, an increase of reactive species, DNA damage, angiogenesis, and other tumorigenesis-favoring processes. Infections by *Mycobacterium tuberculosis*, which causes lung fibrosis, have also been correlated to an increased risk of lung cancer. Lung cancer is also one of the main causes of death in subjects affected by AIDS, due to the immunosuppression determined by the human immunodeficiency virus, inflammation, and concomitant coinfection with other microorganisms, including *Mycobacterium tuberculosis* (Schabath and Cote, 2019; Bade and Dela Cruz, 2020).

Lung tumorigenesis is also influenced by factors such as bad alimentary habits and high body mass index. Saturated fats, red meat, lipids, and food enriched with nitrosodimethylamines and nitrites, have been associated with a higher risk (Bade and Dela Cruz, 2020).

The risk of developing lung cancer is also influenced by genetic predisposition. Different genes, including *TP53*, *ATM*, *TERT*, *SOD2,* have been hypothesized to play a role. Other genes determine the susceptibility to mutagens, like polymorphisms in DNA repair enzymes, including those involved in nucleotide excision repair and mismatch repair, as well as genes involved in inflammation or genes involved in apoptosis. All mentioned factors participate in the lung tumorigenic process (Bade and Dela Cruz, 2020).

Hints of lung anatomy and physiology

Lung cancer can originate from various cell types and different areas of the lung. The lungs are localized into the chest cavity and are mainly deputed to gas exchange between air and blood. The lungs consist of lobes (three in the right lung and two in the left lung) and an airway network. The latter includes the bronchi, arising from the trachea, bronchioles, and alveoli in the distal part. Each structure has a peculiar function and organization (Sainz de Aja et al., 2021; Seguin et al., 2022). Bronchioles are composed of basal cells, bronchioalveolar stem (BASC), club (or Clara cells), goblet, and ciliated cells. The latter represents the most differentiated cells in the lung. Instead, alveoli are lined by rare Clara cells and by alveolar type 1 and 2 cells (also called type I and II pneumocytes), which are involved in gas exchange and production of pulmonary surfactant, respectively (Seguin et al., 2022).

Tumorigenesis

Lung stem cells are involved in the regeneration of the lung throughout life. Similar mechanisms are also activated to overcome tissue injury. However, exposure to risk factors and genetic susceptibility can result in abnormal activation of specific pathways and deregulation of cellular functions, due to DNA double-strand breaks, mutational events, and generation of an inflammatory environment. Long-term exposure to these events leads to the formation of premalignant lesions and of clonal patches, generally characterized by loss of heterozygosity, microsatellite instability, and gene mutations. The most common alterations involve tumor suppressor genes, such as *TP53* and *KEAP1*, or genes encoding receptor tyrosine kinases, such as *EGFR* (Herbst, 2008; Seguin et al., 2022). Additional events, as well as pressure from the tumor microenvironment, promote firstly, the formation of in situ lesions and, subsequently, disease progression (Figure 2).

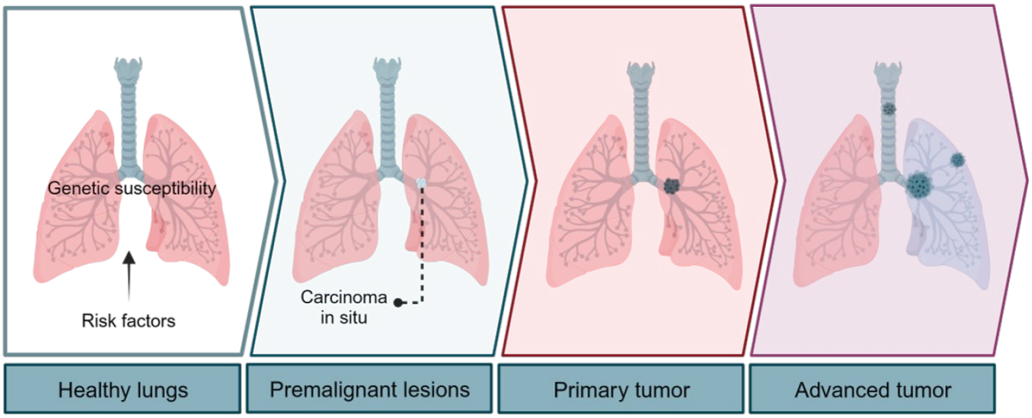

Figure 2. The image schematically represents tumor initiation process. The risk factor exposure (tobacco smoking, occupational carcinogens), together with genetic susceptibility (*TP53* mutations, alterations of tyrosine kinase pathways), determine the formation of premalignant lesions. Long-exposure to these factors initiates carcinogenesis process. Created with Biorender.com.

The early events responsible for lung tumorigenesis have been characterized by creating genetically engineered mouse models (GEMMs). GEMMs have been generated for *KRAS* or *EGFR* mutations (Ji et al., 2006; Herbst, 2008; Chen et al., 2014). However, cellular tumor initiation events and discrimination of driver and passenger mutations require further examination. In this context, patient-derived organoid generation may be useful.

Histological classification of lung cancer

Lung cancer is a heterogeneous disease. Histologically, NSCLC represents the main subtype, comprising 80-85% of cases, the remaining 10-15% of cases are classified as SCLC. The latter arises from small cells secreting hormones; instead, NSCLC generally originates from epithelial cells covering the respiratory tract or mucous-secreting cells. NSCLC is further divided into three different subtypes. Among these, adenocarcinoma (ADC) is the main histological subtype (more than 50% of cases), followed by squamous cell carcinoma (SCC, about 40% of cases), and large cell carcinoma (LCC, 10% of cases). Lung ADCs are generally located in the lung periphery and arise from club cells (a type of bronchiolar epithelial cells) and epithelial type 2 alveolar cells (Figure 3). ADC is the predominant subtype in never-smokers and women (Chen et al., 2014; Schabath and Cote, 2019). Based on histological growth patterns,

lung ADCs are subdivided into lepidic, acinar, papillary, micropapillary, and solid. The lepidic form corresponds to a non-invasive tumor with a good prognosis. An intermediate grade of risk is associated with acinar and papillary forms. The first is characterized by glands with round or oval forms. The papillary pattern is characterized by a fibrovascular structure surrounding neoplastic cells. The micropapillary and solid patterns are characterized by different morphology: detached and without fibrovascular structure the first subtype and enriched with polygonal cells and without gland the second, but both are associated with poor prognosis (Pal et al., 2018). ADCs are usually characterized by distal localization and by the expression of markers coherent with glandular histology, including thyroid transcription factor 1 (TTF1), keratin 7 (KRT7), and napsin A (Chen et al., 2014; Pal et al., 2018). SCCs often originate from the proximal airways and are distinguished by squamous differentiation. The expression of cytokeratin 5, cytokeratin 6 (KRT5/6), the transcription factors SRY-box 2 (SOX2), p40 and/or p63 are commonly used for its immunohistochemical characterization (Figure 4). Based on these features, it has been hypothesized that basal cells give rise to SCC tumors (Figure 3). In the last forty years, the diagnosis of SCC has been in decline due to reduced smoking exposure, which represents the prevalent risk factor for this tumor. NSCLCs without glandular or squamous features are classified as LCC (Chen et al., 2014; Pal et al., 2018). Histological classification is crucial for diagnosis and therapy, but it is inadequate to describe differences in patient progression and response to therapy by itself.

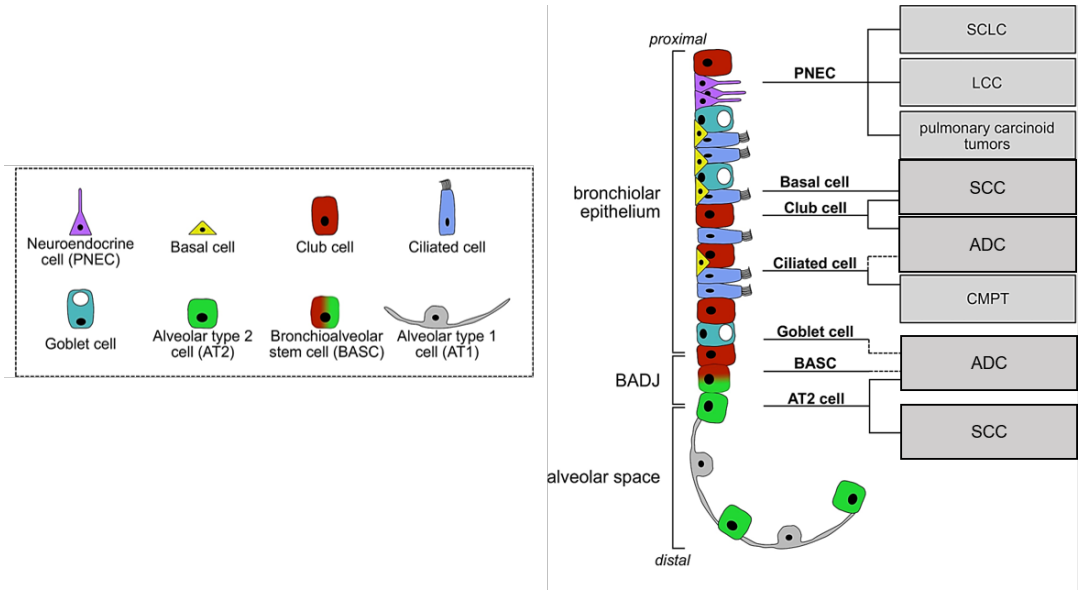

Figure 3. The image shows the origin of lung tumor subtypes from epithelial cells in lungs. ADCs arise from club cells and alveolar epithelial type 2 cells. SCCs originate from basal cells. Modified from Sainz de Aja et al., 2021.

Molecular classification of lung cancer

The diversity observed in lung cancer cases has required a more in-depth understanding of the disease. Specifically, analysis of NSCLC has highlighted a high heterogeneity at the molecular level. The mutational rate is higher in smokers compared to non-smokers, and the mutation spectrum is also different (Imielinski et al., 2012; Testa et al., 2018). Some genes are frequently mutated in NSCLC, including *KRAS*, *EGFR, BRAF*, *ALK*, *ROS1*, and *MET*. Mutations are also common in *PIK3CA*, and *ERBB2 (HER2),* as well as in the tumor suppressor genes *TP53*, *STK11*, *KEAP1*, *NF1*, *RB1*, and *CDKN2A*. Alterations are also described in chromatin-modifying genes, such as *SETD2, ARID1A*, and *SMARCA4* (Cancer Genome Atlas Research Network, 2014; Testa et al., 2018). Differences in the mutation spectrum are influenced by histological subtypes, gender, and ethnical origins.

Lung ADC has been frequently associated with alterations in oncogenes, including *KRAS, EGFR, ALK, ROS1, NRG1, NTRK1, HER2, MET*, and *RET* (Chen et al., 2014).

KRAS mutations account for 30% of lung ADCs and their presence is generally mutually exclusive with *EGFR* and *HER2* alterations. The mutations usually occur at codons 12 or 13 (rarely codon 61) and affect mostly Caucasian people (Herbst, 2008; Pal et al., 2018).

EGFR is located on chromosome 7 and encodes for a receptor tyrosine kinase. Mutations make its activity constitutive, thus sustaining differentiation, proliferation, and survival signals to cells. Alterations commonly occur between exons 18-21, with a higher incidence in tumors arising at younger age, in women, never-smokers, and Asian patients. Indeed, *EGFR* mutations account for about 15% of lung ADC samples, but their frequency reaches 50% in Asian people (Pal et al., 2018; Testa et al., 2018)

Another tyrosine kinase receptor mutated in ADC samples is *ALK*. Its sequence is commonly subjected to breakpoints in exons 19 or 20 of the gene, which is located on chromosome 2, and a subsequent rearrangement with specific gene partners, the most frequent of which is *EML4*. The resulting fusion protein is characterized by constitutive tyrosine kinase activity, transmitting proliferation and survival signals (Testa et al., 2018). *ALK* rearrangements affect about 5% of ADC cases and they are prevalent in patients of younger ages, females, and non-smokers, similar to EGFR mutations (Rodriguez-Canales et al., 2016).

ROS1 is a member of the insulin receptor family, encoded by a gene localized on chromosome 6. Rearrangement of *ROS1* is structurally similar to ALK rearrangements, since the fusion product maintains the tyrosine kinase domain. ROS1 rearrangements represent 1-2% of NSCLC cases. The most common fusion product is CD74-ROS1 (Pal et al., 2018).

Alterations in other oncogenes include: *MET* amplification or splicing mutation in exon 14, which occur in ADCs at advanced stages, as a resistance mechanism to therapy with tyrosine kinase inhibitors; *BRAF* mutations, which affect 4% of NSCLC cases; rearrangements in the *RET* gene or mutations in *NTRK1*.

Fewer oncogenes are mutated in SCC tumors, and mutations are enriched in genes like *DDR2, PI3KCA,* and *PTEN* (Chen et al., 2014).

Identifying driver mutations is crucial to determine the biological processes involved in the initiation of cell transformation and to provide indications for targeted therapy.

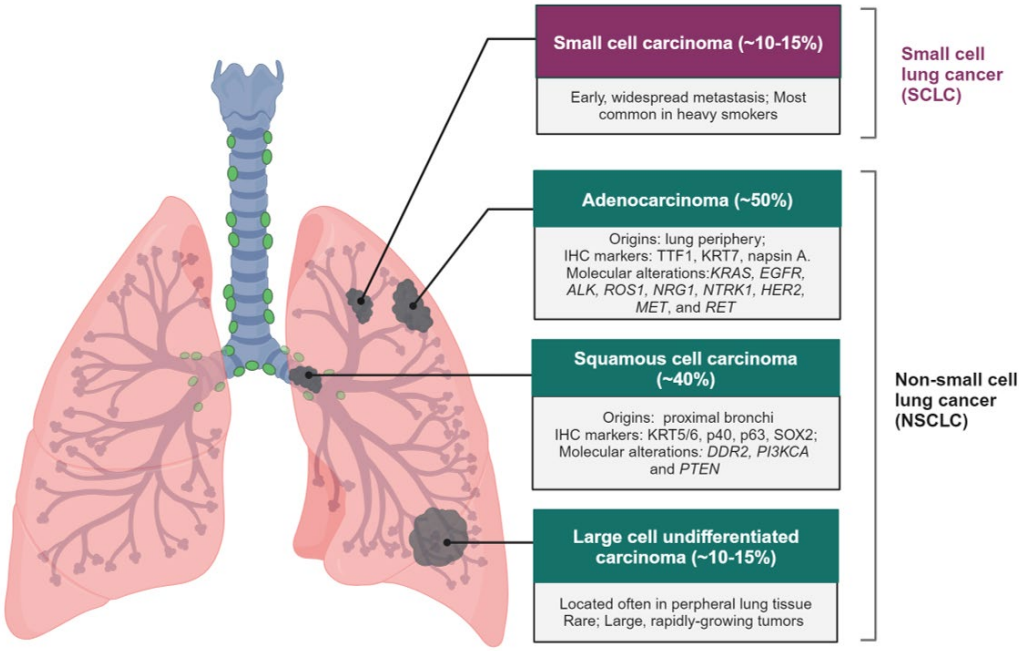

Figure 4. The image shows the histological subtypes of lung cancer and their molecular features. Created with Biorender.com.

Diagnosis of lung cancer

One of the major problems associated with lung cancer and its poor prognosis is that diagnosis often occurs when the tumor becomes symptomatic, at the late stage of the disease.

Following the analysis of medical history, laboratory tests, and physical exams, the key step in lung cancer diagnosis is represented by imaging, mainly chest radiography and computed tomography scans. The latter is used to define the stage of the tumor. In addition, also other techniques such as magnetic resonance can be used (Jantus-Lewintre et al., 2012). To confirm the suspect, a biopsy can be performed (Nooreldeen et al., 2021). The type of biopsy (such as thoracoscopy, or bronchoscopy) is selected based on tumor localization, growth pattern and metastasis presence. The obtained tissue samples are used for immunohistochemistry and/or molecular analysis, to

respectively characterize the type of tumor and detect alterations at genes or chromosome levels, useful for prognosis and/or to adopt the best therapeutic strategy (Rodriguez-Canales et al., 2016). As a rule, the mutation status of *EGFR*, *BRAF*, *ALK*, *ROS1*, *NTRK1, 2*, and *3* are characterized. Moreover, PD-L1 expression is also verified to evaluate the eligibility for immunotherapy treatment. Recently, liquid biopsy, including analysis of circulating tumor cells and circulating tumor DNA, has become a useful non-invasive tool for the early detection and progression analysis of the disease, as well as for assessing the onset of resistance to therapy based on tumor-derived cells or nucleic acids circulating in the blood or present in other biofluids (Pal et al., 2018; Nooreldeen et al., 2021).

Lung cancer treatment

Cancer cells can spread to nearby tissues and through lymph nodes and blood reach distant organs. Based on this consideration, lung cancer is classified using the TNM system, in which three parameters are considered: the extension of the primary tumor (T), the involvement of lymph nodes (N) and the presence of metastasis (M). This type of classification permits a better definition of prognosis and treatment (Nooreldeen et al., 2021; AIOM, 2021). The standard therapy for lung neoplasia at early stages (stages I, II, and in some cases stage III) is represented by surgical resection of the tissue. In addition, adjuvant chemotherapy (cisplatin-based) or radiotherapy can be administered to avoid the permanence of transformed cells in the body.

Tumors at locally advanced stages (stage II and IIIa) are treated with chemotherapy or radiotherapy. Instead, tumors at advanced-stages (stage IIIB, IIIC and IV) require molecular characterization to detect driver mutations treatable with targeted therapies. Two types of targeted therapy are mainly used: monoclonal antibodies and Tyrosine-Kinase Inhibitors (TKIs). Monoclonal antibodies bind to a specific target on cancer cells and then determine its killing. Antibodies against VEGF or EGFR have been developed in this way. TKIs are small molecules able to cross cell membranes and block proliferation signals in cancer cells. TKIs targeting EGFR-activating mutations have been developed for this purpose. The first generation of EGFR-targeted therapies,

gefitinib and erlotinib, are two competitive inhibitors for ATP binding to the kinase domain. The onset of resistance mechanism required the development of novel irreversible inhibitors (second-generation inhibitors, such as afatinib) and then third-generation inhibitors (osimertinib) able to target the canonical EGFR mutations and the resistance mutations (Eck and Yun, 2010). Similarly, other TKIs targeting different oncogenes, like ALK and ROS1 inhibitors, are approved for the treatment of lung cancer.

In some instances, patients with NSCLC can benefit from immunotherapy, exploiting the use of immune checkpoint inhibitors, like those directed against PD-1, PD-L1 (PD-1 ligand) and/or CTLA-4, that target inhibitor receptors on the surface of T cells. Treatment with anti-PD1 is approved as the first-line treatment in patients expressing PD-1 more than 50%, while anti-PD-L1 was approved as the second line of treatment in patients with advanced-stage tumors (Rodriguez-Canales et al., 2016). This without oncogene activation (most SCC cases).

There have been important advancements in lung cancer treatment, but the heterogeneity of lung cancer and the onset of resistance mechanisms limit the benefits of novel strategy treatments. The molecular characterization of the patients and the identification of novel targets and biomarkers of therapy response can further improve the patients' survival (Testa et al., 2018).

EPIDERMAL GROWTH FACTOR RECEPTOR (EGFR)

Most NSCLC cases (about 85%) express the Epidermal Growth Factor Receptor (EGFR) (Gately et al., 2012). EGFR is a member of the Erb tyrosine kinase receptor family. This family includes four receptor glycoproteins, HER1 (EGFR/erbB1), HER2 (neu, erbB2), HER3 (erbB3), and HER4 (erbB4), that transduce extracellular signals into cells, by activating various signaling pathways.

The *EGFR* gene is located on chromosome 7p12, where also other genes involved in signal transduction (such as *MET* and *BRAF*) map. The *EGFR* gene is made up of 28 exons and 27 introns. The complete protein, of 170kDa, is encoded by mRNA transcript variant 1. Through gene alternative splicing, eight variants are produced, including three soluble forms (sEGFRv2, sEGFRv3, and sEGFRv4). The full-length EGFR protein is composed of an extracellular domain, a transmembrane domain, a juxtamembrane domain, and an intracellular domain (Figure 5) (Jorissen et al., 2003; Yasuda et al., 2012; Kobayashi and Mitsudomi, 2016; Abou-Fayçal et al., 2017; Li et al., 2023). The extracellular domain is composed of four subdomains: L1 and L2 are responsible for ligand binding, while Cystein-Rich domains, CR1 and CR2, regulate ligand affinity and receptor dimerization (Yasuda et al., 2012; Abou-Fayçal et al., 2017). The intracellular domain comprises the tyrosine kinase domain, which includes an N-terminal lobe and a C-terminal lobe resides. Among them, the ATP binding site is located. In the monomeric receptor, the rotation of the C-lobe towards the ATP binding site is prevented. In the C-terminal domain tyrosine residues, whose phosphorylation regulates the EGFR transduction signaling, are located, together with serine and threonine residues, whose phosphorylation mediates EGFR downregulation (Jorissen et al., 2003; Li et al., 2023).

Different ligands mediate EGFR activation, among which are EGF, amphiregulin, and TGFα (Jorge et al., 2014). Ligand binding shifts a C-lobe of one EGFR monomer close to the N-lobe of a second monomer, resulting in EGFR homo- or hetero-dimerization. EGFR receptors are also present on the membrane as dimers (Jorissen et al., 2003). The ligand-mediated conformational change results in an active kinase domain, that

triggers the transfer of γ-phosphate from ATP to the C-terminal tyrosine residues. The autophosphorylation of the receptor activates downstream signaling pathways, resulting in cellular proliferation and anti-apoptotic signals (Yasuda et al., 2012).

The physiological role of EGFR was elucidated by loss of function experiments. In mice, the role of EGFR in epithelial cell physiology has been shown by receptor knockdown. EGFR depletion determined severe effects on the development of several organs, including skin, lungs, gastrointestinal tract, brain, and liver, together with hair follicle alterations. The reduced availability of EGF affected the size and thickness of the mammary gland and epidermis (Okamoto and Oka, 1984; Tsutsumi et al., 1987; Threadgill et al., 1995; Jorissen et al., 2003). On the other side, overexpression of EGFR or its ligands is associated with tumorigenesis (Jorissen et al., 2003).

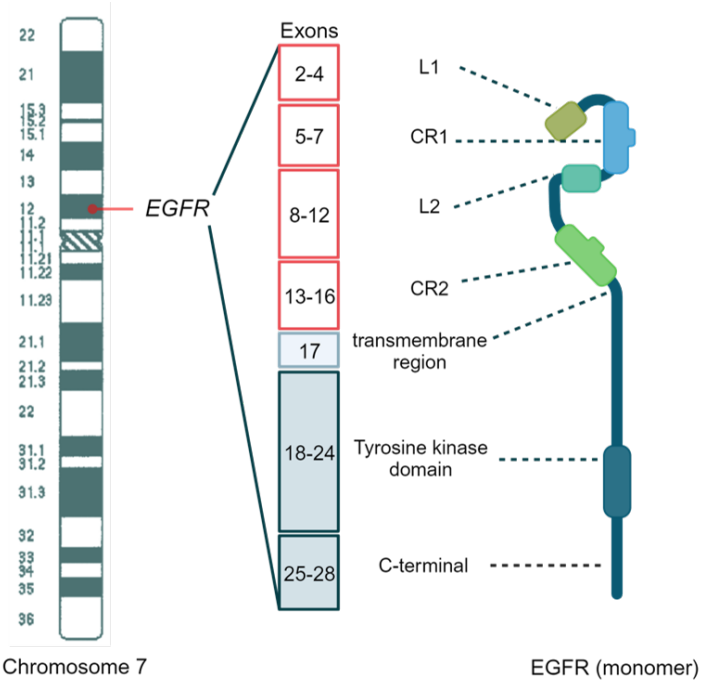

Figure 5. Schematic representation of chromosome 7 and *EGFR* gene. The figure display exons encoding EGFR domains: Ligand binding domain 1 (L1), Cysteine-Rich domain (CR1), L2, CR2, transmembrane domain, tyrosine kinase domain and C-terminal domain. The chromosome 7 ideogram was modified from Lamb et al. 2000. Created with Biorender.com.

Activating *EGFR* mutations

The crucial role of EGFR in cancer was revealed through the identification of its somatic mutations that responded favorably to first-generation TKI inhibitors. This breakthrough discovery highlighted the potential for targeted therapies in oncogene-addicted cancer (Lynch et al., 2004; Paez et al., 2004; Pao et al., 2004; Greulich et al., 2005).

EGFR alterations are typically found in exons 18-21 (Figure 6), which encode for the tyrosine kinase domain. These alterations promote EGFR activation independently of ligands. The most common EGFR mutations involve the deletion of 15 nucleotides within exon 19 (c.2235_2249del), whose consequence is the lack of five amino acids (p.E746-A750del) in the protein and accounts for approximately 45% of all *EGFR* mutations. Equally frequent (40% of *EGFR* mutations) is the exon 21 missense mutation (c.2573T>G), which determines the substitution of a leucine with an arginine residue (p.L858R). Less frequent *EGFR* alterations are an in-frame insertion in exon 20, which accounts for about 5% of all mutations (Yasuda et al., 2012), point mutations in exon 18 at the glycine 719 residue (G719C/S/A, 3% of *EGFR* mutations), the L861Q missense mutation, located in exon 21 (2% of *EGFR* mutations), and in-frame insertions within exon 19 (less than 1% of *EGFR* mutations) (Jorge et al., 2014). All alterations are present in heterozygosity, as only one mutated allele is sufficient for an oncogenic effect.

EGFR mutations are near the ATP binding site. Specifically, the exon 19 deletions are near the C-helix, while the L858R point mutation affects the activation loop. These alterations affect the receptor's affinity for binding with ATP, thereby leading to its activation. The localization of the activating mutations makes them susceptible to the first generation of EGFR inhibitors (gefitinib and erlotinib). The latter are reversible competitive inhibitors with ATP for the binding at lysine 745 (Pao et al., 2004). However, the different ATP affinity among the mutations influences the rate of response to EGFR inhibitors (Lynch et al., 2004; Kancha et al., 2009) Indeed, in-frame deletions at exon 19 are more sensitive compared to the mutation in exon 21, whereas exon 20 insertions

are the least sensitive to EGFR competitive inhibitors (Greulich et al., 2005; Kancha et al., 2009; Da Cunha Santos et al., 2011; Yasuda et al., 2012).

The variability in response to TKIs among activating mutations can be explained by various downstream signals that can be activated. In 2004, Sordella et al. showed that the two most common EGFR variants (p.E746-A750del and p.L858R) are characterized by a peculiar tyrosine phosphorylation pattern in the C-terminal domain. Indeed, these mutations cause increased phosphorylation of tyrosine residues Y992 and Y1068 compared to the wild-type form. In addition, the L858R missense mutation is associated with phosphorylation at residue Y845. The phosphorylation of a specific tyrosine residue activates distinct downstream signals. Phosphorylation at Y845 is associated with STATs signaling, phosphorylation at Y992 is correlated with PLCγ and Shc activation, while phosphorylation of Y1068 is related to the activation of different adaptor proteins, leading to STAT3/5 and/or AKT-mediated signals (Sordella et al., 2004; Amann et al., 2005). Thus, wild-type or mutant EGFR variably activate the different downstream signaling pathways, leading to varying effects on cell survival and response to therapy.

Other *EGFR* mutations, including the point mutations p.T790M and p.C797S, within exon 20, have been shown to have a central role during the onset of resistance to the EGFR-TKIs (Da Cunha Santos et al., 2011; Du et al., 2020)

The substitution of threonine with methionine at codon 790 (p.T790M) leads to increased affinity for ATP binding, causing decreased responsiveness to first- and second-line EGFR inhibitors and accounting for about 50-60% of resistance mechanisms to these inhibitors. It has been shown that the T790M mutation occurs in the same allele of the two most frequent activating mutations (p.E746-A750del and p.L858R) (Da Cunha Santos et al., 2011; Hidaka et al., 2017). The T790M mutation is present prior to EGFR therapy in a small number of cancer cells (Fujita et al., 2012; Li et al., 2014; Watanabe et al., 2015), but it can also emerge during the EGFR-targeted therapy (Hata et al., 2016; Ramirez et al., 2016).

The substitution of cysteine with serine at codon 797 is responsible for 10-26% of acquired resistance to third-line EGFR inhibitors. Indeed, the mutation at codon 797 makes the binding of osimertinib in correspondence with the ATP binding site ineffective (Hidaka et al., 2017; Li et al., 2023).

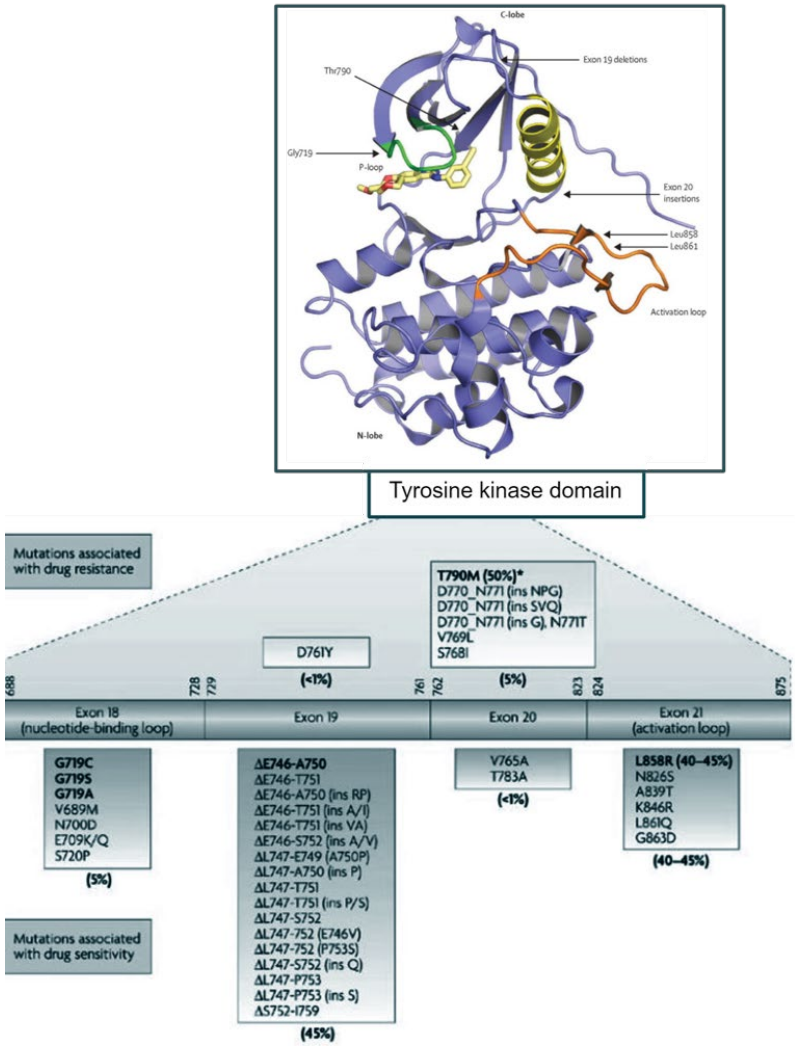

Figure 6. The figure displays the EGFR tyrosine kinase domain with erlotinib and major activating mutations (in the top). The most common EGFR mutations, exon localization, and TKIs sensitivity are shown at the bottom. Modified from Sharma et al., 2007 and Yasuda et al., 2012. Created with Biorender.com.

Moreover, other membrane receptors promote EGFR downstream signaling pathways and thus the survival of tumor cells, thereby bypassing the EGFR activation and limiting

the inhibitory effects of EGFR inhibitors. The amplification of *MET* and *IGFR1* are recognized actors of bypass mechanisms (Da Cunha Santos et al., 2011; Jorge et al., 2014; Du et al., 2021). Other factors can also influence aberrant activation of the EGFR in the tumor, including the high expression of other Erb receptor members, *EGFR* amplification, and/or its altered turnover (Amann et al., 2005; Okabe et al., 2007). The consequences of EGFR activation are determined by the downstream activated pathways.

Signaling pathways downstream of EGFR

EGFR activation recruits adaptor proteins via SH2 or PTB domains, and indirectly activates multiple proteins, serving as docking sites for heterodimers. These events trigger different downstream pathways, often interconnected among themselves. The PI3K-AKT-mTOR and RAS-RAF-MEK-ERK/MAPK pathways, along with the IL6-JAK1/2-STAT3 pathway, are predominantly involved (Figure 7) (Tsiambas et al., 2015). Phosphorylation of EGFR at Y1068 and Y1086 residues determines the recruitment of Grb2/Sos complex to the C-terminal domain. Alternatively, the phosphorylation of Shc tyrosine kinase can also determine the docking site formation for Grb2 recruitment. This event favors Ras and Sos interaction, resulting in GDP/GTP exchange and Ras activation. Consequently, Raf-1, a serine/threonine kinase, MEK and Erk1 and Erk2 are activated, resulting in the activation of several transcription factors (including MYC, NF-KB, c-FOS), involved in the expression of cell-cycle related genes (Jorissen et al., 2003; Li et al., 2023). In addition to Grb2, other proteins involved in cytoskeletal organization, as well as PI3K, are recruited by Shc kinase (Jorissen et al., 2003).

One of the main EGFR downstream pathways includes the activation of the Signal Transducer and Activator of Transcription (STAT) proteins. The STAT protein family of transcription factors consists of seven members (STAT1, STAT2, STAT3, STAT4, STAT5a, STAT5b, and STAT6) involved in many physiological processes, that transmit the extracellular signals to the nucleus. The members of this protein family share a common structural organization, in which the SH2 domain determines the binding to

cytokine receptors (Jorissen et al., 2003; Johnson et al., 2018, Tolomeo et al., 2020, Wang et al., 2022).

Three STAT members, STAT1, STAT3, and STAT5a, are activated by EGFR. EGFR triggers STATs signals via JAK kinase proteins. Alternatively, Src kinase has also been demonstrated to regulate STATs signaling. STATs activation is the mechanism by which EGFR regulates cell proliferation and apoptosis (Jorissen et al., 2003; Li et al., 2023).

EGFR also regulates lipid metabolism, as demonstrated by its effect on phospholipase C-γ (PLCγ), phosphatidylinositol-3-kinase (PI3K), and phospholipase D (PLD). The C-terminal phosphorylation of EGFR at Y992 and Y1173 acts as docking sites for PLCγ, whose activation determines the production of 1,2-diacylglycerol (DAG) and inositol 1,3,5-trisphosphate (IP3). The first molecule modulates the serine/threonine kinase PKC, acting as a cofactor, while IP3 regulates calcium-related signaling, promoting calcium release from intracellular stores.

PI3K is modulated by EGFR directly or via Src activation. PI3K, via phosphatidylinositol-3,4,5-trisphosphate (PIP3), triggers the serine/threonine kinase AKT and consequently, mTOR activation, leading to cell cycle progression (Jorissen et al., 2003; Li et al., 2023).

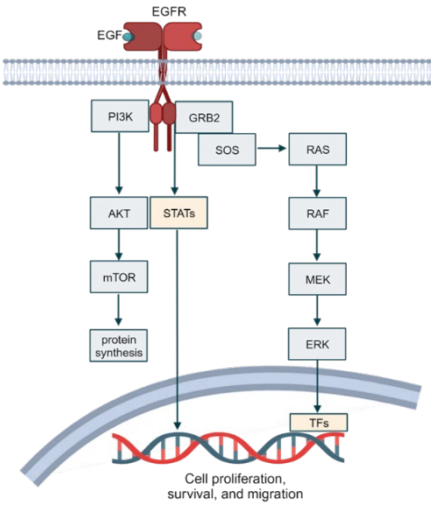

Figure 7. Schematic representation of EGFR downstream signals. The PI3K-AKT-mTOR, RAS-RAF-MEK-ERK/MAPK pathways, and the IL-6-JAK1/2-STAT3 pathway, are predominantly activated by EGFR. Created with Biorender.com.

Signal Transducer and Activator of Transcription 3 (STAT3)

STAT3, a member of the STAT family, is involved in many physiological processes. It transmits the extracellular signals to the nuclei. It is characterized by several domains, including an N-terminal domain, a coiled-coil, a DNA binding domain, a linker, a SH2 domain, and a C-terminal domain. The N-terminal domain mediates the interactions between STAT3 dimers and other proteins, the coiled-coil domain is involved in the STAT3 recruitment to a receptor and its phosphorylation. The DNA binding domain recognizes the consensus sequences into the promoter of its target genes, the SH2 domain has a critical role in STAT3 dimerization, and finally, a C-terminal domain, highly conserved, that functions as the transactivation domain, and includes the residues that, once phosphorylated, promote its transcriptional activity (Figure 8) (Johnson et al., 2018, Tolomeo et al., 2020; Wang et al., 2022).

Figure 8. Schematic representation of STAT3 structure. It consists of seven domains: N-terminal, coiled-coil, DNA binding, linker, SH2, and C-terminal. Here, the localization of two main post-translational modifications, phosphorylation on tyrosine 705 (pY705) and serine (pS727), are shown. From Parakh et al., 2021.

Abnormal activation of STAT3 has been correlated to different pathologies, such as inflammatory and autoimmune diseases and cancers (Yu et al., 2014).

STAT3 activation is mediated by different stimuli. Multiple cytokines are implicated in STAT3 activation: the IL-6 cytokine family, which includes interleukin-6 (IL-6), IL-11, and leukemia inhibitory factor (LIF), but also the IL-10 family (IL-10, IL-22, IL-26) and the IL-12 family (IL-12, IL-23, IL-27, IL-35). There are two main routes of STAT3 activation.

In the classical route, the formation of complexes between cytokines and their receptors determines a conformational change that triggers the activity of their associated tyrosine kinases, mostly belonging to the JAK protein family. The latter phosphorylates the intracellular domain of the β-subunit of the IL-6 receptor (gp130), which permits the binding of the SH2 domain of the STAT3 protein and the

phosphorylation of STAT3 on the tyrosine 705 residue. This event causes the formation of homo- or hetero-dimers of STAT3 and the subsequent translocation into the nucleus by importin-1, where the transcription factors recognize their binding sequence on gene targets. Alternatively, the activation of STAT3 occurs in cells that do not express intramembrane IL-6R but the soluble IL-6 receptor (sIL-6R), generated by alternative splicing of IL-6R mRNA or by its shedding mediated by different members of disintegrin and metalloprotease domain-containing protein 17 (ADAM10 and ADAM17). Indeed, the binding of IL-6/sIL-6R to the gp130 determines the dimerization of β-subunits and the activation of JAK kinase, as described for the classical pathway (Johnson et al., 2018, Huynh et al., 2019; Tosic et al., 2021).

Other stimuli also mediate STAT3 activation: G-protein coupled receptors phosphorylate STAT3 via JAKs proteins, instead, growth factor receptors, like EGFR, the fibroblast growth factor receptor (FGFR), and platelet-derived growth factor receptors (PDGFR) can activate STAT3 via JAK signaling or by direct phosphorylation of the SH2 domain of STAT3 molecules (Yu et al., 2014; Huynh et al., 2019; Wang et al., 2022). In addition, non-receptor protein kinases (like the Src kinase family or ABL) can also activate STAT3 (Huynh et al., 2019, Wang et al., 2022).

In physiological conditions, STAT3 is only transiently activated, due to the action of its negative regulators. Among these, protein tyrosine phosphatases bind active STAT3 and mediate its dephosphorylation. This family includes PTP receptor-type D (PTPRD), PTP receptor-type T (PTPRT), PTP receptor-type K (PTPRK), SH2-domain-containing PTP1 (SHP1), SHP2. The binding STAT3-DNA is instead also blocked by the protein inhibitor of activated STAT (also known as PIAS protein). A critical role in STAT3 negative regulation is determined by the Suppressor of Cytokine Signaling (SOCS) proteins, a family of eight proteins, which binding JAKs protein kinases to prevent phosphorylation or recruitment of STAT3 (Huynh et al., 2019, Wang et al., 2022).

Finally, microRNA and lncRNA have been involved in STAT3 signaling regulation, for example, miR-24 and miR-629 positively regulate STAT3 (Yu et al., 2014; Wang et al., 2022).

PROLINE METABOLISM

Oncogenic mutations trigger the metabolic reprogramming of cancer cells to survive and proliferate (Pavlova and Thompson, 2016). In this context, the role of non-essential amino acids, including L-proline, has been largely demonstrated (Phang et al., 2015).

L-proline has various physiological roles, including nutrient adaptation, stress protection, osmotic regulation, and cellular signaling. It also plays a role in pathological conditions such as neuropsychiatric disorders, aging, and tumor initiation and progression (Phang et al., 2008; Tanner, 2019; Bergers and Fendt, 2021).

L-proline is a proteinogenic secondary amino acid, characterized by an imino-group in a pyrrolidine ring. Because of its peculiar structure, a distinctive set of enzymes is required for L-proline metabolism (Figure 9) (Cappelletti et al., 2018; Tanner et al., 2018).

Dietary proteins are the source of L-proline. Moreover, this amino acid is synthesized endogenously from glutamate or ornithine (Phang et al., 2010; Cappelletti et al., 2018; Tanner et al., 2018).

To produce L-proline, a phosphoryl group from ATP is transferred to L-glutamate, by Glutamate 5-kinase (G5K, EC 2.7.2.11). Consequently, L-glutamate 5-phosphate is reduced to L-glutamate-γ-semialdehyde (GSAL) by γ-glutamate phosphate reductase (γ-GPR, EC 1.2.1.41) in a NADPH-dependent reaction. These two enzymes in higher organisms (plants and animals) are fused to form the P5C synthase (P5CS) enzyme.

Ornithine δ-amino acid transferase (OAT) catalyzes the conversion of ornithine into GSAL (Tanner et al., 2018; Tanner, 2019).

In both biosynthetic routes, the spontaneous removal of a water molecule provides Δ-pyrroline-5-carboxylate (P5C). Finally, the NAD(P)H-dependent P5C reductase (P5CR, EC 1.5.1.2), known as PYCR in humans, reduces the P5C substrate to proline (Tanner et al., 2018; Tanner, 2019; Phang, 2019).

Three PYCR isoforms have been described in humans, with different subcellular localization: PYCR1 and PYCR2 catalyze the reduction of P5C in mitochondria, using

NADH as a reducing equivalent, while PYCR3 reduces P5C in the cytosol in an NADPH-dependent reaction (Bogner et al., 2021).

Alternatively, the breakdown of the extracellular matrix provides the imino acid (Cappelletti et al., 2018; Phang et al., 2010; Tanner et al., 2018).

L-proline is catabolized in the mitochondria by the sequential activity of two enzymes, proline dehydrogenase (PRODH, EC 1.5.5.2) and GSAL dehydrogenase (GSALDH EC 1.2.1.88). PRODH, localized at the inner mitochondrial membrane, mediates the rate-limiting oxidation of proline to P5C. GSAL is obtained by spontaneous hydrolysis of P5C. GSALDH localized in the mitochondrial matrix, oxidases GSAL to glutamate using NAD as a cofactor.

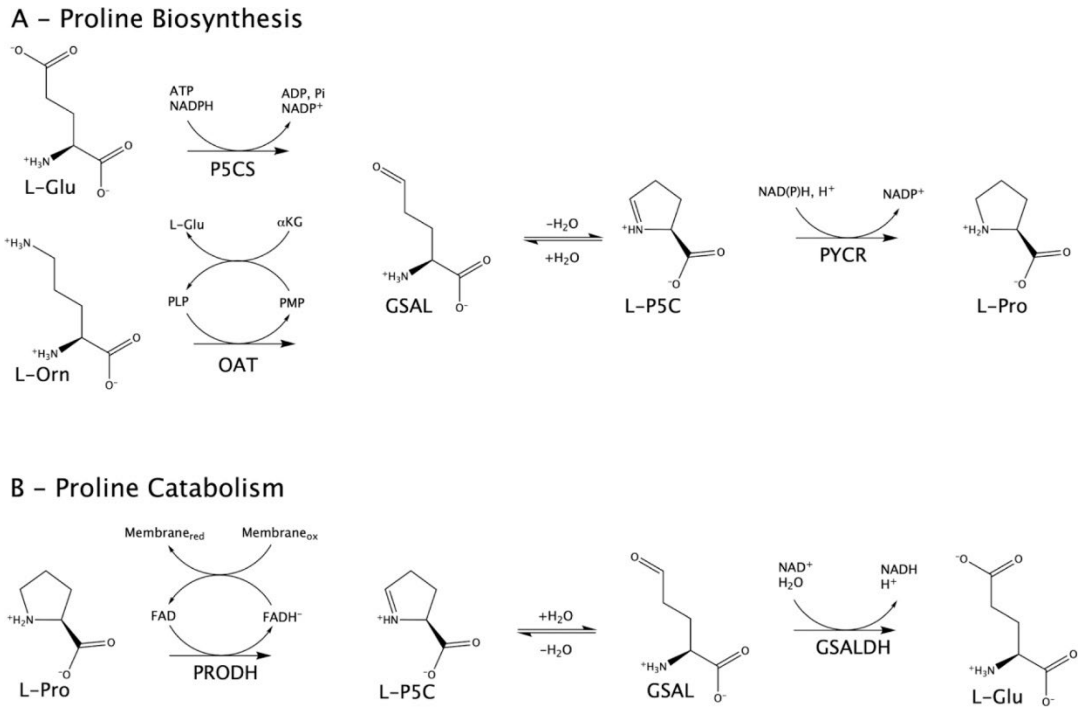

Figure 9. The image shows the distinctive set of enzymes involved in L-proline metabolism. L-proline is synthetized from L-glutamate, via P5CS, or ornithine, through OAT. In both biosynthetic ways, P5C is generated by spontaneous removal of a water molecule. Finally, the PYCR enzyme reduces the P5C substrate to proline. L-proline is catabolized by two mitochondrial enzymes: PRODH and GSALDH (Bogner et al., 2021).

The intermediate P5C is simultaneously the precursor, but also the product of proline metabolism (Phang et al., 2008).

Proline cycle

The interconversion between P5C and proline is known as the proline cycle. It occurs among two cellular compartments: cytosol, and mitochondria (Liu and Phang, 2012; Tanner et al., 2018). The cycle consists of the biosynthetic reaction, in which the cytosolic PYCR enzyme reduces P5C to proline, oxidizing the NADH/NADPH cofactors. Therefore, the availability of $NAD(P)^+$ activates the pentose phosphate pathway, resulting in ribose production and nucleotide synthesis. Moreover, the obtained reducing equivalents are translocated into the electron transport chain to produce ATP (Liu and Phang, 2012; Burke et al., 2020; Bogner et al., 2021). Proline degradation represents the second half of the proline cycle. The mitochondrial PRODH enzyme oxidizes proline to P5C, generating two electrons. These are transferred to the mitochondrial electron transport chain, producing ATP, or ROS species (Figure 10) (Phang et al., 2008; Liu et al., 2012).

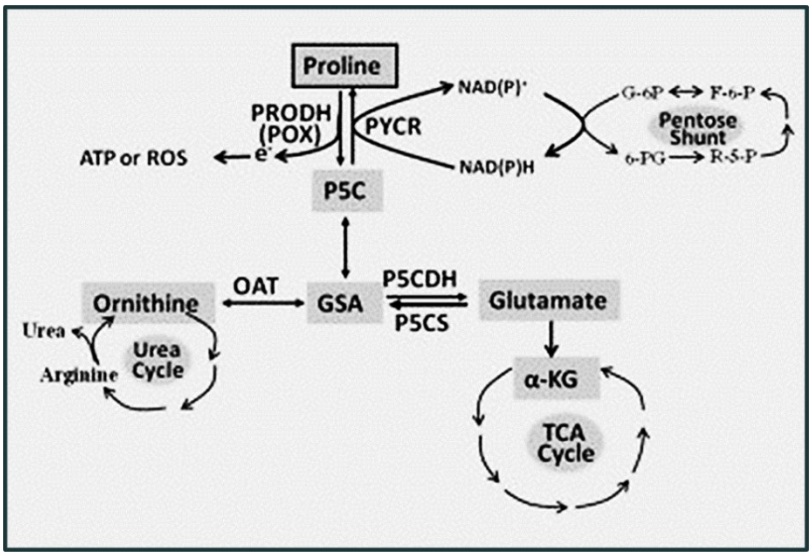

Figure 10. A simplified representation of the proline cycle is shown. In the cytoplasm, PYCR reduces P5C to proline, oxidizing the NADH/NADPH. The second half cycle is catalyzed by PRODH in the mitochondria. Two electrons are generated by proline oxidation, that can be used to produce ATP, or ROS species. P5C can be transformed to then to α-ketoglutarate (α-KG), or into ornithine. Proline metabolism is interconnected to the pentose phosphate pathway, pyrimidine nucleotide synthesis, TCA and urea cycle (Liu and Phang, 2012).

Therefore, proline metabolism is interconnected to the pentose phosphate pathway and pyrimidine nucleotide synthesis. It is linked to cellular bioenergetics and modulates signal transmission via ROS production (Bogner and Tanner, 2022). Moreover, it can originate glutamate in glutamatergic neurons assuming a role in neurotransmission (Bender et al., 2005).

The involvement of the proline cycle in various physiological and pathological conditions underscores its multifaceted role. Alteration in proline metabolism has been associated to cancer progression (Elia et al., 2017). Furthermore, dysregulation in proline metabolism has been associated with neurodisorders. Specifically, hyperprolinemia type I, caused by PRODH deficiency, has been associated with cognitive impairment and developmental delay, and schizophrenia (Willis et al., 2008), likely due to its interconnection with glutamate and glutamatergic transmission.

PRODH gene

Two genes have been annotated as *PRODH* in the human genome: *PRODH1* and the paralog *PRODH2*. They differ in chromosome localization and substrate preference. *PRODH1* is located on chromosome 22q11.21. It consists of 15 exons and encodes proline dehydrogenase (Campbell et al., 1997). Instead, *PRODH2*, encoding for hydroxyproline dehydrogenase, maps on chromosome 19q13.12 (Tanner et al., 2018).

Mutations *in PRODH1* have been associated with hyperprolinemia type 1 and neurodevelopmental disorders, including schizophrenia (Liu et al., 2001; Qin et al., 2021). The high rate of mutations often depends on gene conversion events with the *PRODH* pseudogene (*Ψ-PRODH*).

Ψ-PRODH maps telomeric of *PRODH* on chromosome 22q (Figure 11). It is characterized by 95% homology with *PRODH1*, from which it differs by the deletion of a region between exon 2 and part of exon 7 (Bender et al., 2005).

Hyperprolinemia type I is an autosomal recessive disorder, characterized by PRODH deficiency and higher levels of proline in serum (Willis et al., 2008). In the most serious cases, the disorder is associated with schizophrenia. High proline levels and increased risk of schizophrenia have also been found in patients with Di George syndrome, a

syndrome caused by a 3 Mb deletion in the chromosomal region 22q11.2, mediated by unequal crossing-over events between two low copy repeats containing *Ψ-PRODH* and *DGCR6-like* genes and *PRODH* and *DGCR6* (Karayiorgou and Gogos, 2004; Bender et al., 2005).

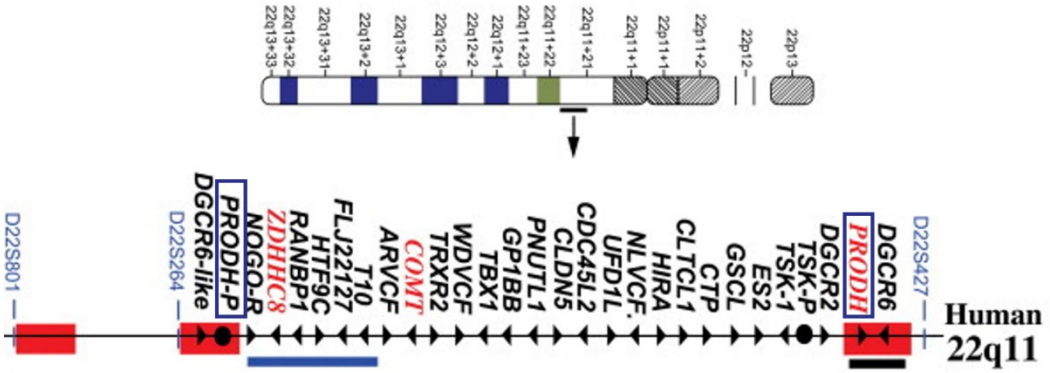

Figure 11. Schematic representation of the 22q11 chromosome region containing the *PRODH* gene and *its* pseudogene (*PRODH-P*)] (blue rectangle). The low-copy repeat sequences mediating unequal crossing-over events that give rise to the microdeletions responsible of the Di George syndrome are indicated in red boxes, and microsatellites are written in blue. Modified from Karayiorgou and Gogos, 2004.

To investigate the role of *PRODH* mutations, the activity of sixteen PRODH missense mutations was measured by Bender et al. (Bender et al., 2005). Four of sixteen mutations (R185Q, L289M, A455S, and A472T) showed less than 30% of catalytic activity reduction, six mutations (Q19P, A167V, R185W, D426N, V427M, and R431H) led to moderate reduction of the flavoenzyme activity, five missense mutations (P406L, L441P, R453C, T466M, and Q521E) determined more than 70% of reduction in PRODH activity, instead the Q521R mutation enhanced its activity (Bender et al., 2005). Regarding cancer, altered expression patterns, rather than missense mutations seem to be prevalent (TCGA data).

Regulation of *PRODH* expression

The *PRODH* gene is expressed in different organs, such as lungs, kidneys, skin, digestive tract, and brain. Different transcription factors regulate *PRODH* expression. Among these, the oncosuppressor p53 was the first identified. Because of that, *PRODH* is also known as *p53-induced gene 6* (*PIG6*) (Polyak et al., 1997). Indeed, Polyak et al. observed an increase in *PRODH* expression following overexpression of

p53 (Polyak et al., 1997). Subsequently, Maxwell et al. investigated the p53 binding on the *PRODH* promoter and identified a sequence -0,9kb upstream of the transcriptional start site (TSS) by Chromatin immunoprecipitation (ChIP) and electrophoretic mobility shift assays (Maxwell and Kochevar, 2008). In comparison to this, the binding of p53 to the intronic responsive elements (RE), in particular, the one located +6.8kb downstream of the TSS, has shown stronger *PRODH* induction . The same RE, located +6,8kb from the TSS, is transactivacted also by p63 and p73, the other members of the p53 family, as demonstrated by luciferase assays (Raimondi et al., 2013). This evidence underlines PRODH's role in response to various types of stress that activate p53, including genotoxic stress.

Other transcription factors are also involved in PRODH regulation. Peroxisome Proliferator-Activated Receptor gamma (PPARγ) is a hormone nuclear receptor, involved in the cellular response to different stimuli: primarily lipid metabolism, inflammation, and cell proliferation (Phang et al., 2012). An increase in *PRODH* expression was observed in HEK293 cells transfected with PPARγ. Promoter activation was also confirmed by the addition of troglitazone, a synthetic ligand of PPARγ. The actual binding of PPARγ to the *PRODH* promoter (between -982 and -969bp upstream of the TSS) was demonstrated by electrophoretic mobility shift and ChIP assays (Pandhare et al., 2006; Phang et al., 2010).

Adenosine Monophosphate-Activated Protein Kinase (AMPK) is an enzyme key in cellular energy homeostasis. It has been observed that this enzyme increases the expression and activity of PRODH during hypoxia and glucose deficiency. The mechanism through which AMPK regulates PRODH expression and activity is still unclear, but the involvement of the mammalian target-of-rapamycin (mTOR) pathway has been suggested (Pandhare et al., 2009; Liu et al., 2012).

On the other side, a putative binding site for the c-MYC transcription factor was found in the *PRODH* promoter. The transcription factor c-MYC plays a fundamental role in the regulation of various cellular processes, including cell growth, proliferation, differentiation, and apoptosis and it is often deregulated in cancer. Despite the evidence, direct binding of the transcription factor to *PRODH* was not demonstrated

by ChIP experiments. Instead, c-MYC downregulates PRODH by increasing miR-23b* expression (Liu et al., 2012). The correlation between PRODH expression and miR-23b* has been investigated among healthy and tumoral tissue in renal cancer. Indeed, the binding of miR-23b* to the PRODH 3'UTR was demonstrated (Liu et al., 2012).
Recently, promoter methylation was also shown to regulate PRODH expression. Switching off PRODH expression was demonstrated to have different prognostic consequences in young and old (>65 years of age) lung cancer patients (Chen et al., 2020).

PRODH: structure and function

In humans, the PRODH full-length sequence consists of 600 amino acids with a molecular mass of 68kDa. The N-terminal sequence determines its close association with the inner mitochondrial membrane (Bender et al., 2005). The eukaryotic structures of the flavin-dependent enzyme have not been characterized. However, PRODH sequence is highly conserved among several species (Liu et al., 2009). Hence, the information about PRODH structure has been obtained by homology studies with the crystal structures of the Proline Utilization A bifunctional enzyme (also known as PutA, in which PRODH and GSAL are fused in one enzyme) from *E. coli* and the monofunctional enzyme from *T. thermophilus* and *D. radiodurans* (Tanner, 2019). The crystal structure of PRODH revealed a catalytic core with $(\beta\alpha)_8$ barrel fold, that is maintained between residues 121 and 579 in humans (Figure 12). Two unknown structural inserts at 150-205 and 241-349 residues have emerged. However, the predicted human structure maintains other residues, including leucine 447, which is crucial for Flavin Adenin Dinucleotide (FAD) binding. In addition, the YXXRRXXE sequence with four conserved amino acids is also maintained within the α8 helix. This sequence is essential for substrate binding.

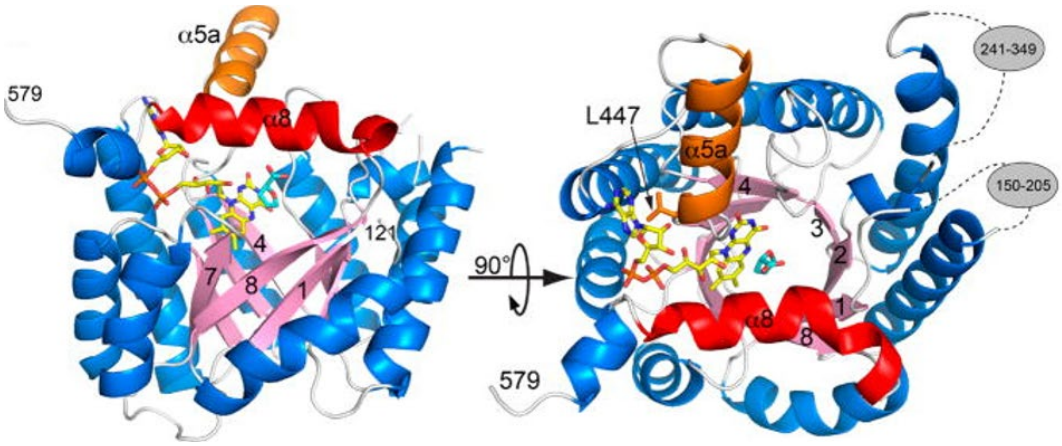

Figure 12. The structure of the human PRODH1 catalytic core was obtained by homology studies made with SWISS-MODEL. FAD is shown in yellow, L-THFA is colored in cyan, the α8 helix is colored in red, and the α5 helix is colored in orange. Uncertain residues are indicated in gray. Modified from Tanner et al., 2018.

In detail, the two arginine (R563 and R564) residues bind the proline carboxylate, the tyrosine residue (Y560) and a leucine residue (L527) interact with the proline ring. Finally, the glutamate residue stabilizes the substrate binding, by packing against R564. The essential residues for substrate binding were characterized in mono- and bifunctional PutA/PRODH enzyme, using an L-proline analog, L-tetrahydro-2-furoic acid (L-THFA) (Tanner et al., 2018; Tanner, 2019). Instead, the use of *N*-propargylglycine (*N*-PPG), a PRODH irreversible inhibitor, shed light on the conformational changes following the cofactor reduction (White et al., 2008; Tanner et al., 2018). In *S. cerevisiae*, PRODH catalyzes the oxidation of L-proline through a two-step ping-pong mechanism. The first step involves FAD reduction, followed by its oxidation by ubiquinone in the second step (Wanduragala et al., 2010).

PRODH converts proline into P5C while reducing its FAD cofactor. To restore its active state, two electrons are transferred to complex II of the mitochondrial electron transport chain. The proline-derived electrons are then transferred to cytochrome c, complex IV, and finally to oxygen. In this way, PRODH generates ATP to provide cell energy. Alternatively, at complex III electrons can reduce oxygen, generating ROS species (Phang, 2010; Phang, 2019). In addition, it has been proposed that FAD is accessible to oxygen to promote direct superoxide anion production (White et al., 2008).

The intermediate P5C can be transferred to the cytosol and recycled for proline synthesis, using reducing equivalents and oxidizing NADPH to NADP. This pathway supports the synthesis of pentoses, that can be used for nucleotide synthesis.
In the mitochondria, the intermediate P5C can be hydrolyzed to GSAL, oxidized to glutamate by P5CDH, and then to α-ketoglutarate, which links proline catabolism to the TCA cycle. Additionally, P5C can be transformed into ornithine and enter the urea cycle (Liu et Phang, 2012).
The dynamic interplay between PRODH and its associated pathways not only contributes to cellular energy production and redox homeostasis, but also integrates proline metabolism into many cellular processes such as nucleotide synthesis, TCA cycle metabolism, and urea cycle participation.

The dual role of PRODH in cancer

The complex interconnection between PRODH and basal cell metabolism often leads to the identification of antagonistic roles of PRODH in tumors.
Several types of cancer, including breast, skin, kidney, bladder, and gastrointestinal tumors, have shown a decrease in PRODH expression compared to that in normal tissues. Restoration of PRODH expression in renal and colorectal cancer cell lines and mouse models has demonstrated an oncosuppressive role for PRODH. Multiple mechanisms have been proposed to explain the antitumor role. In colorectal cancer cells, PRODH overexpression determines DNA damage and cell cycle arrest by inducing the expression of growth arrest and DNA damage-inducible gene (GADD) proteins (Liu et al., 2009). Moreover, PRODH overexpression via superoxide anion production leads to the alteration of mitochondrial membrane potential and subsequent cytochrome c release. These events trigger caspase 3 cleavage and apoptosis (Liu et al., 2005). Alternatively, PRODH also activates caspase 8, inducing NFAT expression and the components of death receptors DR5 and TRAIL (Liu et al., 2006). In addition, in colorectal cancer, ROS have been associated with the regulation of different pathways, including COX2 inhibition and decreased EGFR phosphorylation (Liu et al., 2008).

Similarly, PRODH induces apoptosis in renal cancer cells through ROS production. In renal cancer, PRODH downregulation correlated with miR-23b* expression (Maxwell and Rivera, 2003; Liu et al., 2010). In hepatocarcinoma samples, PRODH expression shows an inverse correlation with increasing tumor stage. High expression is associated with a favourable prognosis (Ding et al., 2020).

In contrast, proline catabolism can be exploited as a source of energy under stress conditions. For example, PRODH has been proposed to contribute to the cellular response in the presence of hypoxia and glucose deprivation: in a hypoxic environment, PRODH induced autophagy by ROS production, but in the concomitant presence of hypoxia and low glucose levels, electrons produced by PRODH were used for ATP production (Liu and Phang, 2012). The pro-tumoral role of PRODH has been demonstrated in pancreatic and prostate cancers. Pancreatic carcinoma cells use proline catabolism to fuel the TCA cycle during low nutrient availability (Olivares et al., 2017). Prostate cancers show a tumor grade-dependent increase in PRODH expression. Moreover, in prostate cancer cells and animal models, PRODH affects the tumor microenvironment, reducing T-cell infiltration through P5C release (Yan et al., 2018).

PRODH contributes to the invasive behavior of breast cancer cells, as indicated by its high expression during the spheroidal growth of breast cancer cells and the formation of metastases *in vivo*. This effect is mediated by ATP production and maintained through PC5 recycling. Inhibition of PRODH by L-THFA leads to decreased ATP levels and affects spheroid formation and metastasis. Increased expression of PRODH has been shown in metastatic tumors compared to primary breast cancers (Elia et al., 2017).

The role of PRODH in lung cancer is more controversial. On one hand, PRODH expression has been associated with the upregulation of mesenchymal markers (vimentin, Slug, and N-cadherin) and increased migratory and invasive abilities. Moreover, ROS, derived from proline catabolism, determines an increase in IKKα phosphorylation, activation of the NF-κB pathway, and upregulation of some inflammatory-related genes (*CXCL1*, *LCN2* and *IL17C*) (Liu et al., 2020).

On the other hand, our laboratory demonstrated that increased PRODH expression, observed in lung ADCs at early stages, correlates with better prognosis. Lung ADC cell lines ectopically expressing PRODH showed delayed growth and elevated ROS levels. We identified senescence as the mechanism responsible for delayed growth in these cells (Grossi et al., 2024).

The involvement of PRODH in cancer biology is influenced by its impact on various cellular processes, as it can regulate the phosphorylation state of different pathways (EGFR, MEK, IKKα) and induce cell cycle arrest, apoptosis, autophagy, and senescence via ROS production (Liu et al., 2005; Liu et al., 2006; Liu et al., 2008; Liu et al 2009; Liu et al., 2012; Nagano et al., 2017; Liu et al., 2020).

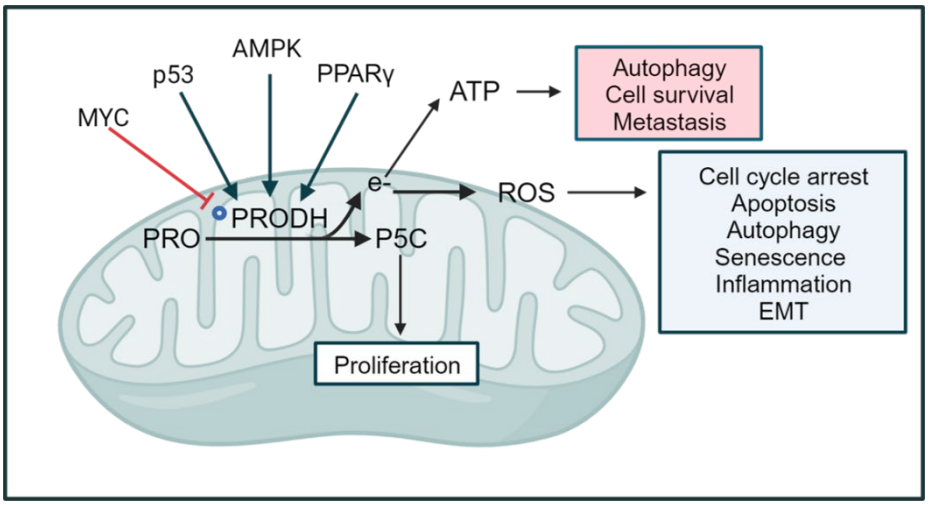

Figure 13. The image show schematically the roles of PRODH in cancer and the oncosuppressor and oncogenes involved in its regulation. Created with Biorender.com.

This has led to the conclusion that PRODH effects depend on the tumor type, the microenvironment, and possibly the genetic background.

AIM OF THE STUDY

Proline dehydrogenase (PRODH) is a p53 inducible enzyme localized in the inner mitochondrial membrane. It catalyzes the key step of proline oxidation in a FAD-dependent reaction and connects proline with basal cell metabolism.

In response to several types of stress, PRODH contributes to several vital cellular processes, such as cell cycle arrest, senescence, survival, and apoptosis.

The multiple outcomes following PRODH induction determine its dual role in tumors, that appear to be organ-, tissue-, and cell-type-dependent. Moreover, the genetic background and tumor stage probably influence PRODH effects as well.

In this context, during an immunohistochemical analysis carried out in collaboration with Prof. Sessa and Dr. Chiaravalli (Pathology unit of Ospedale di Circolo-Fondazione Macchi and the University of Insubria), we found that PRODH is expressed in low-stage lung adenocarcinomas. We also observed a correlation between PRODH expression and EGFR mutations.

The objective of this Ph.D. thesis was to explore the mechanisms by which EGFR regulates the expression of PRODH and its significance for lung cancer. To achieve this, we modulated EGFR expression in various cellular models and investigated the involvement of the JAK/STAT3 downstream signaling pathway in PRODH regulation.

As PRODH has been implicated in cancer progression at a late stage, this study also aimed to assess if PRODH expression may play a role in the resistance of EGFR mutated lung adenocarcinomas to targeted therapy with tyrosine kinase inhibitors.

Ultimately, this project aimed to advance the knowledge of the role of PRODH in lung cancer development and progression.

RESULTS

The following manuscript drafts have been written based on the results of my Ph.D. work:

1) Proline dehydrogenase is negatively regulated by Epidermal Growth Factor (EGFR) via the STAT3 transcription factor
2) The putative role of Proline Dehydrogenase (PRODH) in acquired resistance of lung cancer cells to EGFR inhibitors

In addition, during my Ph.D. I contributed to the following paper:

- Grossi, S., Berno, E., Chiofalo, P., Chiaravalli A.M., Cinquetti, R., Bruno, A., Palano, M.T., Gallazzi, M., La Rosa, S., Sessa, F., Acquati, F., Campomenosi, P. (2024). Proline Dehydrogenase (PRODH) Is Expressed in Lung Adenocarcinoma and Modulates Cell Survival and 3D Growth by Inducing Cellular Senescence. Int J Mol Sci, 25(2):714.

RESULTS -1-

Proline dehydrogenase is negatively regulated by Epidermal Growth Factor (EGFR) via the STAT3 transcription factor

Priscilla Chiofalo[1], Elena Berno[1], Raffaella Cinquetti[1], Vincenza Ciaramella[2,5], Antonino Bruno[3,4], Carminia Maria Della Corte[2], Floriana Morgillo[2] and Paola Campomenosi[1,*]

[1] University of Insubria, Department of Biotechnology and Life Sciences, DBSV, Via J.H. Dunant 3, 21100 Varese, Italy;

[2] University of Naples "L. Vanvitelli", Department of Precision Medicine, Via S. Pansini 5, 80131, Naples, Italy;

[3] Laboratory of Immunology and General Pathology, Department of Biotechnology and Life Sciences, DBSV, Via Monte Generoso 71, 21100 Varese, Italy;

[4] Laboratory of Innate Immunity, Unit of Molecular Pathology, Biochemistry, and Immunology, IRCCS MultiMedica, Via G. Fantoli 16/15, 20138, Milan, Italy;

[5] IRCCS SYNLAB SDN, Via E. Gianturco 113, 80143 Naples, Italy.

*Correspondence: paola.campomenosi@uninsubria.it

ABSTRACT

Lung cancer is the leading cause of cancer mortality and represents a significant health problem worldwide. It is a heterogeneous disease, with Small Cell Lung Cancer (SCLC) accounting for approximately 15% of cases and Non-Small Cell Lung Cancer (NSCLC) accounting for 80-85%. Among these, lung Adenocarcinoma (ADC) represents the predominant histological subtype. The emergence of recurrent molecular alterations, including Epidermal Growth Factor Receptor (EGFR) alterations, characterizing lung ADC, determined the development of different therapeutic options, such as Tyrosine-Kinase Inhibitors (TKIs). However, the heterogeneous response to TKIs calls for a comprehensive analysis of the molecular landscape of EGFR-mutant tumors, to allow a better understanding of EGFR-mutated lung cancer biology and to design better therapeutic approaches.

In this context, proline dehydrogenase (PRODH) could play a role. PRODH is a mitochondrial flavoenzyme catalyzing the first step of proline oxidation, which is important for both cellular bioenergetics and the modulation of signaling transmission via reactive oxygen species (ROS) production.

Here, we demonstrated that EGFR overexpression downregulated PRODH expression, while the inhibition of EGFR small in-frame deletion determined the opposite effects. To clarify the mechanism of PRODH regulation, its promoter was analyzed. Among the possible regulators, we revealed the presence of putative binding sites for STAT3, a transcription factor central to one of the downstream signaling pathways of EGFR.

Our results show that STAT3 significantly decreases PRODH transcript levels, as observed by overexpression or stimulation experiments, whereas STAT3 inhibition increases PRODH expression. These findings provide evidence of EGFR negative regulation of PRODH expression through the STAT3 transcription factor.

Introduction

Lung cancer represents one of the most frequent types of tumor and the leading cause of cancer-related deaths (Siegel et al., 2023). It is a highly heterogeneous disease from the histological and molecular points of view. It is classified as Small Cell Lung Cancer (SCLC, for about 15% of cases) and Non-Small Cell Lung Cancer (NSCLC, approximately 85% of cases), of which lung Adenocarcinoma (ADC) represents the predominant subtype (about 50% of cases).

ADCs arise in the lung periphery, mainly in never-smokers and women. This subtype is characterized by recurrent molecular alterations, including Epidermal Growth Factor Receptor (EGFR).

EGFR-activating mutations frequently occur between exons 18 and 21, leading to constitutive activation of the receptor. Approximately 90% of EGFR alterations are represented by an in-frame deletion in exon 19 and a point mutation in exon 21 (Rodriguez-Canales et al., 2016). Tumors with EGFR-activating mutations rely on their downstream signaling pathways for survival and are vulnerable to Tyrosine Kinase Inhibitors (TKIs). These tumors are considered "oncogene-addicted" (Gazdar et al., 2004; Weinstein and Joe, 2008; Gately et al., 2012).

However, different responses to TKI therapies have been observed in patients with EGFR-mutant tumors. Therefore, a more in-depth characterization of the molecular players involved in tumors and tumor cell lines with mutant EGFR and identification of prognostic and/or predictive markers are required as urgent clinical unmet needs (Kobayashi and Mitsudomi, 2016).

The downstream signaling pathways initiated by the activation of EGFR predominantly involve RAS-RAF-MEK-ERK, PI3K-AKT-mTOR, and JAK-STAT cascades (Li et al., 2023). Even so, differences were observed between EGFR wild-type or the diverse EGFR variants, resulting in subtle differences in tumor behavior (Sordella et al., 2004). These observations led to the in-depth characterization of the metabolic and transcriptomic profile of EGFR mutant tumors. Specifically, EGFR-activating mutations increase glycolytic activity, the pentose phosphate pathway (PPP), drive *de novo*

pyrimidine biosynthesis and influence the concentrations of various amino acids, including proline and aspartate (Makinoshima et al., 2014; Makinoshima et al., 2015). EGFR-mutant lung tumors exhibit a unique gene expression pattern, as revealed by a distinct set of differentially expressed genes, including *PCDHA6*, *WBP1*, and *ERBB3* (Su et al., 2006; Angulo et al., 2008). Interestingly, Angulo et al. proposed a correlation between EGFR and proline dehydrogenase (PRODH) expression.

PRODH is a mitochondrial flavin-dependent enzyme, encoded by *PRODH1*, that maps on chromosome 22q11.21. This enzyme catalyzes the rate-limiting reaction of proline oxidation to Δ1-pyrroline 5-carboxylate (P5C).

In the cytoplasm, P5C can be recycled for proline synthesis, using reducing equivalents and oxidizing NADPH to NADP, which can be used in the PPP. This pathway supports the synthesis of pentoses, that can be used for nucleotide synthesis. In the mitochondria, instead, P5C can be converted to glutamate and then to α-ketoglutarate, which links proline catabolism to the Tricarboxilic Acid Cycle (TCA). By proline oxidation, PRODH also generates two electrons that are transferred to the electron transport chain to produce either ROS or ATP. Additionally, P5C can be transformed into ornithine and enter the urea cycle (Liu et al., 2012; Phang, 2019; Burke et al., 2020; Liu et al., 2021).

PRODH has been associated with various pathologies, including cancer (Liu and Phang, 2012; Tanner et al., 2018). The complex interconnection of PRODH with basal cell metabolism often led to identifying antagonistic roles of PRODH in tumors: it promotes tumor growth in pancreatic tumors (Olivares et al., 2017) and contributes to the invasive phenotype in breast cancer (Elia et al., 2017), while it causes cell cycle arrest and cell death in gastroenteric and renal tumors (Liu et al., 2009). In addition, our group observed increased PRODH expression in early-stage lung ADCs, where its expression seems to correlate with better survival (Grossi et al., 2024). Indeed, the outcome of PRODH expression in cancer depends on the tumor type, its stage, the tumor microenvironment, and possibly the genetic background (Geng et al., 2021; Liu et al., 2021).

Given the expression of PRODH in lung ADCs and the reported metabolic alterations in EGFR mutant tumors, we aimed to investigate the interplay between PRODH and EGFR in this type of tumor. We show that in our experimental models PRODH is negatively regulated by mutant EGFR via STAT3.

Materials and methods

Cell lines and culture conditions

A549, NCI-H1437 (H1437), PC9, HCC827, NCI-H1299 (H1299), and NCI-H1975 (H1975) human lung ADC cell lines were used in this study. In addition, HEK293, an immortalized cell line from human embryonic kidney, MCF7, a breast cancer cell line, and DU145 prostate cancer cell line were used. A549, H1437, PC9, HCC827, and DU145 were grown in RPMI-1640 medium, supplemented with 10% of FBS, and 2mM di L-glutamine. The medium for H1975 cells was also supplemented with 1% sodium pyruvate. HEK293 and MCF7 were cultured in DMEM medium supplemented with 10% of FBS and 2mM L-glutamine.

Culture conditions, tissue origins, and mutational status are summarized in Table 1. Media and reagents for cell cultures were from Euroclone, Milan, Italy.

All cell lines were human and were grown at 37°C in 95% humidity and 5% CO_2. All cells were passaged for no more than one month after thawing. Cells were routinely controlled for mycoplasma contamination by nested PCR (Tang et al., 2000).

Cell line	Tissue	Mutational status	Culture conditions
A549	Lung adenocarcinoma	*KRAS* mutated	RPMI 1640 + FBS 10% + 2mM L-Gln
NCI-H1299	Lung adenocarcinoma	*TP53* null	RPMI 1640 + FBS 10% + 2mM L-Gln
NCI-H1437	Lung adenocarcinoma	*TP53* mutated	RPMI 1640 + FBS 10% + 2mM L-Gln
PC9	Lung adenocarcinoma	*EGFR* p.E746_A750del; *TP53* mutated	RPMI 1640 + FBS 10% + 2mM L-Gln
HCC827	Lung adenocarcinoma	*EGFR* p.E746_A750del; *TP53* mutated	RPMI 1640 + FBS 10% + 2mM L-Gln

NCI-H1975	Lung adenocarcinoma	*EGFR* p.L858R *EGFR* p.T790M *TP53* mutated	RPMI 1640 + FBS 10% + 1% NaPy + 2mM L-Gln
HEK293	Embryonic kidney (immortalized)		DMEM + FBS 10% + 2mM L-Gln
MCF7	Breast adenocarcinoma		DMEM + FBS 10% + 2mM L-Gln
DU145	Prostate adenocarcinoma	*TP53* mutated	RPMI 1640 + FBS 10% + 2mM L-Gln

Table 1. The table resumes culture conditions, tissue origins, and mutational status for *EGFR*, *KRAS*, and *TP53* genes for all cell lines used in the study. The type of mutation is specified only for EGFR. Fetal Bovine Serum (FBS), L-glutamine (L-gln), sodium pyruvate (NaPy).

Cell treatments

For immunoblotting and mRNA analysis, $0{,}3x10^6$ cells were seeded in 60mm Petri dishes for the HCC827 cell line; $0{,}4x10^6$ PC9 cells and $0{,}2x10^6$ H1975 cells were seeded in 100mm Petri dishes. Cells were treated with osimertinib (Selleckem, Aurogene, Milan, Italy; 0,03μM for HCC827 and PC9; 0,06μM for H1975) for 72 hours. MCF7 ($0{,}3x10^6$ cells) were seeded in a 6-well multiwell plate. Twenty-four hours later, cells were stimulated with 50ng/ml IL-6 (Miltenyi Biotec, Bologna, Italy) or with the same dose of IL-6 plus 10ng/ml TNFα (Miltenyi Biotec, Bologna, Italy) and harvested 1 hour later for protein analysis and 14 hours later (or 1, 4, 8, 14, and 24 hours later) for mRNA analysis. For STAT3 inhibition, $0{,}4x10^6$ DU145 cells were seeded in 60mm Petri dishes. After 24 hours, 1μM Pimozide (STAT3 inhibitor, Merck-Sigma Aldrich, Milan, Italy) was added to the medium. Cells were collected after 1 hour for protein analysis and after 4, 8, and 24 hours for mRNA analysis.

Plasmids, constructs and cloning procedures

EGFR-expressing constructs were generated by cloning the EGFR wild-type coding sequence and the sequence encoding the two most common EGFR activating mutations (p.L858R and p.E746-A750del) into the pcDNA3.1Hygro vector, which was already available in the laboratory.

The wild-type sequence was obtained from the cDNA of the H1299 cell line.

Briefly, total RNA was extracted from the H1299 cell line with Tri Reagent (Merck-Sigma Aldrich, Milan, Italy) and cDNA was synthesized with M-MuLV Reverse transcriptase (New England Biolabs, Euroclone, Milan, Italy).

A primer specific to the EGFR sequence was used for cDNA synthesis (5'-GATCTCTAGAACTATCCTCCGTGGTCATGCTC-3'). Amplification of two EGFR fragments was obtained using Q5 Hot Start High-fidelity (HF) DNA polymerase enzyme (New England Biolabs, Euroclone, Milan, Italy) and two different primer pairs: EGFR HindIII primer forward 5'-CCCAAGCTTATTGATCGGGAGAGCCGGAG-3' and EGFR "del" primer reverse 5'-GCCATCACGTAGGCTTCATC-3' for 5' EGFR sequence (size 2,2kbp), EGFR "del" primer forward 5'-CGTTCGGCACGGTGTATAAG-3' and EGFR XbaI primer reverse 5'-GATCTCTAGAACTATCCTCCGTGGTCATGCTC-3' for downstream EGFR sequence (1,5kbp). Subsequently, the external primers and the two PCR amplicons, with 136bp overlapping sequence, were used in equimolar amounts to perform overlap extension PCR (OE-PCR). OE-PCR was performed using different annealing temperatures in the same amplification run (62°C for 5 cycles, 60°C for 5 cycles, and 59°C for 20 cycles).

The full-length EGFR sequence was purified and cloned into pcDNA3.1Hygro expression vector by digestion with HindIII and XbaI enzymes (New England Biolabs, Euroclone, Milan, Italy).

The two most common EGFR activating mutations L858R and p.E746-A750del were obtained respectively from two constructs carrying the desired mutations: pDONR223_EGFR_pELREA746del and pDONR223_EGFR_p.L858R constructs, kind gifts from Jesse Boehm, Matthew Meyerson & David Root, William Hahn & David Root via Addgene (Addgene plasmid #82911; http://n2t.net/addgene:82911; RRID: Addgene_82911 and Addgene plasmid #82906; http://n2t.net/addgene:82906; RRID: Addgene_82906) (Berger et al., 2016).

Both mutant constructs were digested with AfeI restriction enzyme (New England Biolabs, Euroclone, Milan, Italy), to substitute the cassette carrying the mutations into the wild-type backbone. All the constructs were confirmed by Sanger sequencing

(GATC-Biotech, Germany) and compared to the reference sequence using NCBI Blast tools.

The constructs pBabeSTAT3C, carrying a cDNA encoding a constitutively active form of STAT3 (STAT3C), and pBabe, used as a control vector, were obtained from J.E. Darnell's group (Bromberg et al., 1999), thanks to Prof. M. Gariboldi (University of Insubria).

The pGL4.26 vector was obtained from Prof. A. Inga and Prof. Y. Ciribilli's laboratory (University of Trento).

Two constructs were generated, referred to as pGL4.26 PRODH_short and pGL4.26_PRODH_long, carrying part of the *PRODH* sequence from intron 1. The construct pGL4.26 PRODH_long includes all four putative STAT3 response elements (REs), which were identified in the first *PRODH* intron, while pGL4.26 PRODH_short encompasses three of the four STAT3 REs.

These STAT3 putative REs were identified in *PRODH* genomic regions (reference sequence NC_000022.11), using the rVISTA software.

The two fragments were amplified from genomic DNA using Pfu DNA polymerase (Thermo Fisher Scientific, Milan, Italy) and two primer pairs: forward 5'-CAATCTCGAGGAAACGGGTGCCTCCCAAG-3' and reverse 5'-CCAGAAGCTTCCATGGGTGAGTTCAAAGCTG-3' for the PRODH-long segment (size 378bp) and forward 5'- CGATCTCGAGGGAGTATTCTTCATGTTGAGACAAG-3' and reverse 5'-CCAGAAGCTTCCATGGGTGAGTTCAAAGCTG-3' for the smaller fragment (189bp). The PCR amplicons were purified and cloned into the pGL4.26 vector by digestion with XhoI and HindIII restriction enzymes (New England Biolabs, Euroclone, Milan, Italy).

The presence of the insert in the vector was verified through double digestion with the same enzymes. Additionally, digestion with EcoRI was carried out to ensure that the cloned segment had been obtained from the *PRODH1* gene and not from the pseudogene (*Ψ-PRODH*), which carries some single nucleotide variants in the regions of interest. The sequence of the constructs was checked by Sanger sequencing

(GATC-Biotech, Germany) and compared to the reference sequence using the NCBI Blast tool.

Transient transfections

For transient transfection of EGFR wild-type or mutant constructs, A549 and H1437 ($0,3x10^6$ cells) were seeded in 6-well plates to reach 70% confluence on the following day. Control cells were transfected with empty pcDNA3.1Hygro plasmid. For transfection, 2µg of each plasmid and FuGENE HD transfection reagent (Promega, Milan, Italy) were used, according to the manufacturer's protocol. After 48 hours, cells were harvested for protein and RNA analysis. Transient transfections were also carried out in HEK293 cells. Twenty-four hours before transfection, $0,5x10^6$ HEK293 cells were seeded in 60mm dishes. For transfection, 3,5µg of each plasmid and FuGENE HD transfection reagent (Promega, Milan, Italy) were used. To ensure the activation of the EGFR signal transduction pathways, EGF was added to cells transiently transfected with EGFR-expressing constructs. To do so, 24 hours after transfection, cells were serum-starved for 14 hours and then stimulated with Epidermal Growth Factor (EGF) (40ng/ml, Merck-Sigma Aldrich, Milan, Italy). After 20 minutes and 10 hours from stimulation, cells were harvested respectively for protein and RNA extraction.
MCF7 cells were transiently transfected with the construct pBabeSTAT3C, carrying a cDNA encoding a constitutively active form of STAT3 (STAT3C; carrying the p.A661C and p.N663C substitutions), or empty pBabe plasmid, as a control. Twenty-four hours prior to transfection, $0,4x10^6$ MCF7 cells were seeded in a 6-multiwell plate. The following day, cells were transfected with 2µg of the STAT3 expressing construct or equimolar amounts of pBABE vector (complemented with carrier DNA) using the FuGENE HD transfection reagent (Promega, Milan, Italy). Cells were harvested after 42 hours for protein and RNA extraction.

Immunoblotting

To prepare protein extracts, cells were scraped in Phosphate Buffer Saline (PBS) (Euroclone, Milan, Italy), centrifuged, and then resuspended in RIPA buffer (150mM

NaCl, 50mM Tris-HCl pH 7.5, 1% Igepal CA630, 0.1% SDS, and 0.5% Sodium deoxycholate), supplemented with protease and phosphatase inhibitors (PMSF, aprotinin, pepstatin, sodium orthovanadate). After incubating for 45 minutes at 4ºC with gentle rotation, the extracts were centrifuged at 15000xg for 5 minutes at 4°C. The supernatant was transferred to new tubes. Protein concentration was measured by The Quick Start Bradford 1x Dye Reagent (Biorad, Milan, Italy), using bovine serum albumin to build the standard curve. Samples were separated by SDS-PAGE, transferred to nitrocellulose membranes using the Mini-PROTEAN Tetra System (Biorad, Milan, Italy). Membranes were blocked with 4% non-fat milk in PBS-T (0,1% Tween20 in PBS) and target proteins were detected using specific primary antibodies. The following antibodies were used: EGFR (1:1000, #4267, Cell Signaling Technologies, CST), phospho-EGFR Y1068 (1:1000, #3777, CST), STAT3 (1:1000, #9139, CST), phospho-STAT3 Y705 (1:1000, #9145, CST), phospho-STAT3 S727 (1:1000, #34911 CST). For normalization, α-tubulin (1:2000, T9026, Merck-Sigma Aldrich, Milan, Italy or 1:1000, MAB94264, Immunological Sciences, Rome, Italy) was used. Subsequently, the membranes were incubated with goat anti-rabbit HRP-conjugated antibody or anti-mouse HRP-conjugated antibody as appropriate, both diluted 1:900 (ThermoFisher Scientific, Milan, Italy). Each antibody was diluted in 2% non-fat milk in PBS-T. Immunocomplexes were detected with the enhanced chemiluminescent system Westar ηC ultra 2.0 (Cyanagen, Bologna, Italy) and the Odyssey Li-COR FC imaging system (Carlo Erba Reagents, Milan, Italy).

RNA extraction and RT-qPCR

Total RNA was isolated using TRI Reagent (Merck-Sigma Aldrich, Milan, Italy). RNA samples were quantified with a NanoDrop 2000c (ThermoFisher by Life Technologies, Milan, Italy). RNA (500ng) was reverse transcribed using the iScript cDNA synthesis kit (Biorad, Milan, Italy). To generate first-strand cDNA, iScript reaction mix with oligo(dT) and random hexamer primers, RNase H+ MMLV reverse transcriptase, and RNA (500ng) were added to the PCR tube. The reaction was performed at 25°C for 5 minutes, 43°C for 30 minutes, 43°C for 15 minutes and 85°C for 5 minutes in T100

thermal cycler (Biorad, Milan, Italy). Then, cDNA was diluted with distilled water and stored at −20°C.

Relative levels of gene transcripts were determined by quantitative PCR (qPCR), using iTaq Universal Sybr Green (Biorad, Milan, Italy), using primers specific for PRODH (forward: 5'-GCAGAGCACAAGGAGATGGA-3' and reverse: 5'-TGGTATTGCTTGTCCCGCTT-3'), TNFRS1A (forward: 5'-ATTGGACTGGTCCCTCACCT -3' and reverse: 5'- AGTAGGTTCCTTTGTGGCACTT-3'), TWIST (forward: 5'-GCGGCCAGGTACATCGACTT-3' and reverse: 5'-TGCAGCTTGCCATCTTGGAG-3'), and β2M (forward: 5'-ATGGATGAAACCCAGACACA-3' and reverse: 5'-AGGCTATCCAGCGTACTCCA-3'). Oligonucleotides were ordered from Metabion International AG. All reaction mixes were prepared adding primers and iTaq Universal Sybr Green Supermix, which includes hot start iTaq DNA Polymerase, dNTPs, Sybr Green I dye. Each reaction mix was dispensed into the appropriate wells of a qPCR plate and DNA samples were added. The final volume of 10µl was obtained by adding nuclease-free water. Three replicates were prepared for each sample and target. Blanks, containing nuclease-free water instead of cDNA, were included. A CFX Connect real-time PCR instrument was used (Biorad, Milan, Italy). The specificity of the amplification was confirmed by melting curve analysis. Fold change in transcript levels was calculated by the $2^{-\Delta\Delta Ct}$ method (Livak and Schmittgen, 2001).

Luciferase assays

DU145 cells ($6x10^4$) were seeded in a 24-well multiwell plate. After 24 hours, each well was transfected with 423ng of pGL4.26 PRODH_long, equimolar amounts of pGL4.26 PRODH_short or pGL4.26 empty vector (complemented with carrier DNA). In addition, to normalize the readout, each well was transfected with 252ng of pRL-SV40 plasmid carrying the luciferase sequence from *Renilla reniformis* under a constitutive promoter. The Lipofectamine 2000 transfection Reagent (ThermoFisher Scientific, Milan, Italy) was used to perform the transfection, according to the manufacturer's instructions. The following day, cells were treated with 1µM Pimozide (Selleckchem, Aurogene, Milan,

Italy) or vehicle (dimethyl sulfoxide, DMSO, Euroclone, Milan, Italy). Forty-eight hours after transfection, cells were lysed, and luciferase activity was determined using the Dual-Luciferase Reporter Assay System (Promega, Milan, Italy) as recommended by the manufacturer's protocol. Luminescence was measured with a Tecan Infinite 200Pro plate reader (Tecan, Cernusco sul Naviglio, Italy). Renilla luciferase activity was used to normalize firefly luciferase activity.

Statistical analyses

The difference in PRODH expression among cells transfected with the different EGFR constructs was determined by the two-tailed t-test. The difference in PRODH expression between cells transfected with the STAT3C construct or control vector was calculated by the two-tailed t-test. The significance of the difference in transcript levels (PRODH, TNFRS1A, Twist) after qPCR between cells stimulated with cytokines (IL-6 and TNFα), or treated with pimozide, and mock conditions was calculated by applying a two-tailed t-test, depending on the type of comparison. The significance of the difference in Relative Luminescence (RLU) between cells transfected with the "PRODH_short", the "PRODH_long" luciferase constructs or the appropriate control vector, treated with pimozide or with vehicle, were determined by multiple t-test. Data were analyzed using GraphPad Prism8 (San Diego, CA, USA).

Results

EGFR correlates negatively with PRODH expression

To evaluate if EGFR could modulate the expression of the *PRODH* gene, we first performed transient transfections of wild-type and mutant EGFR-expressing constructs in A549 and H1437 lung ADC cell lines. EGFR levels and activation were increased in cells transfected with the different EGFR-expressing constructs, compared to empty vector-transfected cells, as determined by immunoblot analyses (Figure 1, A and B). When PRODH transcript levels were analyzed, we observed a slight decrease in PRODH transcript levels in A549 and H1437 cells transfected with EGFR expression constructs compared to control vector-transfected cells. In both lung ADC cell lines,

the EGFR p.E746-A750del expression construct, in particular, affected PRODH expression (Figure 1A, 1B). We reasoned that the mutations present in lung cancer cell lines (such as *KRAS*, *TP53*, and *NRAS* mutations) could affect the results. Thus, we ectopically expressed wild-type and mutant EGFR expression constructs into HEK293 immortalized human cells. In addition, we stimulated transfected cells with EGF, since some papers proposed that during transient transfections EGFR mutants require ligand addition to fully activate the signal transduction pathways (Lynch et al., 2004; Greulich et al., 2005). In this setting, we observed a significant decrease of PRODH mRNA in HEK293 cells transfected with wild-type or mutant EGFR constructs compared to cells transfected with the empty vector. In all tested cell lines, expression of EGFR p.E746-A750del resulted in the greatest variation in PRODH transcript level in H1437 and HEK293 (Figure 1C).

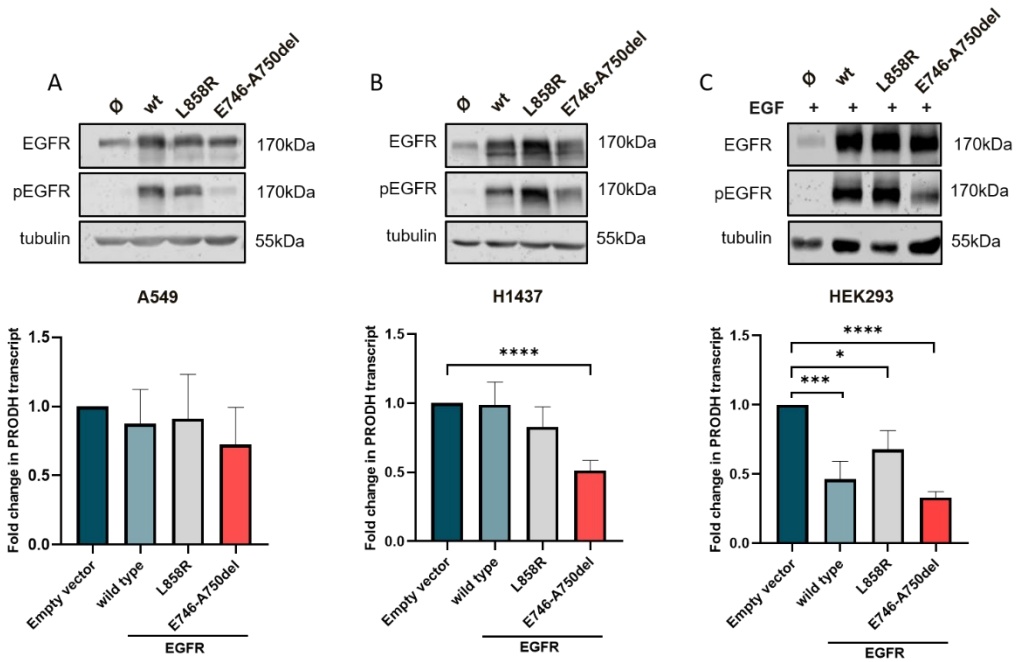

Figure 1. Ectopic expression of EGFR determines a decrease in PRODH transcript levels in human cell lines. A549 (A) and H1437 (B) cells were transfected with the empty vector or constructs expressing EGFR wild-type, EGFR L858R, or EGFR E746-A750del. After 48 hours from transfection, cells were processed for protein and RNA extraction. Whole lysates were analyzed by immunoblotting for total and activated EGFR expression (pEGFR Y1068). α-tubulin was used for normalization. A representative image is shown for each cell line. The expression of PRODH mRNA was determined by RT-qPCR (graphs below). The

graphs represent the mean of three independent experiments ± Standard error (SE) (****p<0.0001, two-tailed t-test). HEK293 (C) cells were transfected, serum-starved for 14 hours, and exposed to EGF (40 ng/mL). After 20 minutes, proteins were extracted and the expression of EGFR, pEGFR Y1068, and α-tubulin were examined by immunoblotting (image above). After 10 hours of stimulation, PRODH transcript levels were determined by qRT-PCR (graph below). The graph represents the mean of two independent experiments ± SE (*p<0.05, ***p<0.001, ****p<0.0001, two-tailed t-test).

As an alternative approach, to confirm the involvement of the two most common EGFR mutations, the effect of EGFR inhibition on PRODH expression was investigated in lung ADC cell lines harboring the EGFR p.E746-A750del short in-frame deletion (PC9, HCC827) or the p.L858R and p.T790M missense mutations (H1975). Treatment with osimertinib inhibited EGFR activation in all tested cell lines (Figure 2, upper panels). In parallel to EGFR inhibition, osimertinib determined an increase in PRODH transcript levels, in particular in the two lung ADC cell lines carrying EGFR deletion at exon 19 (Figure 2, A and B), confirming the observations obtained after transfection of the EGFR p.E746-A750del expression construct.

Only a slight but not consistent increase in PRODH transcript was observed in H1975 cells (Figure 2C).

Collectively, these data indicate that EGFR indeed regulates PRODH expression at the transcriptional or post-transcriptional levels. This regulatory effect is likely influenced by EGFR downstream signaling pathways, as suggested by differences between the two EGFR mutants.

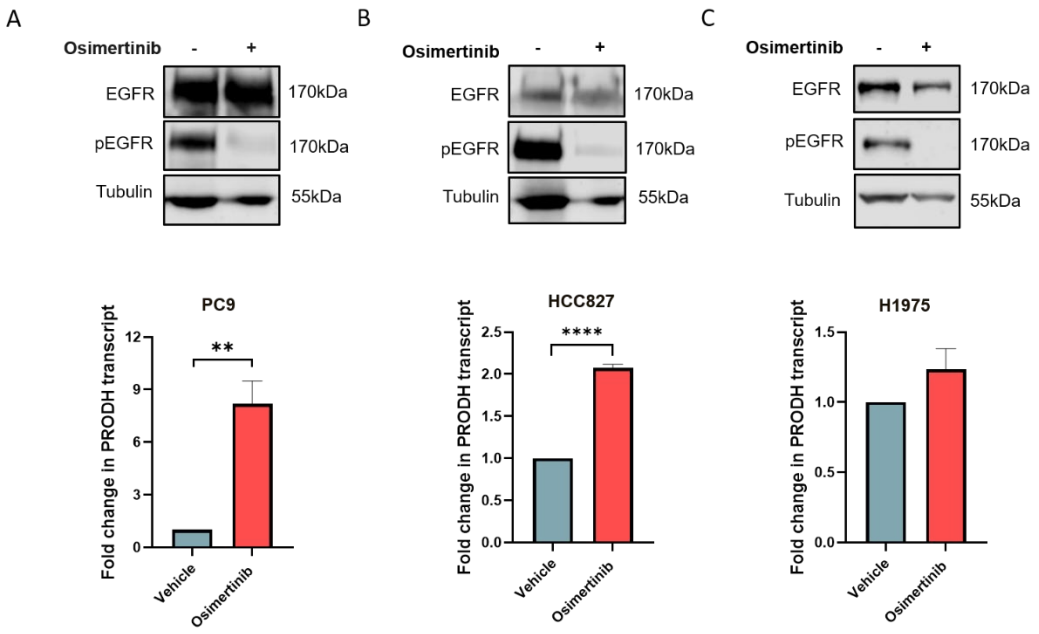

Figure 2. The p. E746-A750del deletion mutant of EGFR affects PRODH expression. PC9 (A), HCC827 (B), and H1975 (C) cells were treated with osimertinib, a third-generation TKI, for 72 hours and then processed for protein and RNA extraction. Protein extracts were analyzed for the expression of EGFR, pEGFR (Y1068), and α-tubulin by immunoblotting (image above). The expression of PRODH mRNA was determined by qRT-PCR (graph below). The graphs represent the mean ± SE of two independent experiments (**p<0.01, ****p<0.0001, two-tailed t-test).

The PRODH gene contains putative binding sites for the STAT3 transcription factor

To investigate the mechanism by which EGFR potentially modulates PRODH expression, the *PRODH* genomic region (reference sequence NC_000022.11) spanning –6000bp to +1000bp from the Transcription Start Site (TSS) was investigated with the rVISTA software, which identifies REs by their conservation throughout evolution (therefore suggesting their biological relevance) and ranks them depending on the available evidence of regulation (Loots and Ovcharenko, 2004). Notably, the analysis revealed four putative STAT3 binding sites mapping downstream of the TSS, within intron 1.

In particular, a full STAT3 RE ggccgtgTCTGGGAAgtcgct (named RE3) was found at +614 from the TSS. By comparing it with the sequence reported in the literature, it includes eight of the nine nucleotides ($TTCN_3GAA$) recognized in the promoter of

STAT3 target genes (Egusquiaguirre et al., 2018; Tošić and Frank, 2021). Close to the larger putative binding sequence, three half-sites (referred to as RE1, RE2, and RE4) were identified. They map +378bp, +592bp, and +662bp respectively from the TSS. All four putative binding sites are located in intron 1 (Figure 3), thus potentially allowing a more efficient regulation.

In addition, putative binding sites for other transcription factors were found in the *PRODH* promoter, including an NF-KB RE, that maps +662bp from the TSS.

STAT3 is one of the major downstream signaling pathways activated by EGFR (Song et al., 2003; Lo et al., 2007). Thus, we hypothesized that EGFR could regulate PRODH expression by activating STAT3 and triggering the transcription factor, alone or in complex with cofactors, to bind to the *PRODH* regulatory regions and repress its transcription.

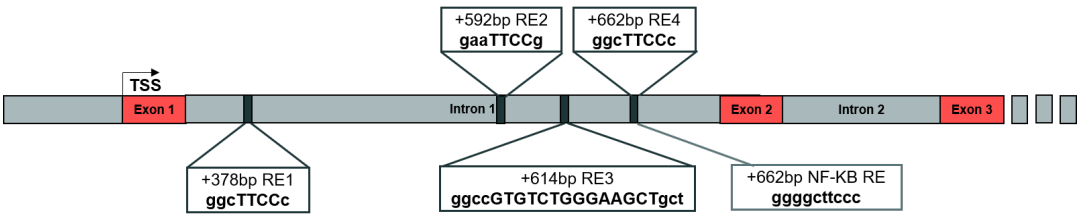

Figure 3. Schematic representation of chromosomal localization and sequence of STAT3 RE1, RE2, RE3 and RE4 and NF-KB putative RE in the *PRODH* gene. The distance from the transcriptional start site (TSS) is reported. Exons are represented by red bars, introns in grey, and putative response elements (REs) in blue. The sequence is not to scale.

Modulation of STAT3, a signaling molecule downstream of EGFR, affects PRODH transcript levels

To investigate if STAT3, for which putative binding sites are present in the first intron of the *PRODH* gene, is the transducer of EGFR effect on PRODH expression, we modulated STAT3 expression into MCF7 and DU145 cell lines, which were selected based on their STAT3 activation status. First, we induced ectopic expression of STAT3 by transfecting a construct encoding a constitutively active version of STAT3 (STAT3C) into MCF7 cells, that express STAT3 in an activatable form (Bromberg et al., 1999). We observed a 30% decrease in PRODH transcript, compared to cells transfected with the empty vector (Figure 4A).

To further clarify the involvement of STAT3 in *PRODH* regulation, we stimulated the expression of the transcription factor into MCF7 cells with IL-6, a cytokine involved in STAT3 activation.

Stimulation conditions were determined by treating MCF7 cells with IL-6 for 1, 4, 8, 14, and 24 hours. After 1 hour of stimulation, STAT3 activation was assessed by immunoblotting analysis, checking the phosphorylation status of tyrosine 705 (Y705) and serine 727 (S727). Modulation of the PRODH transcript was observed after 8 hours and was more evident between 14 and 24 hours. At the same time, we evaluated also changes in mRNA levels of *TNFRS1A* and *TWIST*, two known STAT3 target genes (Egusquiaguirre et al., 2018; Lo et al., 2007) (Figure 4B).

Next, we stimulated STAT3 expression into MCF7 cells, using IL-6, TNFα or their combination. The latter was used to test whether STAT3 cooperates with NF-κB in regulating the *PRODH* gene, since an NF-κB RE is present near the STAT3 REs in intron 1. However, TNFα-induced NF-κB stimulation did not affect PRODH expression. Instead, STAT3 stimulation with IL-6 resulted in a slight decrease in PRODH expression, comparable to that observed with STAT3 overexpression (Figure 4C).

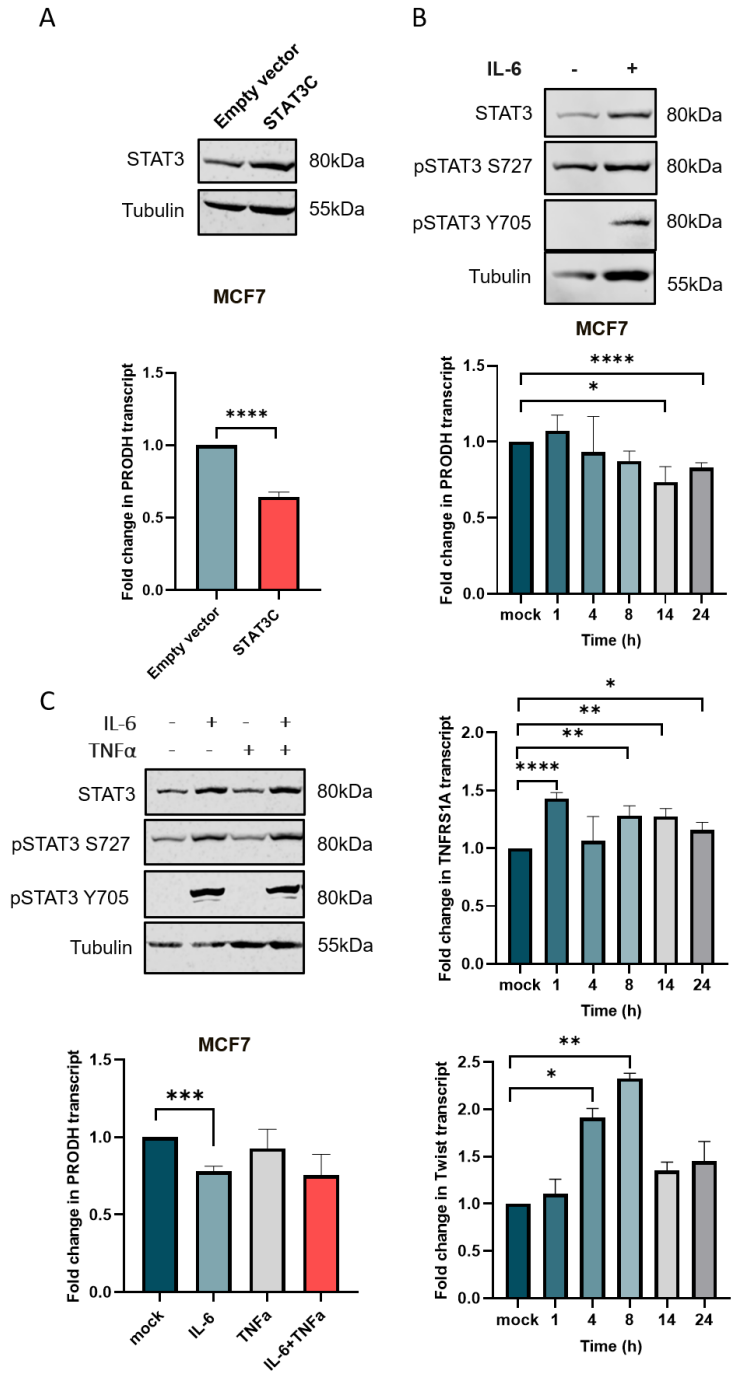
A
Empty vector
STAT3C
STAT3
80kDa
Tubulin
55kDa
MCF7
Fold change in PRODH transcript
****
Empty vector
STAT3C
B
IL-6 - +
STAT3
80kDa
pSTAT3 S727
80kDa
pSTAT3 Y705
80kDa
Tubulin
55kDa
MCF7
Fold change in PRODH transcript
****
*
mock 1 4 8 14 24
Time (h)
C
IL-6 - + - +
TNFα - - + +
STAT3
80kDa
pSTAT3 S727
80kDa
pSTAT3 Y705
80kDa
Tubulin
55kDa
MCF7
Fold change in PRODH transcript
***
mock
IL-6
TNFa
IL-6+TNFa
Fold change in TNFRS1A transcript
*
**
**
****
mock 1 4 8 14 24
Time (h)
Fold change in Twist transcript
**
*
mock 1 4 8 14 24
Time (h)

Figure 4. STAT3 is involved in PRODH transcriptional regulation. MCF7 cells were transfected with the pBabe-STAT3 construct, which expresses constitutively active STAT3 (STAT3C), or pBabe control vector (A). After 42 hours from transfection, cells were then processed and analyzed for expression of STAT3 protein by immunoblot and for PRODH mRNA by qRT-PCR. The graphs represent the mean of three independent experiments (****p<0.0001, two-tailed t-test). MCF7 were stimulated with IL-6 (50ng/ml) (B). One hour after stimulation, cells were processed and protein extracts were analyzed by immunoblot for STAT3 expression and activation (through pSTAT3 Y705 and pSTAT3 S727). α-tubulin was used for normalization. Cells were processed for RNA extraction after 1, 4, 8, 14 and 24 hours. The expression of PRODH, TNFRS1A, and Twist mRNA was determined by qRT-PCR. The graphs represent the mean of n=4 (for PRODH), 3 (for TNFRS1A), or 2 (for Twist) independent experiments ± SE (*p<0.05, **p<0.01, ***p<0.001, ****p<0.0001, two-tailed t-test). MCF7 cells were stimulated with IL-6 and/or TNFα (C). Samples were then analyzed to check STAT3 activation by immunoblot and for PRODH expression by qRT-PCR, respectively 1 and 14 hours after stimulation. The graphs represent the mean ± SE of two independent experiments (***p<0.001, two-tailed t-test).

As a complementary experiment, we inhibited STAT3 with pimozide in DU145 cells, which express STAT3 in a constitutively active form. Inhibition of STAT3 was checked by analysis of the phosphorylation status of Y705 and S727 (Figure 5A). Consistent with the previous findings of an inverse correlation between STAT3 induction and PRODH expression, administration of the STAT3 inhibitor pimozide determined an increase in PRODH transcript levels, that was maximal 24 hours after STAT3 inhibition (Figure 5B).

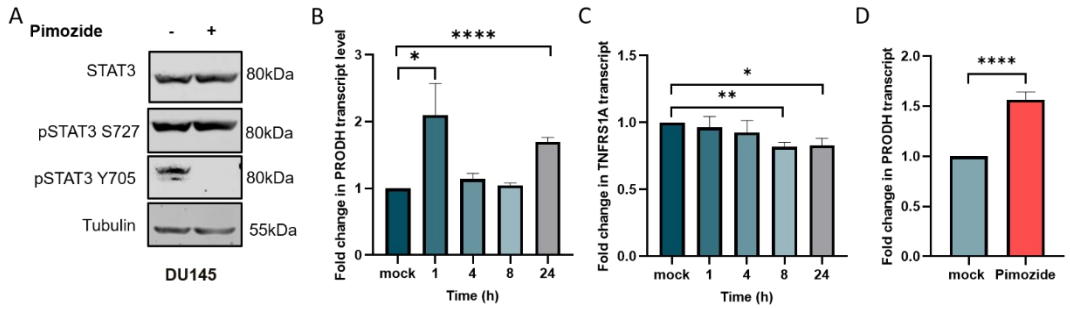

Figure 5. STAT3 inhibition caused an increase in the PRODH transcript. DU145 cells were treated with pimozide (1μM). After 1 hour of stimulation, cells were processed and protein extracts were analyzed by immunoblot (A) for STAT3 expression and activation (through pSTAT3 Y705 and pSTAT3 S727). α-tubulin was used for normalization. Cells were processed for RNA extraction after 1, 4, 8, and 24 hours. The expression of PRODH (B), and TNFRS1A (C) mRNAs was determined by qRT-PCR. The graphs represent the mean of n=2 independent experiments ± SE. One further experiment was performed to analyze the fold change in PRODH transcript by qPCR (D). (*p<0.05, **p<0.01, ***p<0.001, ****p<0.0001, two-tailed t-test).

Concomitantly, a decrease in TNFRS1A transcript levels was observed at 8 and 24 hours (Figure 5C). The 1.6-fold increase in PRODH expression after 24 hours of STAT3 inhibition was confirmed in a further experiment (Figure 5D).

Based on the available data, it appears that PRODH expression is downregulated by STAT3, possibly by transcriptional repression mediated by the putative REs in the *PRODH* gene.

PRODH modulation by STAT3 is mediated by sequences present in intron 1

To investigate whether STAT3 modulates PRODH expression by binding its target sequences in intron 1, we transfected DU145 cells with pGL4.26 as control, pGL4.26 PRODH_short (PRODH_short) or pGL4.26 PRODH_long (PRODH_long) constructs, carrying the smaller and the longer fragment of intron 1, respectively. We performed a luciferase assay after STAT3 inhibition using DU145 cells (Figure 6A).

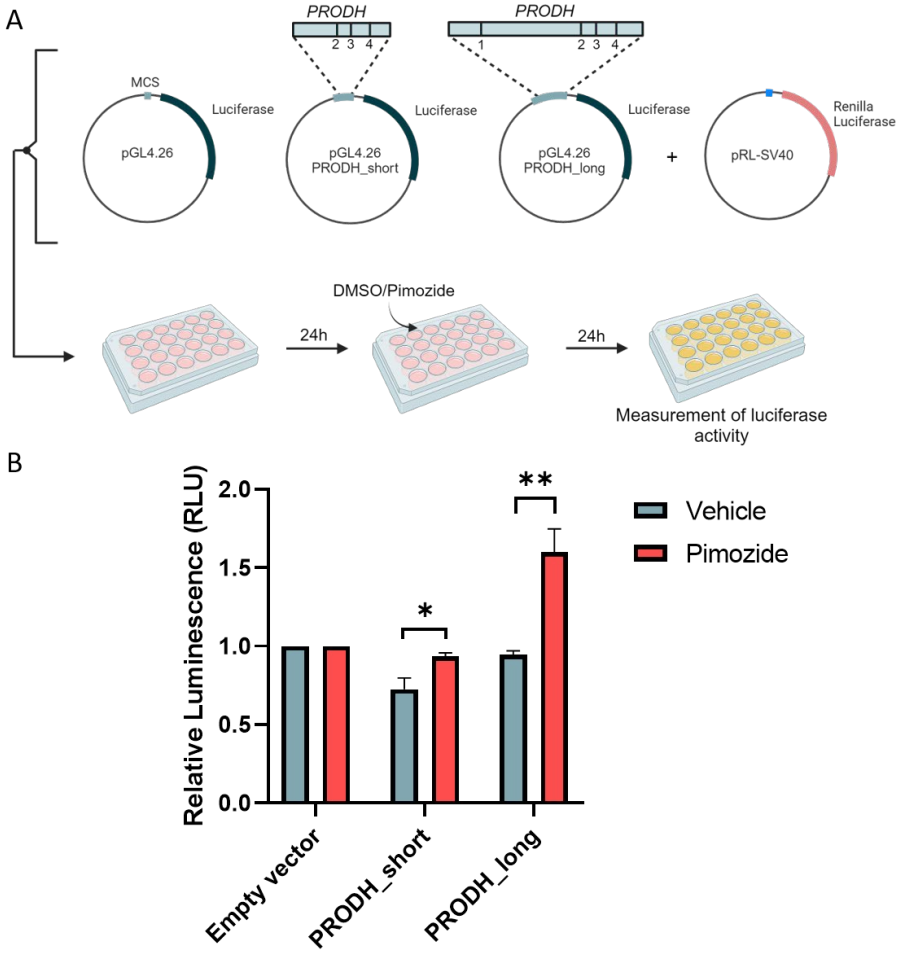

Figure 6. STAT3 inhibition transactivated PRODH expression. DU145 cells were transiently transfected with pGL4.26 as control, pGL4.26 PRODH_short (PRODH_short) or pGL4.26 PRODH_long construcs. Twenty-four hours later, STAT3 was inhibited by pimozide (1µM). After 24 hours, a luciferase assay was performed. Reporter vector pRL-SV40 was used for normalization. A scheme of the transfected constructs and plasmids, the short and long promoter fragments (light blue rectangle) containing putative STAT3 REs (black vertical lines) are indicated. Created with Biorender.com. The graph in (B) shows the change in Relative Luminescence (RLU) of pimozide treated-cells (in red) relative to vehicle-treated cells (in blue), normalized on the empty vector pGL4.26. One preliminary experiment was performed. (*p<0.05, **p<0.01, multiple t-test).

Upon STAT3 inhibition, we observed a significant increase in luciferase activity in DU145 cells transfected with either the short or the long PRODH fragments, as compared to those transfected with the empty pGL4.26 vector. This preliminary result confirms our hypothesis of a direct binding of STAT3 to *PRODH*. The increase in luciferase activity was higher in cells transfected with the PRODH_long construct, which carries all four STAT3 putative REs, as well as additional REs for other transcription factors (Figure 6B), compared to those transfected with the PRODH_short construct. Luciferase activity was also comparable to the change in PRODH transcript by qPCR after treatment of the same cell line with the same inhibitor, suggesting that the modulation occurs through this genomic region. Although preliminary, this observation suggests that either the binding to all REs increases the efficiency of modulation, or that STAT3 binds and represses *PRODH* expression in cooperation with other transcription factors.

Discussion

Tumor cells adapt their metabolism to sustain their rapid growth (Hanahan and Weinberg, 2011). The catabolism of proline has the potential to play an important role in cancer cell development, either positively or negatively. PRODH catalyzes the rate-limiting reaction of proline oxidation to P5C and transfers electrons to its Flavin Adenin Dinucleotide (FAD) cofactor, providing key mediators, like ATP and ROS species, whose balance affects survival, cell cycle arrest and apoptosis (Liu and Phang, 2012; Tanner et al., 2018).

PRODH is encoded by a stress-inducible gene localized on chromosome 22. Currently, various factors have been identified as PRODH regulators. Indeed, PRODH expression is induced by p53 binding to its regulatory sequences in the *PRODH* gene (Raimondi et al., 2013). Also PPARγ was shown to bind to a RE in the *PRODH* promoter (Pandhare et al., 2006); instead, MYC downregulates PRODH expression via miR-23b* binding to PRODH 3'UTR (Liu et al., 2012). To fully understand the role of PRODH in cancer, it is essential to further clarify PRODH regulation.

Interestingly, in 2008, Angulo et al. described the dysregulation of some genes involved in the apoptotic pathway in EGFR-mutant tumors. One of the genes whose expression increased in EGFR-mutated tumors was indeed *PRODH*.

Our laboratory previously observed that PRODH is expressed in a high proportion of early-stage lung ADC cases (Grossi et al., 2024).

We aimed to investigate a possible association between PRODH expression and EGFR mutations, by employing cellular models. Initially, we transfected lung ADC cell lines with EGFR wild-type or mutant constructs. Then we transfected the constructs into HEK293 non-tumor cells alongside EGF administration, to eliminate possible confounding factors, including genetic modifiers (in particular mutations in other genes, such as those of the Ras family), often present in cancer cell lines and fully activate EGFR downstream pathways, as recommended by literature sources (Lynch et al., 2004; Greulich et al., 2005). In each experimental setting, we observed a consistent decrease in PRODH mRNA in cells transiently transfected with wild-type or mutant EGFR compared to cells transfected with empty vector. Notably, the cells transfected with the construct carrying the EGFR p.E746-A750del mutant showed the most significant decrease in PRODH transcript. Accordingly, EGFR inhibition by osimertinib in PC9 and HCC827 cell lines, both carrying the p.E746-A750 EGFR in-frame deletion, led to PRODH mRNA upregulation compared to vehicle-treated cells.

In contrast to the data by Angulo et al, our experimental results suggested a negative correlation between EGFR and PRODH expression (Angulo et al., 2008). It must be underlined that our investigations were conducted *in vitro*, utilizing a limited number of

lung ADC cell lines and modulating EGFR or STAT3 expression by transfection of expression constructs or inhibition.

EGFR mutations in tumors have been linked to increased transcriptional heterogeneity, which is further characterized by the presence of distinct subgroups within EGFR mutant cohorts. Indeed, different studies have described distinct genes variably expressed among EGFR mutant cohorts. Various factors contribute to this heterogeneity, including age, gender, and ethnicity, as well as genomic complexity (Planck et al., 2013). These factors should be considered when examining these tumors. The negative correlation between EGFR and PRODH expression is consistent with our finding of PRODH's antiproliferative role in lung ADC cell lines (Grossi et al., 2024). In addition, PRODH expression reduced EGFR activation in colorectal cancer DLD-1 cells (Liu et al., 2008).

To investigate the mechanism by which EGFR modulated PRODH expression, the *PRODH* regulatory region was examined bioinformatically. Among others, a tandem Signal Transducer and Activator of Transcription 3 (STAT3) binding site attracted our attention. The site consisted of a full RE surrounded by three shorter sequences. The presence of a tandem sequence is crucial for promoting the cooperation of STAT3 factors in the DNA binding of target genes through the N-terminal domain (Hu et al., 2015; Egusquiaguirre et al., 2018).

STAT3 is a key signaling pathway activated by EGFR, wherein the tyrosine kinase receptor, through STAT3 activation, induces the expression of target genes (Lo et al., 2005, Lo et al., 2007), and promotes the survival of lung cancer cells. In addition, a correlation between EGFR-activating mutations and the phosphorylation status of STAT3 was recognized in NSCLCs (Song et al., 2003; Gao et al., 2007).

Considering these assumptions, we investigated the role of STAT3 as a possible link between EGFR and PRODH, by modulating STAT3 in different cancer cell lines.

Ectopic expression or endogenous stimulation of STAT3 led to a decrease in PRODH expression, while its inhibition resulted in higher levels of PRODH transcript, supporting our hypothesis. However, the mechanism by which STAT3 downregulates PRODH has yet to be elucidated. Commonly, STAT3 transactivates target genes by binding to its

nine base pairs RE (sequence: $TTCN_3GAA$). Negative regulation through STAT3 has also been observed (Ivanov et al., 2001; Niu et al., 2005). DNA binding by STAT3 prevents the expression of apoptotic-related genes (Timofeeva et al., 2013). Additionally, STAT3 can regulate gene expression by epigenetic mechanisms (Yu et al., 2014; Tošić and Frank, 2021). Since the main post-translational modification involved in STAT3 transcriptional activity (phosphorylation at tyrosine 705) is required to decrease PRODH expression in MCF7 cells, we hypothesized that STAT3 binds to the *PRODH* promoter directly. This has been confirmed by luciferase assays performed in DU145 cells, where we observed elevated luciferase activity upon STAT3 inhibition in cells transfected with reporter constructs carrying either the short or the long fragments from *PRODH* intron 1, compared to those treated with vehicle. To provide further evidence for the direct binding of STAT3 to the RE on PRODH, we will mutagenize STAT3 REs. Complementary luciferase assay experiments will be carried out in MCF7 cells after STAT3 ectopically expression. Moreover, we plan to do Chromatin Immunoprecipitation assays, although, given the moderate degree of variation, the direct binding of STAT3 to *PRODH* REs may be difficult to detect.

To mediate its effect, STAT3 may also cooperate with other transcription factors. This hypothesis is also supported by the fact that cells transfected with the long fragment from intron 1 of the *PRODH* gene exhibited greater luciferase activity than those transfected with the shorter fragment. As STAT3 often interacts with MYC (Hutchins et al., 2013), it would be tempting to speculate that STAT3 may cooperate with this transcription factor to regulate PRODH expression. It has been previously shown that MYC downregulates PRODH via microRNA miR-23b*. However, this may represent an additional regulatory mechanism (Liu et al., 2012). Another potential factor is NRF2, whose putative binding site is located close to STAT3 RE1 at +384 from TSS. Moreover, p53 might be involved, given that it is downregulated by STAT3 (Niu et al., 2005).

Recent findings have unveiled that acetylation of STAT3 on the lysine residue 685 facilitates the recruitment of the Sin3α complex, which includes histone deacetylases and methyltransferase, thus acquiring the ability to silence tumor suppressor genes

(Gambi et al., 2019). This process has been documented in human breast cancer cells, including MCF7 cells, and was triggered by cytokine stimulation (Gambi et al., 2019; Monteleone and Poli, 2019). It is plausible that a similar mechanism could be triggered by STAT3 to inhibit PRODH expression. A comprehensive understanding of the mechanism by which STAT3 mediates PRODH regulation necessitates further investigations. However, the involvement of STAT3 in proline metabolism has already been documented by other groups (Zhang et al., 2023).

Taken together, these data suggest that EGFR inhibits PRODH expression via STAT3, in order to promote lung ADC cell growth. At the same time, the upregulation of PRODH in response to TKI inhibitors underscores its potential involvement in the induction of apoptosis in treated tumor cells.

The absence of chromatin immunoprecipitation assay and the fact that our experiments were all carried out *in vitro* represent the main limitations of our work.

In conclusion, PRODH emerges as a potential diagnostic and prognostic marker for lung ADCs and could provide valuable insights into the therapeutic responsiveness of lung ADCs.

References

Angulo, B., Suarez-Gauthier, A., Lopez-Rios, F., Medina, P. P., Conde, E., Tang, M., Soler, G., Lopez-Encuentra, A., Cigudosa, J. C., & Sanchez-Cespedes, M. (2008). Expression signatures in lung cancer reveal a profile for EGFR-mutant tumours and identify selective PIK3CA overexpression by gene amplification. Journal of Pathology, 214(3), 347–356.

Berger, A.H., Brooks, A.N., Wu, X., Shrestha, Y., Chouinard, C., Piccioni, F., Bagul, M., Kamburov, A., Imielinski, M., Hogstrom, L., Zhu, C., Yang, X., Pantel, S., Sakai, R., Watson, J., Kaplan, N., Campbell, J. D., Singh, S., Root, D. E., Narayan, R., Natoli, T., Lahr, D. L., Tirosh, I., Tamayo, P., Getz, G., Wong, B., Doench, J., Subramanian, A., Golub, T. R., Meyerson, M., Boehm, J. S. (2016) High-throughput Phenotyping of Lung Cancer Somatic Mutations. Cancer Cell, 30(2):214-28.

Bromberg, J. F., Wrzeszczynska, M. H., Devgan, G., Zhao, Y., Pestell, R. G., Albanese, C., & Darnell, J. E. (1999). Stat3 as an oncogene. Cell, 98(3):295-303.

Burke, L., Guterman, I., Palacios Gallego, R., Britton, R. G., Burschowsky, D., Tufarelli, C., & Rufini, A. (2020). The Janus-like role of proline metabolism in cancer. In Cell Death Discovery, 6:104.

Egusquiaguirre, S. P., Yeh, J. E., Walker, S. R., Liu, S., & Frank, D. A. (2018). The STAT3 Target Gene TNFRSF1A Modulates the NF-κB Pathway in Breast Cancer Cells. Neoplasia (United States), 20(5), 489–498.

Elia, I., Broekaert, D., Christen, S., Boon, R., Radaelli, E., Orth, M. F., Verfaillie, C., Grünewald, T. G. P., & Fendt, S. M. (2017). Proline metabolism supports metastasis formation and could be inhibited to selectively target metastasizing cancer cells. Nature Communications, 8:15267.

Gambi, G., Di Simone, E., Basso, V., Ricci, L., Wang, R., Verma, A., Elemento, O., Ponzoni, M., Inghirami, G., Icardi, L., & Mondino, A. (2019). The transcriptional regulator Sin3A contributes to the oncogenic potential of STAT3. Cancer Research, 79(12), 3076–3087.

Gao, S. P., Mark, K. G., Leslie, K., Pao, W., Motoi, N., Gerald, W. L., Travis, W. D., Bornmann, W., Veach, D., Clarkson, B., & Bromberg, J. F. (2007). Mutations in the EGFR kinase domain mediate STAT3 activation via IL-6 production in human lung adenocarcinomas. Journal of Clinical Investigation, 117(12), 3846–3856.

Gately, K., O'Flaherty, J., Cappuzzo, F., Pirker, R., Kerr, K., & O'Byrne, K. (2012). The role of the molecular footprint of EGFR in tailoring treatment decisions in NSCLC. In Journal of Clinical Pathology, 65(1):1-7.

Gazdar, A. F., Shigematsu, H., Herz, J., & Minna, J. D. (2004). Mutations and addiction to EGFR: The Achilles "heal" of lung cancers? Trends in Molecular Medicine, 10(10), 481–486.

Geng, P., Qin, W., Xu, G. (2021). Proline metabolism in cancer. Amino Acids, 53(12):1769-1777.

Greulich, H., Chen, T. H., Feng, W., Jänne, P. A., Alvarez, J. V., Zappaterra, M., Bulmer, S. E., Frank, D. A., Hahn, W. C., Sellers, W. R., & Meyerson, M. (2005). Oncogenic transformation by inhibitor-sensitive and -resistant EGFR mutants. PLoS Medicine, 2(11), 1167–1176.

Grossi, S., Berno, E., Chiofalo, P., Chiaravalli A.M., Cinquetti, R., Bruno, A., Palano, M.T., Gallazzi, M., La Rosa, S., Sessa, F., Acquati, F., Campomenosi, P.. (2024). Proline Dehydrogenase (PRODH) Is Expressed in Lung Adenocarcinoma and Modulates Cell Survival and 3D Growth by Inducing Cellular Senescence. Int J Mol Sci, 25(2):714.

Hanahan, D. & Weinberg, R. A. (2011). Hallmarks of cancer: The next generation. Cell, 144(5), 646–674.

Hu, T., Yeh, J. E., Pinello, L., Jacob, J., Chakravarthy, S., Yuan, G.-C., Chopra, R., & Frank, D. A. (2015). Impact of the N-Terminal Domain of STAT3 in STAT3-Dependent Transcriptional Activity. Molecular and Cellular Biology, 35(19), 3284–3300.

Hutchins, A. P., Diez, D., & Miranda-Saavedra, D. (2013). Genomic and computational approaches to dissect the mechanisms of STAT3's universal and cell type-specific functions. JAK-STAT, 2(4), e25097.

Ivanov, V. N., Bhoumik, A., Krasilnikov, M., Raz, R., Owen-Schaub, L. B., Levy, D., Horvath, C. M., & Ev Ronai, Z. '. (2001). Whereas nu-clear factor-B (NF-B) activates Fas transcription. Mol Cell, 7(3):517-28.

Kobayashi, Y., & Mitsudomi, T. (2016). Not all epidermal growth factor receptor mutations in lung cancer are created equal: Perspectives for individualized treatment strategy. Cancer Sci, 107(9):1179-86.

Li, Y., Mao, T., Wang, J., Zheng, H., Hu, Z., Cao, P., Yang, S., Zhu, L., Guo, S., Zhao, X., Tian, Y., Shen, H., & Lin, F. (2023). Toward the next generation EGFR inhibitors: an overview of osimertinib resistance mediated by EGFR mutations in non-small cell lung cancer. In Cell Communication and Signaling 21(1):71.

Liu, W., Le, A., Hancock, C., Lane, A. N., Dang, C. V., Fan, T. W. M., & Phang, J. M. (2012). Reprogramming of proline and glutamine metabolism contributes to the proliferative and metabolic responses regulated by oncogenic transcription factor c-MYC. Proceedings of the National Academy of Sciences of the United States of America, 109(23), 8983–8988

Liu, W., & Phang, J. M. (2012). Proline dehydrogenase (oxidase) in cancer. In BioFactors, 38(6):398-406.

Liu, Y., Borchert, G. L., Surazynski, A., & Phang, J. M. (2008). Proline oxidase, a p53-induced gene, targets COX-2/PGE2 signaling to induce apoptosis and inhibit tumor growth in colorectal cancers. Oncogene, 27(53), 6729–6737.

Liu, Y., Borchert, G. L., Donald, S. P., Diwan, B. A., Anver, M., & Phang, J. M. (2009). Proline oxidase functions as a mitochondrial tumor suppressor in human cancers. Cancer Research, 69(16), 6414–6422.

Liu, Y., Mao, C., Liu, S., Xiao, D., Shi, Y., & Tao, Y. (2021). Proline dehydrogenase in cancer: apoptosis, autophagy, nutrient dependency and cancer therapy. Amino Acids, 53(12):1891-1902

Livak, K. J. & Schmittgen, T. D. (2001). Analysis of relative gene expression data using real-time quantitative PCR and the 2(-Delta Delta C(T)) Method. Methods,25(4):402-8.

Lo, H. W., Hsu, S. C., Ali-Seyed, M., Gunduz, M., Xia, W., Wei, Y., Bartholomeusz, G., Shih, J. Y., & Hung, M. C. (2005). Nuclear interaction of EGFR and STAT3 in the activation of the iNOS/NO pathway. Cancer Cell, 7(6), 575–589.

Lo, H. W., Hsu, S. C., Xia, W., Cao, X., Shih, J. Y., Wei, Y., Abbruzzese, J. L., Hortobagyi, G. N., & Hung, M. C. (2007). Epidermal growth factor receptor cooperates with signal transducer and activator of transcription 3 to induce epithelial-mesenchymal transition in cancer cells via up-regulation of TWIST gene expression. Cancer Research, 67(19), 9066–9076.

Loots GG, Ovcharenko I. (2004) rVISTA 2.0: evolutionary analysis of transcription factor binding sites. Nucleic Acids Res, 32(Web Server issue):W217-21.

Lynch, T. J., Bell, D. W., Sordella, R., Gurubhagavatula, S., Okimoto, R. A., Brannigan, B. W., Harris, P. L., Haserlat, S. M., Supko, J. G., Haluska, F. G., Louis, D. N., Christiani, D. C., Settleman, J., Haber, D. A., Departments of Medicine TJL, the, & General, M. (2004). Activating Mutations in the Epidermal Growth Factor Receptor Underlying Responsiveness of Non-Small-Cell Lung Cancer to Gefitinib. In n engl j med, 350(21):2129-39.

Makinoshima, H., Takita, M., Matsumoto, S., Yagishita, A., Owada, S., Esumi, H., & Tsuchihara, K. (2014). Epidermal growth factor receptor (EGFR) signaling regulates global metabolic pathways in EGFR-mutated lung adenocarcinoma. Journal of Biological Chemistry, 289(30), 20813–20823.

Makinoshima, H., Takita, M., Saruwatari, K., Umemura, S., Obata, Y., Ishii, G., Matsumoto, S., Sugiyama, E., Ochiai, A., Abe, R., Goto, K., Esumi, H., & Tsuchihara, K. (2015). Signaling through the phosphatidylinositol 3-kinase (PI3K)/mammalian target of rapamycin (mTOR) axis is responsible for aerobic glycolysis mediated by glucose transporter in epidermal growth factor receptor (EGFR)-mutated lung adenocarcinoma. Journal of Biological Chemistry, 290(28), 17495–17504.

Monteleone, E., & Poli, V. (2019). Where Sin3a meets STAT3: Balancing STAT3-mediated transcriptional activation and repression. Cancer Research, 79(12), 3031–3033.

Niu, G., Wright, K. L., Ma, Y., Wright, G. M., Huang, M., Irby, R., Briggs, J., Karras, J., Cress, W. D., Pardoll, D., Jove, R., Chen, J., & Yu, H. (2005). Role of Stat3 in Regulating p53 Expression and Function. Molecular and Cellular Biology, 25(17), 7432–7440.

Olivares, O., Mayers, J. R., Gouirand, V., Torrence, M. E., Gicquel, T., Borge, L., Lac, S., Roques, J., Lavaut, M. N., Berthezène, P., Rubis, M., Secq, V., Garcia, S., Moutardier, V., Lombardo, D., Iovanna, J. L., Tomasini, R., Guillaumond, F., Vander Heiden, M. G., & Vasseur, S. (2017). Collagen-derived proline promotes pancreatic ductal adenocarcinoma cell survival under nutrient limited conditions. Nature Communications, 8:16031.

Pandhare, J., Cooper, S. K., & Phang, J. M. (2006). Proline oxidase, a proapoptotic gene, is induced by troglitazone: Evidence for both peroxisome proliferator-activated receptor γ-dependent and -independent mechanisms. Journal of Biological Chemistry, 281(4), 2044–2052

Phang, J. M. (2019). Proline metabolism in cell regulation and cancer biology: Recent advances and hypotheses. In Antioxidants and Redox Signaling, 30(4):635-649.

Planck, M., Isaksson, S., Veerla, S., Staaf, J. (2013). Identification of transcriptional subgroups in EGFR-mutated and EGFR/KRAS wild-type lung adenocarcinoma reveals gene signatures associated with patient outcome. Clin Cancer Res. 19(18):5116-26.

Raimondi, I., Ciribilli, Y., Monti, P., Bisio, A., Pollegioni, L., Fronza, G., Inga, A., & Campomenosi, P. (2013). P53 Family Members Modulate the Expression of PRODH, but Not PRODH2, via Intronic p53 Response Elements. PLoS ONE, 8(7): e69152.

Rodriguez-Canales, J., Parra-Cuentas, E., & Wistuba, I. I. (2016). Diagnosis and molecular classification of lung cancer. In Cancer Treatment and Research, 170:25-46.

Song, L., Turkson, J., Karras, J. G., Jove, R., & Haura, E. B. (2003). Activation of Stat3 by receptor tyrosine kinases and cytokines regulates survival in human non-small cell carcinoma cells. Oncogene, 22(27), 4150–4165.

Sordella, R., Bell, D. W., Haber, D. A., & Settleman, J. (2004). Gefitinib-sensitizing EGFR Mutations in Lung Cancer Selectively Activate Anti-apoptotic Pathways. Science, 305(5687):1163-7.

Su, H., Bodenstein, C., Dumont, R. A., Seimbille, Y., Dubinett, S., Phelps, M. E., Herschman, H., Czernin, J., & Weber, W. (2006). Monitoring tumor glucose utilization by positron emission tomography for the prediction of treatment response to epidermal growth factor receptor kinase inhibitors. Clinical Cancer Research, 12(19), 5659–5667.

Tang, J., Hu, M., Lee, S., Roblin, R. (2000). A polymerase chain reaction based method for detecting Mycoplasma/Acholeplasma contaminants in cell culture. J Microbiol Methods, 39(2):121-6.

Tanner, J. J., Fendt, S. M., & Becker, D. F. (2018). The Proline Cycle As a Potential Cancer Therapy Target. Biochemistry, 57(25), 3433–3444.

Timofeeva, O. A., Tarasova, N. I., Zhang, X., Chasovskikh, S., Cheema, A. K., Wang, H., Brown, M. L., & Dritschilo, A. (2013). STAT3 suppresses transcription of proapoptotic genes in cancer cells with the involvement of its N-terminal domain. Proc Natl Acad Sci U S A, 110(4), 1267–1272.

Tošić, I. & Frank, D. A. (2021). STAT3 as a mediator of oncogenic cellular metabolism: Pathogenic and therapeutic implications. Neoplasia, ;23(12):1167-1178.

Weinstein, I. B., & Joe, A. (2008). Oncogene addiction. In Cancer Research (Vol. 68, Issue 9, pp. 3077–3080).

Yu, H., Lee, H., Herrmann, A., Buettner, R., Jove, R. (2014). Revisiting STAT3 signalling in cancer: new and unexpected biological functions. Nat Rev Cancer, 14(11):736-46.

Zhang, L., Zhao, X., Wang, E., Yang, Y., Hu, L., Xu, H., & Zhang, B. (2023). PYCR1 promotes the malignant progression of lung cancer through the JAK-STAT3 signaling pathway via PRODH-dependent glutamine synthesize. Translational Oncology, 32: 101667.

RESULTS -2-

The putative role of Proline Dehydrogenase (PRODH) in lung cancer cells acquired resistance to EGFR inhibitors

Priscilla Chiofalo[1], Elena Berno[1], Laura Pulze[1], Antonino Bruno[3,4], Vincenza Ciaramella[2, 5], Raffaella Cinquetti[1], Carminia Maria Della Corte[2], Floriana Morgillo[2] and Paola Campomenosi[1]

Affiliations

[1] University of Insubria, Department of Biotechnology and Life Sciences, DBSV, Via J.H. Dunant 3, 21100 Varese, Italy;

[2] University of Naples "L. Vanvitelli", Department of Precision Medicine, Via S. Pansini 5, 80131, Naples, Italy;

[3] Laboratory of Immunology and General Pathology, Department of Biotechnology and Life Sciences, DBSV, Via Monte Generoso 71, 21100 Varese, Italy;

[4] Laboratory of Innate Immunity, Unit of Molecular Pathology, Biochemistry, and Immunology, IRCCS MultiMedica, Via G Fantoli 16/15, 20138, Milan, Italy;

[5] IRCCS SYNLAB SDN, Via E. Gianturco 113, 80143 Naples, Italy.

ABSTRACT

Non-Small Cell Lung Cancer (NSCLC) is a highly heterogenous disease from a molecular and histological point of view. The high mutation burden of this type of tumor led to different therapeutic options, including targeted therapies and immunotherapies. EGFR alterations confer susceptibility to Tyrosine-Kinase Inhibitors (TKIs). However, the emergence of resistance mechanisms determines the failure of TKI treatment and disease relapse. Resistance is determined by the acquisition of specific additional mutations in the *EGFR* gene, such as the p.T790M, or from activation of alternative pathways, such as *MET* amplification. Peculiar transcriptome characterizes lung cancer cells with acquired resistance to EGFR TKIs. One such feature is the enrichment of genes related to the proline metabolism.

Proline dehydrogenase (PRODH) is a flavin-dependent enzyme localized to the inner mitochondrial membrane, catalyzing the first reaction of proline degradation.

The product, Δ-pyrroline-5-carboxylate is interconnected with the main metabolic cell pathways. Moreover, electrons derived from the reaction can be used for ATP or ROS production. Thus, PRODH plays a role either as an oncosuppressive or a pro-tumoral factor, based on the tumor type, the microenvironment, the type of stress acting on the cells and the genetic landscape.

Here, we describe an increased expression of PRODH in lung cancer cells with *in vitro* acquired resistance to EGFR TKIs, compared to their TKI-sensitive parental cell lines. We observed that HCC827-GR5 cells, which are resistant to gefitinib, were sensitive to PRODH inhibition or silencing. PRODH inhibition impaired 3D growth and the viability of EGFR mutant, TKI-resistant, lung cancer cells but not that of the TKI-sensitive counterpart. These findings suggest that PRODH plays a role in the development of resistance to TKIs and that its targeting concomitantly with treatment with TKIs could be a potential therapeutic strategy for lung cancer.

Introduction

Tumor cells reprogram their metabolism to obtain energy and building blocks required for their survival and growth. Metabolic adaptation is largely mediated by the alteration of oncogenes and oncosuppressor factors, including MYC and p53 (De Berardinis and Chandel, 2016; Phang et al., 2012). In a context-dependent manner, proline metabolism can provide energy and the amino acid for protein synthesis, recycle NADP for nucleotide biosynthesis, and control redox homeostasis under stress conditions (Burke et al., 2020; Phang et al., 2015). In fact, the peculiar structure of proline, with a secondary amine group enclosed into the pyrrolidine ring of the lateral chain, requires a unique set of enzymes for its metabolism, localized in the cytoplasm and mitochondria. Proline is synthesized from glutamate or ornithine by P5C synthase (P5CS) or ornithine δ-amino acid transferase (OAT), respectively (Tanner et al., 2018; Tanner, 2019).

The key enzyme in proline degradation is proline dehydrogenase (PRODH), localized to the inner mitochondrial membrane. This enzyme catalyzes proline oxidation to Δ-pyrroline-5-carboxylate (P5C). Proline-derived electrons are transferred to the electron transport chain to produce ATP. Alternatively, electrons can be used to reduce oxygen, resulting in the production of ROS species (Phang, 2010; Phang, 2019). The intermediate P5C can be transferred to the cytosol and recycled for proline synthesis by P5C reductases (PYCR), using reducing equivalents and oxidizing NAD(P)H to NAD(P) (Burke et al., 2020). This pathway supports the synthesis of pentoses, that can be used for nucleotide synthesis. In the mitochondria, the intermediate P5C can be used as a precursor of glutamate, or ornithine, by which proline catabolism is linked respectively to the Tricarboxylic Acid Cycle (TCA) and the urea cycle (Liu and Phang 2012).

PRODH has been recognized to contribute to cancer development, exhibiting either promoting or inhibitory roles on tumor growth. By increasing ROS production, PRODH induces cell cycle arrest, apoptosis, and senescence (Liu et al., 2005; Liu et al., 2006; Liu et al., 2009; Liu et al., 2012; Nagano et al., 2017). On the other hand, ROS

production can also induce autophagy, thus sustaining tumor growth in response to nutrient stress (Liu et al., 2012; Zareba et al., 2018). In addition, it provides ATP to support energetic needs for tumor growth and metastasis formation (Liu et al., 2012; Elia et al., 2017). The role of PRODH in lung cancer was previously investigated by Liu et al., who showed that PRODH promotes tumor growth, invasion, and the production of inflammatory cytokines (Liu et al., 2020).

Recently, during an immunohistochemical characterization of PRODH expression in lung cancer samples, our laboratory found high levels of PRODH in stage I-II adenocarcinoma. Patients with PRODH-positive tumors had a better prognosis compared to those with PRODH-negative tumors. Expression appeared to decrease at late stages of the disease. Moreover, we observed that restoration of PRODH expression in lung adenocarcinoma (ADC) cell lines affected tumor growth by inducing ROS production and cellular senescence (Grossi et al., 2024). In addition, in our previous experiments, we identified a negative correlation between EGFR and PRODH expression.

Epidermal growth factor receptor (EGFR) inhibitors have recently been introduced as effective treatments for lung cancer. There are three generations of inhibitors currently in clinical use. The first generation, which includes erlotinib and gefitinib, and the second generation, represented by afatinib, target the ATP-binding site of the receptor, inhibiting its activity. These targeted therapies have been effective in NSCLC patients whose tumors carry EGFR-activating mutations. However, the efficacy of EGFR inhibitors in clinical settings is restricted by the development of resistance mechanisms within 15 months from the start of administration. Approximately 50-60% of drug resistance mechanisms are attributable to the T790M mutation, occurring in exon 20 of *EGFR*. Nowadays, the third-generation TKI, osimertinib, represents the gold standard for treating lung ADCs with EGFR-activating mutations and the T790M resistance mutation. Nevertheless, the emergence of EGFR-dependent and independent resistance mechanisms determines treatment failure (Schmid et al., 2020; Du et al., 2021; Gkountakos et al., 2022).

Here, following the observation that PRODH expression is increased in TKI-resistant cell lines compared to their parental, TKI-sensitive counterpart, we aimed to investigate the possible role of PRODH in the onset of resistance of EGFR-mutant tumors. We show that EGFR-mutant, TKI-resistant, lung cancer cell lines are very sensitive to PRODH inhibition or silencing during 2D and 3D cultures.

Materials and Methods

Cell lines, culture conditions and treatment

Human lung ADC cell lines HCC827 and HCC827-GR5, a derivative of HCC827 resistant to Gefitinib, were obtained from University of Parma; PC9 and the Osimertinib Resistant PC9-OR derivative cells were obtained from Prof. Ciardiello's group (University of Naples "Luigi Vanvitelli"). HCC827 and PC9 cells were cultured in RPMI-1640 medium, supplemented with 10% of FBS and 2mM di L-glutamine, whereas HCC827-GR5 and PC9-OR were maintained in RPMI-1640 complete medium supplemented respectively with osimertinib (27μM) or gefitinib (1μM) to keep a selection pressure during *in vitro* propagation.

All the cells were grown at 37°C under 95% humidity and 5% CO_2. Cells were passaged for no more than one month after thawing. Absence of mycoplasma was routinely checked by the method described in Tang et al. (Tang et al., 2000). Media and reagents for cell culture were obtained from Euroclone (Milan, Italy).

HCC827-GR5 ($0{,}35x10^6$) cells were seeded in 60 mm Petri dishes. After 24 hours, cells were treated with 6,8mM of L-tetrahydro-2-furoic acid, L-THFA (SC-253674, Aurogene, Rome, Italy), a reversible inhibitor of PRODH, and then collected after 10, 24, and 48 hours for protein and RNA analysis.

PRODH silencing

HCC827 and HCC827-GR5 cells were seeded in 96-well plates at a density $5x10^3$ cells/well. The day after, cells were silenced using 50nM of ON-TARGETplus Smart Pool siRNA against PRODH (L-009543-00) and its control siRNA (D-001810-10) (Dharmacon, Aurogene, Rome, Italy). Silencing was performed using Lipofectamine

2000 reagent (ThermoFisher Scientific, Milan, Italy) according to the manufacturer's instructions. Subsequently, silenced cells were used for MTT assay.

Immunoblotting

To prepare protein extracts, cells were scraped in Phosphates Buffer Saline (PBS) (Euroclone, Milan, Italy), centrifuged, and then resuspended in RIPA buffer (150mM NaCl, 50mM Tris-HCl pH 7.5, 1% Igepal CA630, 0.1% SDS, and 0.5% Sodium deoxycholate), supplemented with protease and phosphatase inhibitors (PMSF, aprotinin, pepstatin, sodium orthovanadate). After incubating for 45 minutes at 4ºC with gentle rotation, the extracts were centrifuged at 15000xg for 5 minutes at 4ºC. The supernatant was transferred to new tubes. Protein concentration was measured using The Quick Start Bradford 1x Dye Reagent (Biorad, Milan, Italy), using bovine serum albumin for the standard curve. For SDS-PAGE 35µg of extracts were used. Samples were separated by SDS-PAGE and transferred to nitrocellulose membranes (Amersham Hybond ECL, GE Healthcare Life Sciences, by Euroclone, Milan, Italy) using the Mini-PROTEAN Tetra System (Biorad, Milan, Italy). After blocking with 4% non-fat milk in PBS-T (0,1% Tween20 in PBS), specific antibodies were used to identify target proteins. The following primary antibodies were used: fibronectin (1:20000, #F3648, Sigma-Aldrich,), E-cadherin (1:1000, #5296, CST), caspase-9 (1:1000, #9502, CST), caspase-8 (1:1000, #9746, CST) For normalization, α-tubulin (1:2000, T9026, Sigma-Aldrich) was used. Subsequently, the membranes were incubated with goat anti-rabbit HRP-conjugated antibody or anti-mouse HRP-conjugated antibody as appropriate, both diluted 1:900 (ThermoFisher Scientific, Milan, Italy). Each antibody was diluted in 2% non-fat milk in PBS-T. Immunocomplexes were detected with the enhanced chemiluminescent system Westar ηC ultra 2.0 (Cyanagen, Bologna, Italy) and the Odyssey Li-COR FC imaging system.

Cell proliferation assay

HCC827-GR5 cells were seeded in 96-well plates at $5x10^3$ cells/well and treated with 0; 2,5; 5; 7,5; 10 and 15mM of L-THFA (SC-253674, Santa Cruz Biotechnology,

Aurogene, Milan, Italy) for 72 hours. Then 3-[4,5-dimethylthiazol-2-yl]-2,5 diphenyl tetrazolium bromide (MTT) assay was performed.

After 24, 48, and 72 hours from silencing, cell proliferation of HCC827 and HCC827-GR5 was assessed by MTT assay.

For the MTT assay, cells were first washed with PBS, and then MTT working solution was added to each well (0,5mg/ml in RPMI-1640). After incubating for over 2 hours, the MTT was removed. Each well was washed with PBS and then incubated with DMSO (dimethyl sulfoxide, Euroclone, Milan, Italy) for 30 minutes to dissolve the MTT crystals. The absorbance was measured at 595nm using the Tecan Infinite 200Pro plate reader (Tecan, Cernusco sul Naviglio, Italy).

RNA extraction and RT-qPCR

Total RNA was isolated using TRI Reagent (Merck-Sigma Aldrich, Milan, Italy). RNA was reverse transcribed using the iScript cDNA synthesis kit (Biorad, Milan, Italy). To generate total first-strand cDNA, iScript reaction mix, RNase H+ MMLV reverse transcriptase, and RNA (500ng) were mixed into a PCR tube. The reaction was performed at 25°C for 5 minutes, 43°C for 30 minutes, 43°C for 15 minutes and 85°C for 5 minutes in T100 thermal cycler (Biorad, Milan, Italy). Then, cDNA was diluted with distilled water and stored at −20°C.

Relative levels of gene transcripts were determined by quantitative PCR using a CFX Connect real-time PCR instrument (Biorad, Milan, Italy), iTaq Universal Sybr Green (Biorad, Milan, Italy), and primers specific for the targets of interest.

The following primers were used:

PUMA (forward: 5'-TGGAGGGTCCTGTACAATCTCA-3' and reverse: 3'-TCTGTGGCCCCTGGGTAAG-3'),

p21 (forward: 5'-CTGGAGACTCTCAGGGTCGAAA-3' and reverse: 5'-GATTAGGGCTTCCTCTTGGAGAA-3'),

Bcl-2 (forward: 5'-TTGTGGCCTTCTTTGAGTTCGG-3' and reverse: 5'-GTGCCGGTTCAGGTACTCAG-3'),

SNAIL (forward: 5'-CGAGCCCAGGCAGCTATTTC-3' and reverse: 5'-CCCGACAAGTGACAGCCATT-3'),

Fibronectin (forward: 5'-ACCGTGGGCAACTCTGTCAA-3' and reverse: 5'-CCCACTCATCTCCAACGGCA-3') and

β2M reference gene (forward: 5'- ATGGATGAAACCCAGACACA-3' and reverse: 5'-AGGCTATCCAGCGTACTCCA-3').

Oligonucleotides were ordered from Metabion International AG. All reaction mixes were prepared and dispensed into the wells of a qPCR plate, and cDNA samples were added. Three replicates were prepared for each sample and target. Blanks, containing nuclease-free water instead of cDNA, were included. qPCR run using a CFX Connect real-time PCR instrument (Biorad, Milan, Italy). Specificity of amplification was confirmed by melting curve analysis. Fold change in transcript levels was calculated by the $2^{-\Delta\Delta Ct}$ method (Livak and Schmittgen, 2001).

Spheroid formation

HCC827-GR5 cells and their parental cell line were seeded in a 96-multiwell plate with highly anti-adhesive properties (BIOFLOAT, Sarstedt, Trezzano sul Naviglio (MI), Italy) at $5x10^3$ cells/well. When spheroids had formed, 24 hours later, they were treated with 6,8mM of L-THFA or vehicle (PBS) and cultured for 17 days, replacing half of the medium every 3 days. Spheroid images were taken daily. The mean diameter of the cultured spheroids was calculated on days 1, 7, and 14. The average size of the cultured spheroids was reported as mean diameter ± SE.

Measurement of spheroid viability by live/dead assay

The viability of HCC827-GR5 spheroids treated with L-THFA compared to vehicle-treated spheroids was determined by the Live/Dead assay (R37601, ThermoFisher Scientific, Milan, Italy). On day 17, spheroids were collected in a tube and centrifuged at 800xg for 5 minutes. Then standard complete medium was replaced with RPMI-1640 without serum and phenol red. After 20 minutes, almost all medium was

discarded and then Live/Dead staining was added into the tube, according to the manufacturer's instructions. Spheroids were incubated for 30 minutes at 37°C. Subsequently, spheroids were centrifuged, live/dead staining was removed by an additional washing step with RPMI-1640 medium without serum and phenol red, and spheroids were prepared for confocal microscopy analysis.

Confocal microscopy analysis

Cells were counterstained with the far-red fluorescent probe DRAQ5 10μM (Thermo Scientific, Milan Italy) in PBS for 20 minutes and then mounted with Citifluor (Citifluor Ltd., London, UK). Images were obtained using an inverted laser scanning confocal microscope (TCS SP5, Leica Microsystems, Wetzlar, Germany), equipped with a 40x/1.3 immersion objective.

Confocal image stacks (ten sections with optimized thickness) were acquired using the Leica TCS software (Leica Microsystems) with a sequential mode. The images were mounted with Adobe Photoshop (Adobe Systems, San Jose, CA, USA).

Statistical analysis

The significance of the difference in PUMA, p21, Snail, Fibronectin mRNA levels from cells treated with L/THFA at different time points compared to mock condition, evaluated by qPCR, was calculated by applying two-tailed t-test. The difference in absorbance between PRODH or control silenced (scrambled) cells, as evaluated by MTT assay, was determined by the two-tailed t-test. The diameter of L-THFA spheroids was compared to mock-treated spheroids by the multiple t-test. Data were analyzed using GraphPad Prism8 (San Diego, CA, USA).

Results

EGFR-mutated, TKI-resistant, lung cancer cells upregulate PRODH expression

In our previous study, we observed an increased PRODH expression in the TKI-resistant cell line, HCC827-GR5, compared to HCC827 cells at both transcript and protein levels (Grossi et al., 2024). To address if this was a general feature of TKI-

resistant cells, we investigated PRODH expression in the osimertinib-resistant cells PC9-OR compared to their parental cells (PC9) by immunoblotting. PC9-OR cells were previously developed by some of us at the University of Naples “Luigi Vanvitelli”.

In line with what was observed with HCC827-GR5, we found that PRODH expression levels were increased in PC9-OR compared to parental cells (Figure 1A).

In our previous study (Results -1-), we observed an increase in PRODH expression following osimertinib treatment in EGFR-mutated lung cancer cell lines. Hence, we aimed to determine whether PRODH played a role in the development of resistance or whether its expression depended on EGFR inhibition. Thus, we cultured HCC827-GR5 cells in the absence of gefitinib for extended periods, namely 3, 10, and 20 days.

Immunoblot results showed that the absence of selective pressure did not lead to a decrease in PRODH expression when compared to cells cultured with gefitinib (Figure 1B). Thus, PRODH may play a role in the development or maintenance of acquired resistance to TKI inhibitors.

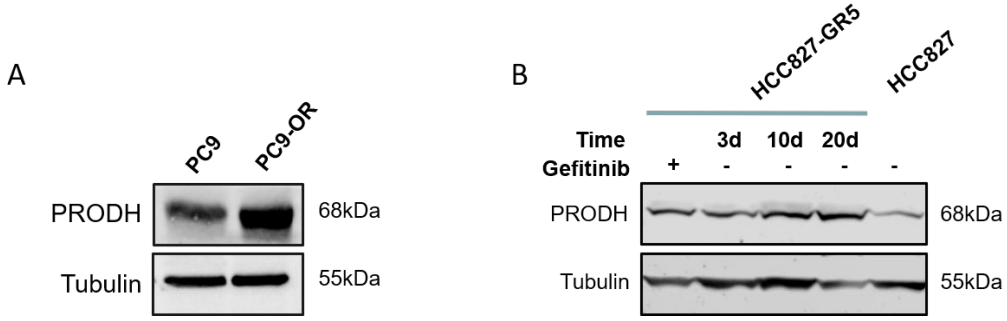

Figure 1. EGFR-mutated, TKI-resistant, lung cancer cells upregulated PRODH expression independently of the presence of TKIs. PRODH expression was checked in PC9-OR EGFR-mutant, TKI-resistant, lung adenocarcinoma cells compared to the parental cell line (A) and in HCC827-GR5 cells grow without gefitinib for 3, 10, and 20 days (B). Protein extracts were analyzed by immunoblotting for PRODH expression and α-tubulin was used for normalization.

PRODH inhibition affects the proliferation ability of EGFR-mutated, TKI-resistant, lung cancer cells

To examine the possible role of PRODH in the development of resistance to TKIs, we treated HCC827-GR5 cells with increasing doses of L-THFA, a reversible PRODH inhibitor. PRODH inhibition affected cell proliferation in HCC827-GR5 cells, as shown

by the MTT assay (Figure 2A). As a complementary approach, we silenced the expression of PRODH in HCC827-GR5 and their parental cells for 24, 48 or 72 hours. PRODH silencing resulted in decreased proliferation of EGFR-mutated, TKI-resistant, lung cancer cells compared to scrambled siRNA-treated cells, but did not affect the proliferation ability of HCC827 cells (Figure 2B). These results confirmed that the TKI-resistant cell line is more sensitive to PRODH inhibition or silencing than its parental, TKI-sensitive counterpart.

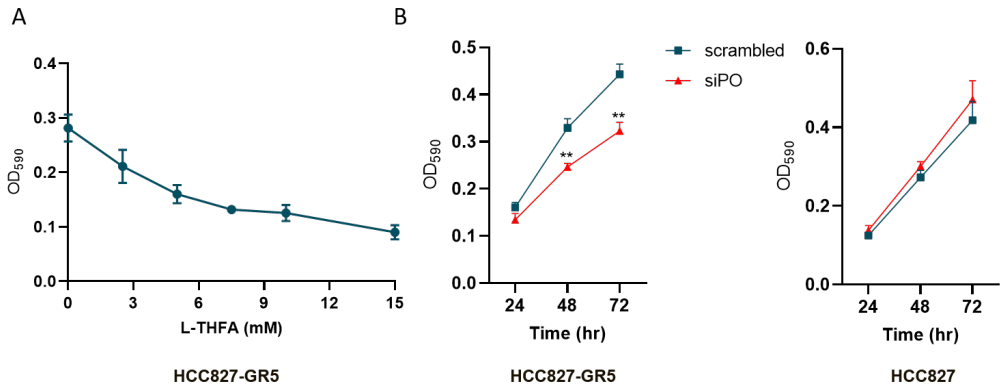

Figure 2. PRODH inhibition or silencing affects the proliferation ability of EGFR-mutated, TKI-resistant, lung cancer cells. A) HCC827-GR5 cells were treated with increasing concentrations of the PRODH inhibitor, L-THFA. After 72 hours, the cell proliferation ability was tested by MTT assay. The graph is representative of three independent experiments ± Standard error (SE). B) HCC827 and HCC827-GR5 cells were transfected with siRNA targeting PRODH or with a scrambled control siRNA. The MTT assay was performed at 24, 48, and 72 hours from silencing. The graph is representative of two independent experiments. Asterisks represent significant differences in the growth of PRODH-silenced cells compared to scrambled (**p<0.01, two-tailed t-test).

PRODH inhibition influences the expression of cell cycle arrest and EMT markers in HCC827-GR5 cells

To determine whether PRODH affected cell cycle arrest, apoptosis, or changes in Epithelial-Mesenchimal Transition (EMT) markers in EGFR-mutated TKI-resistant cell lines, we inhibited PRODH in HCC827-GR5 for different time points (Figure 3). After 48 hours of treatment, there was a noticeable increase in the protein level of cleaved-caspase 8 in L-THFA-treated compared to vehicle-treated HCC827-GR5 cells (Figure 3A).

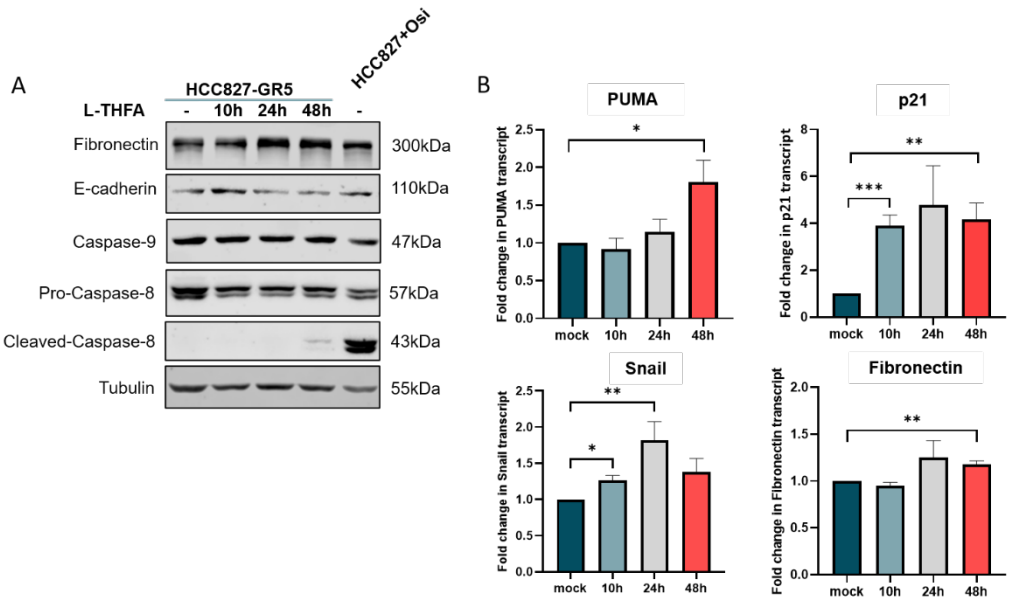

Figure 3. PRODH inhibition influences the expression of cell cycle arrest and EMT markers in HCC827-GR5 cells. HCC827-GR5 cells were treated with L-THFA (6,8mM) for 10, 24, and 48 hours. Protein samples were then prepared and analyzed by immunoblot (A) for Fibronectin, E-cadherin, caspase-9, and caspase-8 proteins. α-tubulin was used for normalization. A representative immunoblot is shown. RNA samples were analyzed by qRT-PCR (B) for expression of PUMA, p21, Snail, and Fibronectin mRNAs. The graphs represent the mean of n=2 independent experiments ± SE (*p<0.05, **p<0.01, ***p<0.001, two-tailed t-test).

We also observed an increase in PUMA mRNA, a pro-apoptotic marker, in L-THFA-treated cells at 48 hours. Moreover, a significant increase in p21 transcript, a marker of cell cycle arrest, was observed starting from 10 hours after treatment with L-THFA compared to vehicle-treated cells. The increase was maintained also at later times. The reduced survival and proliferation observed during PRODH inhibition may thus be caused by a combination of growth arrest and apoptosis induction. Furthermore, the levels of Snail transcript (a key marker of EMT) and fibronectin (also involved in EMT) transcript and protein were increased in HCC827-GR5 cells after treatment with L-THFA (Figure 3, A and B), whereas E-cadherin protein (epithelial protein) was slightly decreased (Figure 3A). Thus, PRODH could potentially regulate the invasive properties of TKI-resistant, EGFR-mutated lung cancer cells, but further investigations are necessary to confirm this result.

PRODH inhibition affects the 3D-growth ability and the viability of EGFR-mutated, TKI-resistant, lung cancer cells

The putative role of PRODH in the acquisition of TKI-resistance of EGFR-mutant lung cancer cells during 3D growth was investigated in HCC827-GR5 and their corresponding parental cells after PRODH inhibition. Cell spheroids were cultured with L-THFA or vehicle (PBS) for 17 days after spheroid formation. Morphology differences were observed during the treatment. Vehicle treated HCC827-GR5 spheroids grew steadily during this period. When treated with L-THFA, HCC827-GR5 spheroids showed a less compact cell core compared to vehicle-treated cells, starting from a few days after inhibition (Figure 4A). Instead, vehicle-treated HCC827 spheroids showed a small compact core and irregular edges compared with L-THFA-treated spheroids (Figure 4C). Importantly, inhibition of PRODH hampered the 3D growth of HCC827-GR5 spheroids in comparison to vehicle-treated cells, as underlined by the difference in the diameter of spheroids after 7 and 14 days of treatment (Figure 4B), whereas treatment with L-THFA seemed to increase the growth ability of HCC827 parental cells compared to the same cells treated with vehicle after 14 days of treatment (Figure 4D). Our data suggest that inhibition of PRODH has different effects on EGFR-mutated TKI-resistant and TKI-sensitive cells.

Altogether, our data suggest that PRODH inhibition has a different effect on EGFR-mutated TKI-resistant cells, where it restricts the growth ability, compared to their EGFR-mutated, TKI-sensitive counterpart, where growth ability is stimulated.

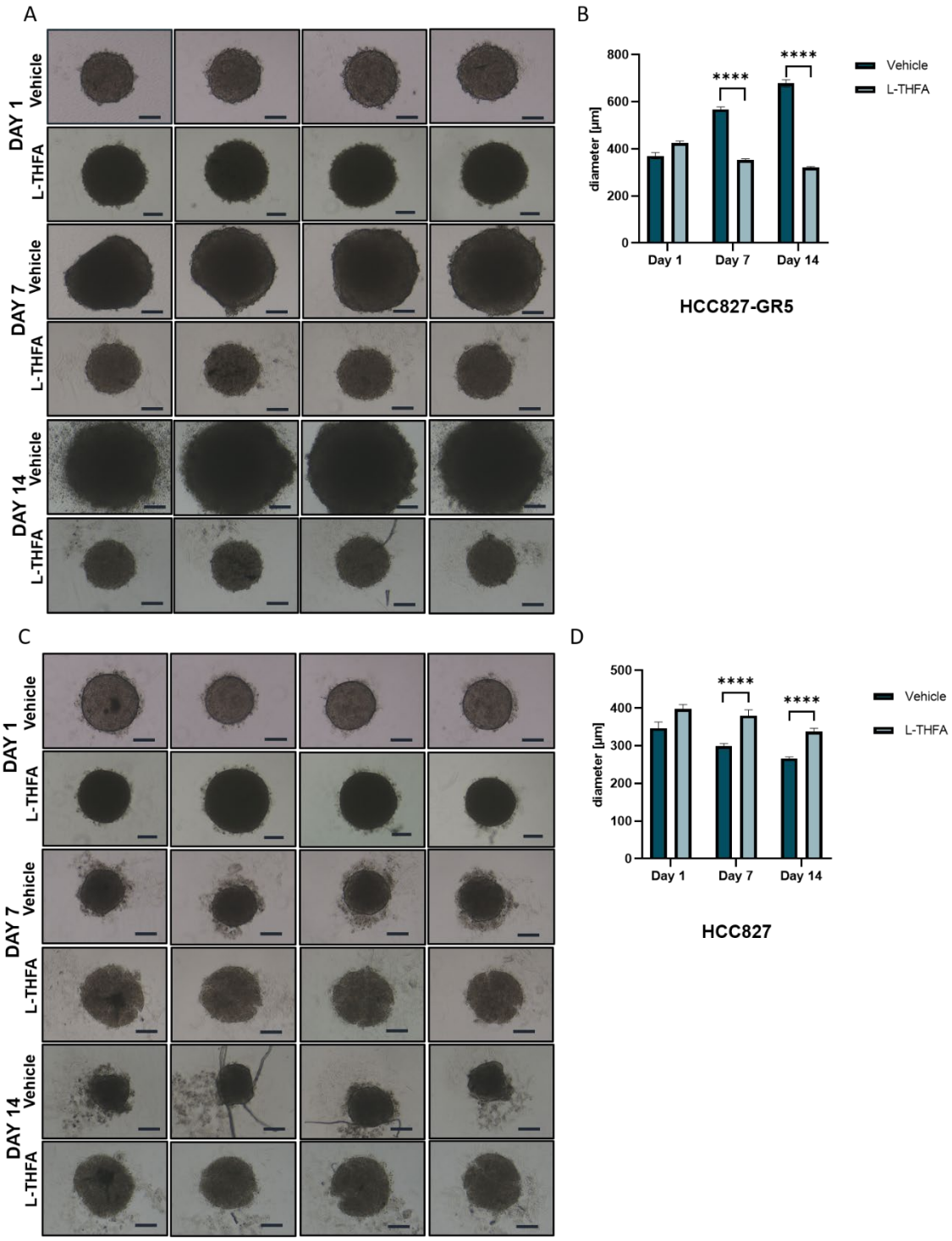

Figure 4. PRODH inhibition affects the ability to grow of EGFR-mutated, TKI-resistant, lung cancer cells. Representative images of HCC827-GR5 (A) and HCC827 (C) spheroids on days 1, 7, and 14 days are

shown. Magnification 40x. The bar indicates 143μm. HCC827 and HCC827-GR5 cells were seeded into a 96-multiwell with anti-adhesive properties to allow for spheroids formation. Then, they were treated with L-THFA (6,8mM) for 17 days. The diameter of each spheroid for HCC827-GR5 (B) and HCC827 (D) was calculated and compared to mock-treated spheroids, as shown by the graph. The graphs represent the mean of n=3 independent experiments ± SE (****p<0.0001, multiple t-test).

To address if the decrease in 3D growth of HCC827-GR5 spheroids treated with L-THFA in comparison to vehicle-treated cells was determined by a reduced cell viability, we performed the live/dead assay. We observed an alteration of membrane integrity in PRODH-inhibited spheroids, as evidenced by an increased diffuse red signal (indicating dead cells) and a smaller number of live cells (green signal) in comparison to vehicle-treated spheroids. According to the hypoxic and necrotic area, which is characteristic of larger spheroids (Däster et al., 2017), vehicle-treated spheroids exhibited an increase in red signal at the core level (Figure 5). In conclusion, our experiment confirmed that PRODH inhibition affected the ability of EGFR mutated, TKI-resistant HCC827-GR5 cells to grow and form 3D spheroids, by compromising their viability.

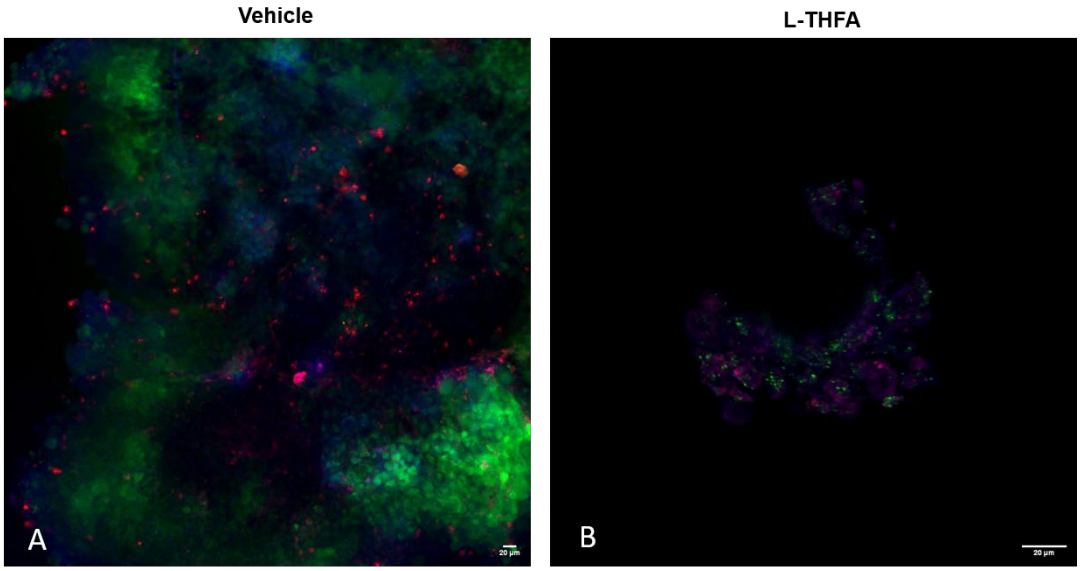

Figure 5. PRODH inhibition affects the viability of EGFR-mutated, TKI-resistant, lung cancer cells. HCC827-GR5 cells were seeded into a 96-multiwell with anti-adhesive properties to allow for spheroids formation. When spheroids had formed (24 hours later), they were treated with L-THFA (6,8mM) for 17 days. On day 17, they were stained with live/dead staining agent and imaged with the Leica TCS SP5, confocal microscope. The image stacks (ten sections with optimized thickness) were acquired using the Leica TCS software (Leica Microsystems) with a sequential mode. Magnification 200x. Representative

images of vehicle-treated HCC827-GR5 spheroids (A) and L-THFA-treated spheroids (B) are shown. In the image, live cells are shown in green, dead cells in red and nuclei in blue.

Discussion

The discovery that tumors with EGFR mutations are dependent on this oncogene and its downstream signaling for survival, and that inhibiting its function with TKIs restrains tumor progression, has greatly advanced the treatment of lung cancer. This has led to a significant improvement in patient survival rates and tolerance to therapy. However, resistance mechanisms arise in the medium to long term. Approximately 50-60% of acquired-resistant cases to the first-generation EGFR inhibitors are attributed to the T790M EGFR mutation. Other resistance mechanisms, both EGFR-dependent and independent, determine therapy failure (Du et al., 2021; Wei et al., 2020). EGFR-dependent mechanisms include mutation at exons 18 (the most frequent of which is L718Q), 19 (L844V mutation), 20 (such as the C797 mutation), *EGFR* amplification, and defective receptor degradation (Du et al., 2021). In addition, the activation of other bypass pathways, mediated by *MET*, *HER2*, and *IGFR1* amplification, the EMT, and transformation into small-cell lung cancer have been also identified as resistance mechanisms (Du et al., 2021). Moreover, gene expression and metabolic reprogramming have been described in EGFR mutant, TKI-resistant tumors (Li et al., 2021; Wei et al., 2020). Identifying new targets that have the potential to resensitize cancer cells to EGFR inhibitors, or novel prognostic biomarkers are key to improving lung cancer treatment.

In this scenario, we showed that PRODH expression was stably increased in EGFR-mutant lung cancer cells with *in-vitro* acquired resistance to TKIs, suggesting a putative role for the mitochondrial flavoenzyme in the onset of resistance. Our hypothesis was in line with the enrichment in the p53 pathway, hypoxia, and arginine and proline metabolism shown in PC9 gefitinib-resistant cells compared to their parental cells previously described (Wei et al., 2020).

PRODH, which is the first enzyme in proline degradation, exhibits a dual role in tumor development. It induces cell deaths in colorectal and renal cancer via ROS production. PRODH expression is downregulated in these tumors types, as well as in

hepatocarcinoma samples (Maxwell and Rivera, 2003; Liu et al., 2005; Liu et al., 2006, Liu et al., 2008; Liu et al., 2009; Ding et al., 2020), where it is associated with a tumor suppressor role. On the other side, PRODH promotes tumor growth under nutrient deprivation in pancreatic cancer (Olivares et al., 2017), it influences tumor growth and T cell infiltration in prostate cancer, and EMT in lung cancer (Olivares et al., 2017; Yan et al., 2018; Liu et al., 2020). Furthermore, PRODH effects may be different depending on the stage of the tumor, as it appears in breast cancer. Its upregulation mediates apoptosis of the MCF7 breast cancer cell line (Zareba et al., 2018). PRODH expression has also been shown to promote 3D growth *in vitro* and metastasis formation *in vivo* of breast cancer cells (Elia et al., 2017).

Here, we demonstrated that PRODH silencing/inhibition affected the proliferation ability of HCC827-GR5 TKI-resistant cells, but did not influence the proliferation of their TKI-sensitive parental cells. These effects appeared to be mediated by induction of cell cycle arrest and apoptosis, as shown by the expression of markers specific to these processes. One may speculate that PRODH is an important effector of EGFR induced survival and proliferation in TKI-resistant lung cancer cells, but further investigations are needed to test this hypothesis.

It is recognized that monolayer cultures are not sufficiently representative of the hypoxic and necrotic tumor environment, which is often critical in the acquisition of therapy resistance (Däster et al., 2017).

Moreover, differences in proline metabolism between 2D and 3D cultures were observed in cellular models from other tumor types (Elia et al., 2017; Choi et al., 2020). When we investigated the effects of PRODH inhibition on 3D growth, we found that L-THFA treatment also impaired the 3D growth ability of HCC827-GR5 spheroids, whereas it weakly supported the 3D growth ability of parental cells in comparison to vehicle-treated cells, according to our previous data (Grossi et al., 2024). Moreover, PRODH inhibition also affected the proportion of live/dead cells during spheroid formation. These data suggested a putative role for PRODH during progression of advanced-stage lung cancer, like that observed in breast cancer (Elia et al., 2017) and during the onset of TKI resistance.

The mechanism by which PRODH expression may promote survival and growth under the selective pressure of EGFR inhibitors has yet to be characterized.

We previously demonstrated that PRODH can induce cellular senescence in lung ADC cells (Grossi et al., 2024). It is known that different drugs have a critical role in senescence, as well as the inhibition of oncogenic factors. By secreting a wide range of growth factors, cytokines, and chemokines (referred to as the senescence-associated secretory phenotype, SASP), senescent cells exert a dual role, as they can either suppress tumor growth or mediate tumor progression. The different role is also influenced by the stage of the tumor (Eggert et al., 2016; Calcinotto et al., 2019; Abuawad et al., 2020).

The role of PRODH in the regulation of the tumor microenvironment composition has been demonstrated in lung cancer cell lines, and in prostate cancer (Yan et al., 2018; Liu et al., 2020). In addition, the metabolism of non-essential amino acids, including proline, is fundamental for M2 macrophages (Abuawad et al., 2020; Burke et al., 2020). Given this background, it is plausible that PRODH may contribute to tumor resistance, inducing senescence and modulating the tumor microenvironment.

It has been previously demonstrated that ATP production and the proline cycle can sustain cancer cell growth during tumor development (Elia et al., 2017; Olivares et al., 2017; Zareba et al., 2018). Similarly, these processes may play a role in supporting lung cancer cell growth in late-stage tumors.

In summary, our data suggest that PRODH inhibition impaired 2D and 3D growth in EGFR mutant, TKI-resistant cells. Further investigations are warranted to clarify the mechanism by which L-THFA impairs tumor growth and to verify the effects of associating PRODH inhibitor with TKI therapy on tumor growth *in vivo* in animal models. For this purpose, we will also investigate the possibility of sensitizing cancer cells to therapy by using PRODH irreversible inhibitors (*N*-propargylglycine) (Scott et al., 2019).

Our study has some limitations: first of all, we carried out most of the experiments on a single lung ADC cell line resistant to TKIs. Indeed, we are developing other TKI resistant cell lines to verify that our findings regarding a role of PRODH in the resistance to TKI

of lung ADC cell lines represent a general feature. A second limitation is that all experiments were carried out *in vitro*. The use of appropriate GEMMs could help to shed light on the role of PRODH in TKI resistance.

A full understanding of the PRODH role in lung tumorigenesis and TKI resistance needs further investigation. Indeed, from the data shown here and in our previous work, it appears that PRODH may exert different roles in early- and late-stage lung cancer.

References

Abuawad, A., Mbadugha, C., Ghaemmaghami, A. M., & Kim, D. H. (2020). Metabolic characterization of THP-1 macrophage polarisation using LC–MS-based metabolite profiling. Metabolomics, 16(3):33.

Burke, L., Guterman, I., Palacios Gallego, R., Britton, R. G., Burschowsky, D., Tufarelli, C., & Rufini, A. (2020). The Janus-like role of proline metabolism in cancer. In Cell Death Discovery, 6:104.

Calcinotto, A., Kohli, J., Zagato, E., Pellegrini, L., Demaria, M., & Alimonti, A. (2019). Cellular Senescence: Aging, Cancer, and Injury. Physiol Rev, 99, 1047–1078.

Choi, U. Y., Lee, J. J., Park, A., Zhu, W., Lee, H. R., Choi, Y. J., Yoo, J. S., Yu, C., Feng, P., Gao, S. J., Chen S., Eoh, H., Jung, J. U. (2020). Oncogenic human herpesvirus hijacks proline metabolism for tumorigenesis. 117(14) 8083-8093.

Däster, S., Amatruda, N., Calabrese, D., Ivanek, R., Turrini, E., Droeser, R. A., Zajac, P., Fimognari, C., Spagnoli, G. C., Iezzi, G., Mele, V., & Muraro, M. G. (2017). Induction of hypoxia and necrosis in multicellular tumor spheroids is associated with resistance to chemotherapy treatment. In Oncotarget, 8(1):1725-1736.

De Berardinis, R. J., & Chandel, N. S. (2016). Fundamentals of cancer metabolism. In Science Advances 2(5):e1600200.

Ding, Z., Ericksen, R. E., Escande-Beillard, N., Lee, Q. Y., Loh, A., Denil, S., Steckel, M., Haegebarth, A., Wai Ho, T. S., Chow, P., Toh, H. C., Reversade, B., Gruenewald, S., & Han, W. (2020). Metabolic pathway analyses identify proline biosynthesis pathway as a promoter of liver tumorigenesis. Journal of Hepatology, 72(4), 725–735.

Du, X., Yang, B., An, Q., Assaraf, Y. G., Cao, X., Xia, J. Acquired resistance to third-generation EGFR-TKIs and emerging next-generation EGFR inhibitors. Innovation (Camb), 2(2): 2(2):100103.

Eggert, T., Wolter, K., Ji, J., Ma, C., Yevsa, T., Klotz, S., Medina-Echeverz, J., Longerich, T., Forgues, M., Reisinger, F., Heikenwalder, M., Wang, X. W., Zender, L., & Greten, T. F. (2016). Distinct Functions of Senescence-Associated Immune Responses in Liver Tumor Surveillance and Tumor Progression. Cancer Cell, 30(4), 533–547.

Elia, I., Broekaert, D., Christen, S., Boon, R., Radaelli, E., Orth, M. F., Verfaillie, C., Grünewald, T. G. P., & Fendt, S. M. (2017). Proline metabolism supports metastasis formation and could be inhibited to selectively target metastasizing cancer cells. Nature Communications, 8:15267.

Gkountakos, A., Centonze, G., Vita, E., Belluomini, L., Milella, M., Bria, E., Milione, M., Scarpa, A., & Simbolo, M. (2022). Identification of Targetable Liabilities in the Dynamic Metabolic Profile of EGFR-Mutant Lung Adenocarcinoma: Thinking beyond Genomics for Overcoming EGFR TKI Resistance. Biomedicines, 10(2):277.

Grossi, S., Berno, E., Chiofalo, P., Chiaravalli A.M., Cinquetti, R., Bruno, A., Palano, M.T., Gallazzi, M., La Rosa, S., Sessa, F., Acquati, F., Campomenosi, P.. (2024). Proline Dehydrogenase (PRODH) Is Expressed in Lung Adenocarcinoma and Modulates Cell Survival and 3D Growth by Inducing Cellular Senescence. Int J Mol Sci, 25(2):714.

Li, N., Mao, W., Gao, Y., Wang, D., Song, Z., & Chen, Z. (2021). Liquid chromatography-mass spectrometry based metabolic characterization of pleural effusion in patients with acquired EGFR-TKI resistance. Journal of Pharmaceutical and Biomedical Analysis, 202:114147.

Liu, W., Glunde, K., Bhujwalla, Z. M., Raman, V., Sharma, A., & Phang, J. M. (2012). Proline oxidase promotes tumor cell survival in hypoxic tumor microenvironments. Cancer Research, 72(14), 3677–3686.

Liu, Y., Borchert, G. L., Donald, S. P., Diwan, B. A., Anver, M., & Phang, J. M. (2009). Proline oxidase functions as a mitochondrial tumor suppressor in human cancers. Cancer Research, 69(16), 6414–6422.

Liu, Y., Borchert, G. L., Donald, S. P., Surazynski, A., Hu, C. A., Weydert, C. J., Oberley, L. W., & Phang, J. M. (2005). MnSOD inhibits proline oxidase-induced apoptosis in colorectal cancer cells. Carcinogenesis, 26(8), 1335–1342.

Liu, Y., Borchert, G. L., Surazynski, A., Hu, C. A., & Phang, J. M. (2006). Proline oxidase activates both intrinsic and extrinsic pathways for apoptosis: The role of ROS/superoxides, NFAT and MEK/ERK signaling. Oncogene, 25(41), 5640–5647.

Liu, Y., Borchert, G. L., Surazynski, A., & Phang, J. M. (2008). Proline oxidase, a p53-induced gene, targets COX-2/PGE2 signaling to induce apoptosis and inhibit tumor growth in colorectal cancers. Oncogene, 27(53), 6729–6737.

Liu, Y., Mao, C., Wang, M., Liu, N., Ouyang, L., Liu, S., Tang, H., Cao, Y., Liu, S., Wang, X., Xiao, D., Chen, C., Shi, Y., Yan, Q., & Tao, Y. (2020). Cancer progression is mediated by proline catabolism in non-small cell lung cancer. Oncogene, 39(11), 2358–2376.

Livak, K. J. & Schmittgen, T. D. (2001). Analysis of relative gene expression data using real-time quantitative PCR and the 2(-Delta Delta C(T)) Method. Methods,25(4):402-8.

Maxwell, S. A., & Rivera, A. (2003). Proline oxidase induces apoptosis in tumor cells, and its expression is frequently absent or reduced in renal carcinomas. Journal of Biological Chemistry, 278(11), 9784–9789.

Nagano, T., Nakashima, A., Onishi, K., Kawai, K., Awai, Y., Kinugasa, M., Iwasaki, T., Kikkawa, U., & Kamada, S. (2017). Proline dehydrogenase promotes senescence through the generation of reactive oxygen species. Journal of Cell Science, 130(8), 1413–1420. https://doi.org/10.1242/jcs.196469

Olivares, O., Mayers, J. R., Gouirand, V., Torrence, M. E., Gicquel, T., Borge, L., Lac, S., Roques, J., Lavaut, M. N., Berthezène, P., Rubis, M., Secq, V., Garcia, S., Moutardier, V., Lombardo, D., Iovanna, J. L., Tomasini, R., Guillaumond, F., Vander Heiden, M. G., & Vasseur, S. (2017). Collagen-derived proline promotes pancreatic ductal adenocarcinoma cell survival under nutrient limited conditions. Nature Communications, 8:16031.

Phang, J. M. (2019). Proline metabolism in cell regulation and cancer biology: Recent advances and hypotheses. In Antioxidants and Redox Signaling, 30(4):635-649.

Phang, J. M., Liu, W., Hancock, C., & Christian, K. J. (2012). The proline regulatory axis and cancer. In Frontiers in Oncology, 2-60.

Phang, J. M., Liu, W., Hancock, C. N., & Fischer, J. W. (2015). Proline metabolism and cancer: Emerging links to glutamine and collagen. In Current Opinion in Clinical Nutrition and Metabolic, 18(1):71-7.

Phang, J. M., Liu, W., & Zabirnyk, O. (2010). Proline metabolism and microenvironmental stress. In Annual Review of Nutrition, 30:441-63

Schmid, S., Li, J. J. N., & Leighl, N. B. (2020). Mechanisms of osimertinib resistance and emerging treatment options. In Lung Cancer, 147:123-129.

Tang, J., Hu, M., Lee, S., Roblin, R. (2000). A polymerase chain reaction based method for detecting Mycoplasma/Acholeplasma contaminants in cell culture. J Microbiol Methods, 39(2):121-6.

Tanner, J. J. (2019). Structural biology of proline catabolic enzymes. In Antioxidants and Redox Signaling, 30(4):650-673.

Tanner, J. J., Fendt, S. M., & Becker, D. F. (2018). The Proline Cycle As a Potential Cancer Therapy Target. Biochemistry, 57(25), 3433–3444.

Wei, N., Song, Y., Zhang, F., Sun, Z., & Zhang, X. (2020). Transcriptome Profiling of Acquired Gefitinib Resistant Lung Cancer Cells Reveals Dramatically Changed Transcription Programs and New Treatment Targets. Frontiers in Oncology, 10:1424.

Yan, Y., Chang, L., Tian, H., Wang, L., Zhang, Y., Yang, T., Li, G., Hu, W., Shah, K., Chen, G., & Guo, Y. (2018). 1-Pyrroline-5-carboxylate released by prostate Cancer cell inhibit T cell proliferation and function by targeting SHP1/cytochrome c oxidoreductase/ROS Axis. Journal for ImmunoTherapy of Cancer, 6(1):148.

Zareba, I., Celinska-Janowicz, K., Surazynski, A., Miltyk, W., & Palka, J. (2018). Proline oxidase silencing induces proline-dependent pro-survival pathways in MCF-7 cells. Oncotarget, 9(17):13748-13757.

CONCLUSIONS AND FUTURE PERSPECTIVES

The multifaceted role of PRODH in cancer has been extensively described. It appears to be influenced by different factors, including the tumor type and subtype and the tumor microenvironment.

In lung cancer, PRODH expression in low-stage ADC is associated with a better prognosis. In this context, we found that PRODH expression decreased cell proliferation, mediating cellular senescence (Grossi et al., 2024). On the other hand, other groups have shown that PRODH promotes epithelial-mesenchymal transition and the expression of inflammatory genes, by altering IKKα phosphorylation and function of the NF-KB pathway (Liu et al., 2020). These aspects seem contradictory, but senescence may be responsible for the induction of inflammatory genes and for the epithelial-mesenchymal transition.

Moreover, we expect that the genetic background may influence PRODH contribution to lung cancer.

To test this hypothesis, we investigated the correlation between EGFR and PRODH expression, which had emerged both from our immunohistochemical analysis, carried out in collaboration with Prof. Sessa and Dr. Chiaravalli (Pathology unit of Ospedale di Circolo-Fondazione Macchi and University of Insubria), and from literature data (Angulo et al., 2008).

Surprisingly, we found a negative correlation between EGFR and PRODH expression, in lung ADC cell lines and human immortalized cells ectopically expressing wild-type or mutant EGFR. According to the data described here, EGFR inhibition in lung cells carrying *EGFR* deletion in exon 19 determined an increase in PRODH mRNA.

We went on to propose that the JAK/STAT3 signal transduction pathway, downstream of EGFR, may be involved in the control of *PRODH* expression, since we had identified four putative binding sites for STAT3 in intron 1 of the *PRODH* gene (Gao et al., 2007; Song et al., 2003). The tandem sequence, which includes a full putative binding site and three partial REs, is like that described in the promoter of known STAT3 target genes (Hu et al., 2015; Egusquiaguirre et al., 2018).

Our hypothesis was confirmed by modulating STAT3 expression in different cell lines, which were selected based on their STAT3 activation status. Indeed, ectopic expression of STAT3, or its endogenous stimulation, determined a decrease in PRODH expression, whereas its inhibition resulted in higher levels of PRODH transcript, as EGFR modulation had done.

EGFR-activating mutations often activate STAT3 signaling to promote cancer cell survival (Parakh et al., 2021). In this context, PRODH inhibition may represent an emerging mechanism by which STAT3 contributes to tumor progression.

Upon activation, STAT3 translocates to the nucleus and binds to specific sequences thus regulating the transcription of target genes, including pro-survival, angiogenetic, and metastatic genes. STAT3 is also known as a repressor of *TP53*, which is one of the best characterized transcriptional regulators of *PRODH* expression (Ivanov et al., 2001; Niu et al., 2005: Raimondi et al., 2013). Additionally, STAT3 can modulate the activity of the mitochondrial electron transport chain, or regulate gene expression by epigenetic changes (Yu et al., 2014; Tošić and Frank, 2021;).

Thus, the mechanism by which STAT3 downregulates PRODH could be multiple. To preliminarily determine whether STAT3 directly binds to PRODH, we conducted a luciferase assay, using constructs in which a short (featuring three out of four STAT3 REs) or a long (containing all four STAT3 REs) *PRODH* sequence from intron 1 were cloned upstream of a minimal promoter controlling luciferase expression. In both instances, upon STAT3 inhibition, we observed elevated luciferase activity in DU145 cells transfected with either the “PRODH_short” or the “PRODH_long” constructs, as compared to the same transfected cells treated with vehicle.

Our observations indicated that cells transfected with the “PRODH_long” construct exhibited greater luciferase activity than those transfected with the “PRODH_short” construct, suggesting that the regulation of PRODH involves the cooperation of multiple sequences, or alternatively, that additional transcription factors, whose REs are present in the “PRODH-long” construct, may cooperate in STAT3 mediated repression. We ruled out the involvement of NF-KB, which has a putative binding site near RE4 and has been known to interact directly or indirectly with STAT3 to regulate gene targets (Yeh

et al., 2015), because its stimulation with TNFα did not have an additive effect with STAT3 stimulation with IL-6 (Results-1). Another potential factor is NRF2, whose putative binding site is located close to the STAT3 RE1 at +384 from the TSS. Both transcription factors have been involved in controlling tumor progression and cancer therapy resistance, and have also been shown to play a role in protecting against oxidative stress (Gao et al., 2017; Tian et al., 2022). To test if STAT3 directly binds to the described REs on *PRODH*, we intend to mutagenize the sequences of interest as well as those for other transcription factors that may be cooperating with STAT3, and repeat luciferase assays. Clarifying *PRODH* regulation is important to define its role in lung cancer.

The research presented in the second paper deals with the possible role that PRODH may have in mediating resistance to TKIs used to treat advanced cancer. The first evidence that PRODH may indeed have a role in the onset of resistance was the observation that its expression was increased in two different EGFR-mutant lung cancer cells with *in-vitro* acquired resistance to TKIs, compared to their relative TKI-sensitive parental counterpart.

In TKI-resistant cells, PRODH inhibition impaired cell growth. These effects are in agreement with an increased expression of markers of cell cycle arrest (p21) and apoptosis (PUMA, caspase 8), but the mechanism by which TKI resistance leads to an increase in PRODH levels and how PRODH inhibition delayed cell growth needs to be further investigated. Our hypothesis is that PRODH inhibition may induce apoptosis of EGFR-mutant, TKI-resistant, lung cancer cells and Annexin V staining experiments are ongoing to investigate this aspect.

As multicellular tumor spheroids recapitulate tumor structure, with hypoxic and necrotic areas (Nath & Devi, 2016; Däster et al., 2017), we generated spheroids of HCC827 and HCC827-GR5 cell lines, to examine the effects of PRODH inhibition on their growth.

We showed that PRODH inhibition negatively affected the 3D growth ability of EGFR mutant, TKI-resistant, but not that of TKI-sensitive cells. Moreover, our preliminary data

showed that PRODH inhibition impaired the viability of HCC827-GR5. Thus, PRODH may have a role in the progression (proliferation and resistance to therapy) of advanced-stage lung cancer, similar to what observed in breast cancer (Elia et al., 2017).

This role needs to be confirmed and mechanistically clarified, for example by investigating the induction of cell cycle arrest and apoptosis in 3D culture or performing viability assays at different time points during spheroid growth.

Moreover, as the role of PRODH in EMT was previously described in lung cancer (Liu et al., 2020), we aim to analyze the expression of proteins related to gap junctions (such as connexins) and markers of differentiation state (including cytokeratin) to explore this role in advanced stages.

From the data shown here, PRODH may exert different roles in early- and late-stage lung cancer, based on the activated signaling pathways.

This hypothesis is further supported by data from the UALCAN database, which indicate changes in PRODH expression across different stages of lung cancer. This information was sourced from the database on November 30, 2023 (http://www.uab.edu).

It is tempting to speculate that those advanced-stage lung ADCs that show increased PRODH expression may be the ones that will develop resistance to TKI.

Given that cancer cell metabolism adapts dynamically to the stage of the tumor (Bergers and Fendt, 2021), the use of PRODH inhibitors may sensitize EGFR-mutant tumors to TKIs.

N-propargylglycine (*N*-PPG) is a promising candidate for this purpose, as it binds to the K234 lysine residue of PRODH and the N5 atom of its cofactor, thereby irreversibly inactivating the enzyme. The safety of *N*-PPG has already been established *in vivo* (Scott et al., 2019).

Thus, to fully comprehend the regulation and role of PRODH in lung cancer, it is essential to consider the tumor stage, as PRODH may function as a prognostic marker at early stages or target for lung cancer therapy at advanced stages.

Abbreviations

ADAM disintegrin and metalloprotease

ADC adenocarcinoma

AMPK adenosine monophosphate-activated protein kinase

BASC bronchioalveolar stem cells

ChIP chromatin immunoprecipitation

COPD chronic obstructive pulmonary disease

CR cystein-rych

DAG 1,2-diacylglycerol

DMSO dimethyl sulfoxide

EGF Epidermal Growth Factor

EGFR Epidermal Growth Factor Receptor gene

EMT epithelial-mesenchymal transition

FAD flavin adenin dinucleotide

FBS fetal bovine serum

FGFR fibroblast growth factor receptor

G5K, Glutamate 5-kinase

GADD growth arrest and DNA damage-inducible gene

GEMM genetically engineering mouse models

GSAL L-glutamate-γ-semialdehyde

GSALDH GSAL dehydrogenase

IL interleukin

IL-6R interleukin-6 receptor

IP3 inositol 1,3,5-trisphosphate

KRT5 cytokeratin 5

KRT6 cytokeratin 6

KRT7 cytokeratin 7

LCC large cell carcinoma

L-gln L-glutamine

LIF leukemia inhibitory factor

L-THFA L-tetrahydro-2-furoic acid

mTOR mammalian target-of-rapamycin

MTT 3-[4,5-dimethylthiazol-2-yl]-2,5 diphenyl tetrazolium bromide

NaPy sodium pyruvate

N-PPG *N*-propargylglycine

NSCLC non-small cell lung cancer

OAT ornithine δ-amino acid transferase

OE-PCR overlap extension PCR

P5C Δ-pyrroline-5-carboxylate

P5CR P5C reductase

P5CS P5C synthase

PBS phosphate buffer saline

PDGFR platelet-derived growth factor receptors

PI3K phosphatidylinositol-3-kinase

PIAS protein inhibitor of activated STAT

PIG6 p53-induced gene 6

PIP3 phosphatidylinositol-3,4,5-trisphosphate

PLCγ phospholipase C-γ

PLD phospholipase D

PPARγ proliferator-activated receptor gamma

PPP pentose phosphate pathway

PRODH proline dehydrogenase

PTPRD PTP receptor-type D

PTPRK PTP receptor-type K

PTPRT PTP receptor-type T

PutA Proline Utilization A enzyme

qPCR quantitative PCR

RE response element

RLU relative luminescence

ROS reactive oxygen species

SASP senescence-associated secretory phenotype

SCC squamous cell carcinoma

SCLC small cell lung cancer

SE standard error

SHP SH2-domain-containing PTP1

sIL-6R soluble IL-6 receptor

SOC Suppressor of Cytokine Signaling

SOX2 SRY-box 2

STAT Signal Transducer and Activator of Transcription

TCA Tricarboxylic Acid Cycle

TKI tyrosine-kinase inhibitors

TSS transcriptional start site

TTF1 thyroid transcription factor 1

γ-GPR γ-glutamate phosphate reductase

REFERENCES

Abou-Fayçal, C., Hatat, A. S., Gazzeri, S., & Eymin, B. (2017). Splice variants of the RTK family: Their role in tumour progression and response to targeted therapy. In International Journal of Molecular Sciences, 18(2):383.

Amann, J., Kalyankrishna, S., Massion, P. P., Ohm, J. E., Girard, L., Shigematsu, H., Peyton, M., Juroske, D., Huang, Y., Salmon, J. S., Kim, Y. H., Pollack, J. R., Yanagisawa, K., Gazdar, A., Minna, J. D., Kurie, J. M., & Carbone, D. P. (2005). Aberrant Epidermal Growth Factor Receptor Signaling and Enhanced Sensitivity to EGFR Inhibitors in Lung Cancer.

Angulo, B., Suarez-Gauthier, A., Lopez-Rios, F., Medina, P. P., Conde, E., Tang, M., Soler, G., Lopez-Encuentra, A., Cigudosa, J. C., & Sanchez-Cespedes, M. (2008). Expression signatures in lung cancer reveal a profile for EGFR-mutant tumours and identify selective PIK3CA overexpression by gene amplification. Journal of Pathology, 214(3), 347–356.

Bade, B. C., & Dela Cruz, C. S. (2020a). Lung Cancer 2020: Epidemiology, Etiology, and Prevention. In Clinics in Chest Medicine (Vol. 41, Issue 1, pp. 1–24).

Bender, H.-U., Almashanu, S., Steel, G., Hu, C.-A., Lin, W.-W., Willis, A., Pulver, A., & Valle, D. (2005). Functional Consequences of PRODH Missense Mutations. In Am. J. Hum. Genet, 76(3):409-20. .

Bergers, G., & Fendt, S. M. (2021). The metabolism of cancer cells during metastasis. In Nature Reviews Cancer, 21(3):162-180.

Bogner, A. N., Stiers, K. M., & Tanner, J. J. (2021). Structure, biochemistry, and gene expression patterns of the proline biosynthetic enzyme pyrroline-5-carboxylate reductase (PYCR), an emerging cancer therapy target. In Amino Acids, 53(12):1817-1834.

Bogner, A. N., & Tanner, J. J. (2022). Structure-affinity relationships of reversible proline analog inhibitors targeting proline dehydrogenase. Organic and Biomolecular Chemistry, 20(4), 895–905.

Burke, L., Guterman, I., Palacios Gallego, R., Britton, R. G., Burschowsky, D., Tufarelli, C., & Rufini, A. (2020). The Janus-like role of proline metabolism in cancer. In Cell Death Discovery, 6:104.

Campbell, H. D., Webb, G. C, & Young, I.G. (1997)A human homologue of the Drosophila melanogaster sluggish-A (proline oxidase) gene maps to 22q11.2, and is a candidate gene for type-I hyperprolinaemia. Hum Genet,101(1):69-74.

Cappelletti, P., Tallarita, E., Rabattoni, V., Campomenosi, P., Sacchi, S., & Pollegioni, L. (2018). Proline oxidase controls proline, glutamate, and glutamine cellular concentrations in a U87 glioblastoma cell line. PLoS ONE, 13(4).

Chen, C., We,i Y., We,i L., Chen, J., Chen, X., Dong, X., He, J., Lin, L., Zhu, Y., Huang, H., You, D., Lai, L., Shen, S., Duan, W., Su, L., Shafer, A., Fleischer, T., Bjaanæs, M. M., Karlsson, A., Planck, M., Wang, R., Staaf, J., Helland, Å., Esteller, M., Zhang, R., Chen, F., Christiani, D. C. (2020) Epigenome-wide gene-age interaction analysis reveals reversed effects of PRODH DNA methylation on survival between young and elderly early-stage NSCLC patients. Aging (Albany NY);12(11):10642-10662.

Chen, Z., Fillmore, C. M., Hammerman, P. S., Kim, C. F., & Wong, K. K. (2014b). Non-small-cell lung cancers: a heterogeneous set of diseases. Nat Rev Cancer. Aug;14(8):535-46. Erratum in: Nat Rev Cancer. 2015 Apr;15(4):247.

Cancer Genome Atlas Research Network (2014). Comprehensive molecular profiling of lung adenocarcinoma: The cancer genome atlas research network. Nature, 511(7511), 543–550.

Da Cunha Santos, G., Shepherd, F. A., & Tsao, M. S. (2011). EGFR mutations and lung cancer. Annual Review of Pathology: Mechanisms of Disease, 6, 49–69.

Däster, S., Amatruda, N., Calabrese, D., Ivanek, R., Turrini, E., Droeser, R. A., Zajac, P., Fimognari, C., Spagnoli, G. C., Iezzi, G., Mele, V., & Muraro, M. G. (2017). Induction of hypoxia and necrosis in multicellular tumor spheroids is associated with resistance to chemotherapy treatment. In Oncotarget, 8(1):1725-1736.

Du, X., Yang, B., An, Q., Assaraf, Y. G., Cao, X., Xia, J. Acquired resistance to third-generation EGFR-TKIs and emerging next-generation EGFR inhibitors. Innovation (Camb), 2(2): 2(2):100103.

Ding, Z., Ericksen, R. E., Escande-Beillard, N., Lee, Q. Y., Loh, A., Denil, S., Steckel, M., Haegebarth, A., Wai Ho, T. S., Chow, P., Toh, H. C., Reversade, B., Gruenewald, S., & Han, W. (2020). Metabolic pathway analyses identify proline biosynthesis pathway as a promoter of liver tumorigenesis. Journal of Hepatology, 72(4), 725–735.

Eck, M. J., & Yun, C. H. (2010). Structural and mechanistic underpinnings of the differential drug sensitivity of EGFR mutations in non-small cell lung cancer. In Biochimica et Biophysica Acta - Proteins and Proteomics, 1804(3):559-66.

Egusquiaguirre, S. P., Yeh, J. E., Walker, S. R., Liu, S., & Frank, D. A. (2018). The STAT3 Target Gene TNFRSF1A Modulates the NF-κB Pathway in Breast Cancer Cells. Neoplasia (United States), 20(5), 489–498.

Elia, I., Broekaert, D., Christen, S., Boon, R., Radaelli, E., Orth, M. F., Verfaillie, C., Grünewald, T. G. P., & Fendt, S. M. (2017). Proline metabolism supports metastasis formation and could be inhibited to selectively target metastasizing cancer cells. Nature Communications, 8:15267.

Fujita, Y., Suda, K., Kimura, H., Matsumoto, K., Arao, T., Nagai, T., Saijo, N., Yatabe, Y., Mitsudomi, T., Nishio, K. (2012) Highly sensitive detection of EGFR T790M mutation using colony hybridization predicts favorable prognosis of patients with lung cancer harboring activating EGFR mutation. J Thorac Oncol. Nov;7(11):1640-4.

Gao, S., Zhan, L., Yang, Z., Shi, R., Li, H., Xia, Z., Yuan, S., Wu, Q. P., Wang, T., & Yao, S. (2017). Remote Limb Ischaemic Postconditioning Protects Against Myocardial Ischaemia/Reperfusion Injury in Mice: Activation of JAK/STAT3-Mediated Nrf2-Antioxidant Signalling. Cellular Physiology and Biochemistry, 43(3), 1140–1151.

Gately, K., O'Flaherty, J., Cappuzzo, F., Pirker, R., Kerr, K., & O'Byrne, K. (2012). The role of the molecular footprint of EGFR in tailoring treatment decisions in NSCLC. In Journal of Clinical Pathology, 65(1):1-7.

Greulich, H., Chen, T. H., Feng, W., Jänne, P. A., Alvarez, J. V., Zappaterra, M., Bulmer, S. E., Frank, D. A., Hahn, W. C., Sellers, W. R., & Meyerson, M. (2005). Oncogenic transformation by inhibitor-sensitive and -resistant EGFR mutants. PLoS Medicine, 2(11), 1167–1176.

Grossi, S., Berno, E., Chiofalo, P., Chiaravalli A.M., Cinquetti, R., Bruno, A., Palano, M.T., Gallazzi, M., La Rosa, S., Sessa, F., Acquati, F., Campomenosi, P.. (2024). Proline Dehydrogenase (PRODH)

Is Expressed in Lung Adenocarcinoma and Modulates Cell Survival and 3D Growth by Inducing Cellular Senescence. Int J Mol Sci, 25(2):714.

Hata, A. N., Niederst, M. J., Archibald, H. L., Gomez-Caraballo, M., Siddiqui, F. M., Mulvey, H. E., Maruvka, Y. E., Ji, F., Bhang, H. E. C., Radhakrishna, V. K., Siravegna, G., Hu, H., Raoof, S., Lockerman, E., Kalsy, A., Lee, D., Keating, C. L., Ruddy, D. A., Damon, L. J., Crystal, A. S., Costa, C., Piotrowska, Z., Bardelli, A, Iafrate, A. J, Sadreyev, R. I., Stegmeier, F., Getz, G., Sequist, L. V., Faber, A. C., Engelman JA. Engelman, J. A. (2016). Tumor cells can follow distinct evolutionary paths to become resistant to epidermal growth factor receptor inhibition. Nature Medicine, 22(3), 262–269.

Herbst, R. S., Heymach, J. V., Lippman, S M. (2008) Lung cancer. N Engl J Med, 359(13):1367-80.

Hidaka, N., Iwama, E., Kubo, N., Harada, T., Miyawaki, K., Tanaka, K., Okamoto, I., Baba, E., Akashi, K., Sasaki, H., & Nakanishi, Y. (2017). Most T790M mutations are present on the same EGFR allele as activating mutations in patients with non–small cell lung cancer. Lung Cancer, 108, 75–82.

Hori, M., Tanaka, H., Wakai, K., Sasazuki, S., & Katanoda, K. (2016). Secondhand smoke exposure and risk of lung cancer in Japan: A systematic review and meta-analysis of epidemiologic studies. Japanese Journal of Clinical Oncology, 46(10), 942–951.

Hu, T., Yeh, J. E., Pinello, L., Jacob, J., Chakravarthy, S., Yuan, G.-C., Chopra, R., & Frank, D. A. (2015). Impact of the N-Terminal Domain of STAT3 in STAT3-Dependent Transcriptional Activity. Molecular and Cellular Biology, 35(19), 3284–3300.

Huynh, J., Chand, A., Gough, D., Ernst, M. (2019). Therapeutically exploiting STAT3 activity in cancer - using tissue repair as a road map. Nat Rev Cancer, 19(2):82-96.

Imielinski, M., Berger, A. H., Hammerman, P. S., Hernandez, B., Pugh, T. J., Hodis, E., Cho, J., Suh, J., Capelletti, M., Sivachenko, A., Sougnez, C., Auclair, D., Lawrence, M. S., Stojanov, P., Cibulskis, K., Choi, K., De Waal, L., Sharifnia, T., Brooks, A., Greulich, H., Banerji, S., Zander, T., Seidel, D., Leenders, F., Ansén, S., Ludwig, C., Engel-Riedel, W., Stoelben, E., Wolf, J., Goparju, C., Thompson, K., Winckler, W., Kwiatkowski, D., Johnson, B. E., Jänne, P. A., Miller, V. A., Pao, W., Travis, W.D., Pass, H.I., Gabriel, S.B., Lander, E.S., Thomas, R.K., Garraway, L.A., Getz, G., Meyerson, M. (2012). Mapping the hallmarks of lung adenocarcinoma with massively parallel sequencing. Cell, 150(6), 1107–1120.

Italian Association for Medical Oncology. The numbers of cancer in Italy (2022). https://www.aiom.it/i-numeri-del-cancro-in-italia/

Italian Association for Medical Oncology. Guidelines lung neoplasms 2021 edition (2021). https://www.aiom.it/linee-guida-aiom/

Ivanov, V. N., Bhoumik, A., Krasilnikov, M., Raz, R., Owen-Schaub, L. B., Levy, D., Horvath, C. M., & Ev Ronai, Z. '. (2001). Whereas nu-clear factor-B (NF-B) activates Fas transcription. Mol Cell, 7(3):517-28.

Jantus-Lewintre, E., Usó, M., Sanmartín, E., Camps, C. (2012) Update on biomarkers for the detection of lung cancer. Lung Cancer (Auckl), 3:21-29.

Ji, H., Li, D., Chen, L., Shimamura, T., Kobayashi, S., McNamara, K., Mahmood, U., Mitchell, A., Sun, Y., Al-Hashem, R., Chirieac, L. R., Padera, R., Bronson, R. T., Kim, W., Jänne, P. A., Shapiro, G. I., Tenen, D., Johnson, B. E., Weissleder, R., Sharpless, N. E., Wong, K. K. (2006). The impact of human EGFR kinase domain mutations on lung tumorigenesis and in vivo sensitivity to EGFR-targeted therapies. Cancer Cell, 9(6), 485–495.

Johnson, D. E., O'Keefe, R. A, Grandis, J. R. (2018). Targeting the IL-6/JAK/STAT3 signalling axis in cancer. Nat Rev Clin Oncol,15(4):234-248.

Jorge, S. E. D. C., Kobayashi, S. S., & Costa, D. B. (2014). Epidermal growth factor receptor (EGFR) mutations in lung cancer: Preclinical and clinical data. In Brazilian Journal of Medical and Biological Research, 47(11):929-39.

Jorissen, R. N., Walker, F., Pouliot, N., Garrett, T. P. J., Ward, C. W., & Burgess, A. W. (2003). Epidermal growth factor receptor: Mechanisms of activation and signalling. In Experimental Cell Research 284(1):31-53.

Kancha, R. K., Von Bubnoff, N., Peschel, C., & Duyster, J. (2009). Functional analysis of epidermal growth factor receptor (EGFR) mutations and potential implications for EGFR targeted therapy. Clinical Cancer Research, 15(2), 460–467.

Karayiorgou, M. & Gogos, J. A. (2004). The molecular genetics of the 22q11-associated schizophrenia. Brain Res Mol Brain Res, 132(2):95-104.

Kim, A. S., Ko, H. J., Kwon, J. H., & Lee, J. M. (2018). Exposure to secondhand smoke and risk of cancer in never smokers: A meta-analysis of epidemiologic studies. International Journal of Environmental Research and Public Health, 15(9).

Yasuda, H., Kobayashi, S., Costa, D.B. (2012). EGFR exon 20 insertion mutations in non-small-cell lung cancer: preclinical data and clinical implications. Lancet Oncol, 13(1):e23-31.

Yeh, J. E. & Frank, D. A. (2016). STAT3-Interacting Proteins as Modulators of Transcription Factor Function: Implications to Targeted Cancer Therapy. ChemMedChem, 11(8):795-801.

Lamb, J. A., Moore, J., Bailey, A., Monaco, A. P. (2000). Autism: recent molecular genetic advances. Hum Mol Genet., 9(6):861-8.

Li, H., Hu, H., Wang, R., Pan, Y., Wang, L., Li, Y., Zhang, Y., Ye, T., Zhang, Y., Li, B., Shen, L., Sun, Y., & Chen, H. (2014). Primary concomitant EGFR T790M mutation predicted worse prognosis in non-small cell lung cancer patients. OncoTargets and Therapy, 7, 513–524.

Li, Y., Mao, T., Wang, J., Zheng, H., Hu, Z., Cao, P., Yang, S., Zhu, L., Guo, S., Zhao, X., Tian, Y., Shen, H., & Lin, F. (2023). Toward the next generation EGFR inhibitors: an overview of osimertinib resistance mediated by EGFR mutations in non-small cell lung cancer. In Cell Communication and Signaling 21(1):71.

Liu, H., Heath, S. C., Sobin, C., Roos, J. L., Galke, B. L., Blundell, M. L., Lenane, M., Robertson, B., Wijsman, E. M., Rapoport, J. L., Gogos, J. A., & Karayiorgou, M. (2001). Genetic variation at the 22q11 PRODH2DGCR6 locus presents an unusual pattern and increases susceptibility to schizophrenia. Proc Natl Acad Sci U S A, 99(6):3717-22.

Liu, W., Glunde, K., Bhujwalla, Z. M., Raman, V., Sharma, A., & Phang, J. M. (2012). Proline oxidase promotes tumor cell survival in hypoxic tumor microenvironments. Cancer Research, 72(14), 3677–3686.

Liu, W., Le, A., Hancock, C., Lane, A. N., Dang, C. V., Fan, T. W. M., & Phang, J. M. (2012). Reprogramming of proline and glutamine metabolism contributes to the proliferative and metabolic responses regulated by oncogenic transcription factor c-MYC. Proceedings of the National Academy of Sciences of the United States of America, 109(23), 8983–8988.

Liu, W., & Phang, J. M. (2012). Proline dehydrogenase (oxidase) in cancer. In BioFactors, 38(6):398-406.

Liu, W., Zabirnyk, O., Wang, H., Shiao, Y. H., Nickerson, M. L., Khalil, S., Anderson, L. M., Perantoni, A. O., & Phang, J. M. (2010). MiR-23b targets proline oxidase, a novel tumor suppressor protein in renal cancer. Oncogene, 29(35), 4914–4924.

Liu, Y., Borchert, G. L., Donald, S. P., Diwan, B. A., Anver, M., & Phang, J. M. (2009). Proline oxidase functions as a mitochondrial tumor suppressor in human cancers. Cancer Research, 69(16), 6414–6422.

Liu, Y., Borchert, G. L., Donald, S. P., Surazynski, A., Hu, C. A., Weydert, C. J., Oberley, L. W., & Phang, J. M. (2005). MnSOD inhibits proline oxidase-induced apoptosis in colorectal cancer cells. Carcinogenesis, 26(8), 1335–1342.

Liu, Y., Borchert, G. L., Surazynski, A., Hu, C. A., & Phang, J. M. (2006). Proline oxidase activates both intrinsic and extrinsic pathways for apoptosis: The role of ROS/superoxides, NFAT and MEK/ERK signaling. Oncogene, 25(41), 5640–5647.

Liu, Y., Borchert, G. L., Surazynski, A., & Phang, J. M. (2008). Proline oxidase, a p53-induced gene, targets COX-2/PGE2 signaling to induce apoptosis and inhibit tumor growth in colorectal cancers. Oncogene, 27(53), 6729–6737.

Liu, Y., Mao, C., Wang, M., Liu, N., Ouyang, L., Liu, S., Tang, H., Cao, Y., Liu, S., Wang, X., Xiao, D., Chen, C., Shi, Y., Yan, Q., & Tao, Y. (2020). Cancer progression is mediated by proline catabolism in non-small cell lung cancer. Oncogene, 39(11), 2358–2376.

Lynch, T. J., Bell, D. W., Sordella, R., Gurubhagavatula, S., Okimoto, R. A., Brannigan, B. W., Harris, P. L., Haserlat, S. M., Supko, J. G., Haluska, F. G., Louis, D. N., Christiani, D. C., Settleman, J., Haber, D. A., Departments of Medicine TJL, the, & General, M. (2004). Activating Mutations in the Epidermal Growth Factor Receptor Underlying Responsiveness of Non-Small-Cell Lung Cancer to Gefitinib. In n engl j med, 350(21):2129-39.

Maxwell, S. A., & Kochevar, G. J. (2008). Identification of a p53-response element in the promoter of the proline oxidase gene. Biochemical and Biophysical Research Communications, 369(2), 308–313.

Maxwell, S. A., & Rivera, A. (2003). Proline oxidase induces apoptosis in tumor cells, and its expression is frequently absent or reduced in renal carcinomas. Journal of Biological Chemistry, 278(11), 9784–9789.

Nagano, T., Nakashima, A., Onishi, K., Kawai, K., Awai, Y., Kinugasa, M., Iwasaki, T., Kikkawa, U., & Kamada, S. (2017). Proline dehydrogenase promotes senescence through the generation of reactive oxygen species. Journal of Cell Science, 130(8), 1413–1420.

Nath, S., & Devi, G. R. (2016). Three-dimensional culture systems in cancer research: Focus on tumor spheroid model. In Pharmacology and Therapeutics, 163:94-108.

Niu, G., Wright, K. L., Ma, Y., Wright, G. M., Huang, M., Irby, R., Briggs, J., Karras, J., Cress, W. D., Pardoll, D., Jove, R., Chen, J., & Yu, H. (2005). Role of Stat3 in Regulating p53 Expression and Function. Molecular and Cellular Biology, 25(17), 7432–7440.

Nooreldeen, R., & Bach, H. (2021). Current and future development in lung cancer diagnosis. In International Journal of Molecular Sciences, 2(16):8661.

Okabe, T., Okamoto, I., Tamura, K., Terashima, M., Yoshida, T., Satoh, T., Takada, M., Fukuoka, M., & Nakagawa, K. (2007). Differential constitutive activation of the epidermal growth factor receptor in non-small cell lung cancer cells bearing EGFR gene mutation and amplification. Cancer Research, 67(5), 2046–2053.

Okamoto, S., & Oka, T. (1984). Developmental Biology Evidence for physiological function of epidermal growth factor: Pregestational sialoadenectomy of mice decreases milk production and increases offspring mortality during lactation period (salivary gland/mammary gland/growth and differentiation/lactogenesis). In Proc. Nati. Acad. Sci. USA, 81(19):6059-63.

Olivares, O., Mayers, J. R., Gouirand, V., Torrence, M. E., Gicquel, T., Borge, L., Lac, S., Roques, J., Lavaut, M. N., Berthezène, P., Rubis, M., Secq, V., Garcia, S., Moutardier, V., Lombardo, D., Iovanna, J. L., Tomasini, R., Guillaumond, F., Vander Heiden, M. G., & Vasseur, S. (2017). Collagen-derived proline promotes pancreatic ductal adenocarcinoma cell survival under nutrient limited conditions. Nature Communications, 8:16031.

Paez, J. G., Jänne, P. A., Lee, J.C., Tracy, S., Greulich H, Gabriel S, Herman P, Kaye FJ, Lindeman N, Boggon TJ, Naoki K, Sasaki H, Fujii Y, Eck MJ, Sellers, W. R., Johnson, B. E., Meyerson M. (2004) EGFR mutations in lung cancer: correlation with clinical response to gefitinib therapy. Science, 304(5676):1497-500.

Pal, P., Cabanero, M., & Tsao, M. S. (2018). Pulmonary Adenocarcinoma-Pathology and Molecular Testing. In Pulmonary Adenocarcinoma: Approaches to Treatment (pp. 13–33). Elsevier.

Pandhare, J., Cooper, S. K., & Phang, J. M. (2006). Proline oxidase, a proapoptotic gene, is induced by troglitazone: Evidence for both peroxisome proliferator-activated receptor γ-dependent and -independent mechanisms. Journal of Biological Chemistry, 281(4), 2044–2052.

Pandhare, J., Donald, S. P., Cooper, S. K., & Phang, J. M. (2009). Regulation and function of proline oxidase under nutrient stress. Journal of Cellular Biochemistry, 107(4), 759–768.

Pao, W., Miller, V., Zakowski, M., Doherty, J., Politi, K., Sarkaria, I., Singh, B., Heelan, R., Rusch, V., Fulton, L., Mardis, E., Kupfer, D., Wilson, R., Kris, M., & Varmus, H. (2004). EGF receptor gene mutations are common in lung cancers from '"never smokers"' and are associated with sensitivity of tumors to gefitinib and erlotinib, 101(36):13306-11.

Parakh, S., Ernst, M., Poh, A. R. (2021). Multicellular Effects of STAT3 in Non-small Cell Lung Cancer: Mechanistic Insights and Therapeutic Opportunities. Cancers (Basel), 13(24):6228.

Pavlova, N. N., & Thompson, C. B. (2016). The Emerging Hallmarks of Cancer Metabolism. In Cell Metabolism 23(1):27-47.

Phang, J. M. (2019). Proline metabolism in cell regulation and cancer biology: Recent advances and hypotheses. In Antioxidants and Redox Signaling, 30(4):635-649.

Phang, J. M., Donald, S. P., Pandhare, J., & Liu, Y. (2008). The metabolism of proline, a stress substrate, modulates carcinogenic pathways. In Amino Acids, 35(4):681-90.

Phang, J. M., Liu, W., Hancock, C., & Christian, K. J. (2012). The proline regulatory axis and cancer. In Frontiers in Oncology, 2-60.

Phang, J. M., Liu, W., Hancock, C. N., & Fischer, J. W. (2015). Proline metabolism and cancer: Emerging links to glutamine and collagen. In Current Opinion in Clinical Nutrition and Metabolic, 18(1):71-7.

Phang, J. M., Liu, W., & Zabirnyk, O. (2010). Proline metabolism and microenvironmental stress. In Annual Review of Nutrition, 30:441-63.

Polyak, K., Xia, Y., Zweier, J. L., Kinzler, K. W., & Vogelstein, B. (1997). A model for p53-induced apoptosis. Nature. 1997, 389(6648):300-5.

Qin, X., Chen, J., & Zhou, T. (2021). 22q11.2 deletion syndrome and schizophrenia. In Acta Biochimica et Biophysica Sinica (Vol. 52, Issue 11, pp. 1181–1190). Oxford University Press, 52(11):1181-1190.

Raimondi, I., Ciribilli, Y., Monti, P., Bisio, A., Pollegioni, L., Fronza, G., Inga, A., & Campomenosi, P. (2013). P53 Family Members Modulate the Expression of PRODH, but Not PRODH2, via Intronic p53 Response Elements. PLoS ONE, 8(7):e69152.

Ramirez, M., Rajaram, S., Steininger, R. J., Osipchuk, D., Roth, M. A., Morinishi, L. S., Evans, L., Ji, W., Hsu, C. H., Thurley, K., Wei, S., Zhou, A., Koduru, P. R., Posner, B. A., Wu, L. F., & Altschuler, S. J. (2016). Diverse drug-resistance mechanisms can emerge from drug-tolerant cancer persister cells. Nature Communications, 7.

Rodriguez-Canales, J., Parra-Cuentas, E., & Wistuba, I. I. (2016). Diagnosis and molecular classification of lung cancer. In Cancer Treatment and Research, 170:25-46.

Sainz de Aja, J., Dost, A. F. M., & Kim, C. F. (2021). Alveolar progenitor cells and the origin of lung cancer. Journal of Internal Medicine, 289(5), 629–635.

Schabath, M. B., & Cote, M. L. (2019b). Cancer progress and priorities: Lung cancer. Cancer Epidemiology Biomarkers and Prevention, 28(10), 1563–1579.

Scott, G. K., Yau, C., Becker, B. C., Khateeb, S., Mahoney, S., Jensen, M. B., Hann, B., Cowen, B. J., Pegan, S. D., & Benz, C. C. (2019). Targeting Mitochondrial Proline Dehydrogenase with a Suicide Inhibitor to Exploit Synthetic Lethal Interactions with p53 Upregulation and Glutaminase Inhibition. Molecular Cancer Therapeutics, 18(8), 1374–1385.

Seguin, L., Durandy, M., & Feral, C. C. (2022). Lung Adenocarcinoma Tumor Origin: A Guide for Personalized Medicine. In Cancers (Basel), 14(7):1759.

Siegel, R. L., Miller, K. D., Wagle, N. S., & Jemal, A. (2023). Cancer statistics, 2023. CA: A Cancer Journal for Clinicians, 73(1), 17–48.

Sharma, S.V., Bell, D.W., Settleman J., Haber D.A. (2007). Epidermal growth factor receptor mutations in lung cancer. Nat Rev Cancer, 7(3):169-81.

Song, L., Turkson, J., Karras, J. G., Jove, R., & Haura, E. B. (2003). Activation of Stat3 by receptor tyrosine kinases and cytokines regulates survival in human non-small cell carcinoma cells. Oncogene, 22(27), 4150–4165.

Sordella, R., Bell, D. W., Haber, D. A., & Settleman, J. (2004). Gefitinib-sensitizing EGFR Mutations in Lung Cancer Selectively Activate Anti-apoptotic Pathways. Science, 305(5687):1163-7.

Sung, H., Ferlay, J., Siegel, R. L., Laversanne, M., Soerjomataram, I., Jemal, A., & Bray, F. (2021). Global Cancer Statistics 2020: GLOBOCAN Estimates of Incidence and Mortality Worldwide for 36 Cancers in 185 Countries. CA: A Cancer Journal for Clinicians, 71(3), 209–249.

Tanner, J. J. (2019). Structural biology of proline catabolic enzymes. In Antioxidants and Redox Signaling, 30(4):650-673.

Tanner, J. J., Fendt, S. M., & Becker, D. F. (2018). The Proline Cycle As a Potential Cancer Therapy Target. Biochemistry, 57(25), 3433–3444.

Testa, U., Castelli, G., & Pelosi, E. (2018). Lung cancers: Molecular characterization, clonal heterogeneity and evolution, and cancer stem cells. In Cancers (Basel), 10(8):248.

Threadgill, D. W., Dlugosz, A. A, Hansen, L. A, Tennenbaum, T., Lichti, U., Yee, D., LaMantia, C., Mourton, T., Herrup, K., Harris, R. C, et al. (1995). Targeted disruption of mouse EGF receptor: effect of genetic background on mutant phenotype. Science, 269(5221):230-4.

Tian, Y., Liu, H., Wang, M., Wang, R., Yi, G., Zhang, M., & Chen, R. (2022). Role of STAT3 and NRF2 in Tumors: Potential Targets for Antitumor Therapy. Molecules, 27(24):8768.

Tolomeo, M., Cascio, A. (2021). The Multifaced Role of STAT3 in Cancer and Its Implication for Anticancer Therapy. Int J Mol Sci, 22(2):603.

Tošić, I. & Frank, D. A. (2021). STAT3 as a mediator of oncogenic cellular metabolism: Pathogenic and therapeutic implications. Neoplasia, ;23(12):1167-1178.

Tsiambas, E., Ragos, V., Lefas, A. Y., Georgiannos, S. N., Grapsa, D., Grapsa, D., Patsouris, E., Syrigos, K. (2015). Chromosome 7 deregulation in non-small cell lung carcinoma molecular landscape. J BUON, 20(6):1635-9.

Tsutsumi, O., Kubota, Y., & Oka, T. (1987). Effect of sialoadenectomy, treatment with epidermal growth factor (EGF) antiserum and replacement of EGF on the epidermis in mice. In J. Endocr, 113(2):193-7.

Wanduragala, S., Sanyal, N., Liang, X., & Becker, D. F. (2010). Purification and characterization of Put1p from Saccharomyces cerevisiae. Archives of Biochemistry and Biophysics, 498(2), 136–142.

Wang, H. Q., Man, Q. W., Huo, F. Y., Gao, X., Lin, H., Li, S. R., Wang, J., Su, F. C., Cai, L., Shi Y., Liu B., Bu, L. L. (2020) STAT3 pathway in cancers: Past, present, and future. MedComm, 3(2):e124.

Watanabe, M., Kawaguchi, T., Isa, S. I., Ando, M., Tamiya, A., Kubo, A., Saka, H., Takeo, S., Adachi, H., Tagawa, T., Kakegawa, S., Yamashita, M., Kataoka, K., Ichinose, Y., Takeuchi, Y., Sakamoto, K., Matsumura, A., & Koh, Y. (2015). Ultra-sensitive detection of the pretreatment EGFR T790M mutation in non-small cell lung cancer patients with an EGFR-activating mutation using droplet digital PCR. Clinical Cancer Research, 21(15), 3552–3560.

White, T. A., Johnson, W. H., Whitman, C. P., & Tanner, J. J. (2008). Structural basis for the inactivation of Thermus thermophilus proline dehydrogenase by N-propargylglycine. Biochemistry, 47(20), 5573–5580.

Willis, A., Bender, H. U., Steel, G., & Valle, D. (2008a). PRODH variants and risk for schizophrenia. In Amino Acids, 35(4):673-9.

Yan, Y., Chang, L., Tian, H., Wang, L., Zhang, Y., Yang, T., Li, G., Hu, W., Shah, K., Chen, G., & Guo, Y. (2018). 1-Pyrroline-5-carboxylate released by prostate Cancer cell inhibit T cell proliferation and function by targeting SHP1/cytochrome c oxidoreductase/ROS Axis. Journal for ImmunoTherapy of Cancer, 6(1):148.

Yasuda, H., Kobayashi, S., Costa, D. B. (2012). EGFR exon 20 insertion mutations in non-small-cell lung cancer: preclinical data and clinical implications. Lancet Oncol, 13(1):e23-31.

Yu, H., Lee, H., Herrmann, A., Buettner, R., Jove, R. (2014). Revisiting STAT3 signalling in cancer: new and unexpected biological functions. Nat Rev Cancer, 14(11):736-46.